

**Analysis of Blast/Explosion Resistant
Reinforced Concrete *Solid Slab and T-Beam*
Bridges**

by

Firas A. Abdelahad

A Thesis Submitted to the Faculty of
The College of Engineering
in Partial Fulfillment of the Requirements for the degree of
Master of Science

**Florida Atlantic University
Boca Raton, Florida
May 2008**

Copyright by Firas A. Abdelahad 2008

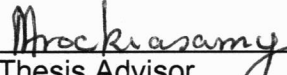
Analysis of Blast/Explosion Resistant Reinforced Concrete Solid Slab and T-Beam Bridges



by

Firas A. Abdelahad

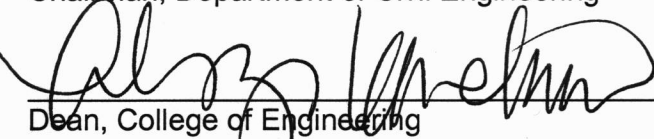
This thesis was prepared under the direction of the candidate's thesis advisor, Dr. Arockiasamy, Department of Civil Engineering, and has been approved by the members of the supervisory committee. It was submitted to the faculty of The College of Engineering and was accepted in partial fulfillment of the requirements for the degree of Master of Science

SUPERVISORY COMMITTEE:


Thesis Advisor


Chairman, Department of Civil Engineering


Dean, College of Engineering


Dean, Graduate College


Date

ACKNOWLEDGMENTS

The author would like to express his sincere gratitude to his supervisor, Dr. M. Arockiasamy, Professor of Civil Engineering, and Director of the Center of Infrastructure and Constructed Facilities, Florida Atlantic University, for his excellent guidance, encouragement, input, great interest throughout the research, and the considerable amount of time he spent at every stage of this thesis. Without his advice, engineering judgment, and the unfailing support throughout the study and the manuscript review, this research would not have been possible. The author would like to record his sincere appreciation to the financial support extended to him from the Dean, College of Engineering.

Appreciation is expressed to Dr. Yan Yong, Professor of Civil Engineering, and Dr. Chi-Tay Tsai, Professor of Mechanical Engineering (Committee Members), Florida Atlantic University, for their valuable suggestions and input. Thanks are extended to Dr. Pete Scarlatos, Professor and Chair Department of Civil Engineering, Florida Atlantic University.

The author would like to extend his sincere gratitude to his parents, Abboud and Claudette, brothers Samer and Kamil, Aunt Elizabeth and Uncle Toni and his family. Acknowledgements are also due to his aunt Madeleine and his uncle Nabil for their generous support, thanks go to his

Uncle Richard and his family as well as the author cousins Sami, Rola and her family. Special thanks are extended to the author friends, Abboud Saadeh, Toni Dallal, George Haddad, Dani Nouneh, Rami Saba, Alaa Hanna, Irina Chang, Jamie Fraser, Juan Bolivar, Elisabeth Gundersen, Akira Tsunemi, Riti Waghray, Sarah Hatfield, Pierre Msaed, Anthony Theodorou, Unal Coban and Dayana Martillo to their encouragement, support and affection throughout the research. Last, but not least, Digna Mejia, Dr. Fred Bloetscher, Dr. D. V. Reddy, Dr. K. Sobhan, Dr. R. Teegavarapu, and Dr. E. Kaiser owe the author special thanks for their supports.

Very Special thanks are due to the author father and mother, role model who continue to instill the motivation and optimism necessary to overcome life's challenges.

ABSTRACT

Author: Firas A. Abdelahad
Title: Analysis of Blast/Explosion Resistant Reinforced
Concrete Solid Slab and T-Beam Bridges

Institution: Florida Atlantic University
Thesis Advisor: Dr. M. Arockiasamy
Degree: Masters of Science
Year: 2008

This study presents and illustrates a methodology to calculate the capacity of an existing reinforced concrete bridge under a non-conventional blast load due to low and intermediate pressures. ATBlast program is used to calculate the blast loads for known values of charge weight and stand off distance. An excel spreadsheet is generated to calculate ultimate resistance, equivalent elastic stiffness, equivalent elastic deflection, natural period of the beam, the maximum deflection, and the maximum rotation in the support for a simple span solid slab and T-Beam bridges. The allowable rotation could be taken as to two degrees. Naval Facility Engineering Command (NAVFAC) approach was adopted, where the inputs were material properties, span length, and area of reinforcement. The use of the Fiber Reinforced Polymer for increasing the capacity of an existing bridge is also presented in this study.

Parametric studies were carried out to evaluate the performance of the solid slab and T-Beam bridges under the assumed blast load.

To My Family

Table of Contents

TABLE OF CONTENTS	VII
LIST OF TABLES	X
TABLE OF FIGURES.....	XI
CHAPTER 1: INTRODUCTION.....	1
1.1 BACKGROUND	1
1.2 OBJECTIVE.....	1
1.3 APPROACH.....	2
1.4 SCOPE.....	2
CHAPTER 2: LITERATURE REVIEW.....	4
2.1 INTRODUCTION	4
2.2 IMPORTANCE OF STUDY	4
2.3 BLAST/DAMAGE TO STRUCTURES	6
2.4 FLEXURAL STRENGTHENING OF BEAMS USING EXTERNALLY BONDED COMPOSITE MATERIALS.....	15
2.4.1 <i>Overview</i>	15
2.4.2 <i>Importance of FRP Composites</i>	16
CHAPTER 3: MATERIAL BEHAVIOR AT HIGH STRAIN RATES	18
3.1 OVERVIEW	18
3.2 PROPERTIES OF CONCRETE AND REINFORCING STEEL UNDER STATIC LOADS.....	18
3.2.1 <i>Modulus of Elasticity</i>	18
3.2.1.1 Concrete	18
3.2.1.2 Reinforcing Steel.....	19
3.2.1.3 Modular Ratio	19
3.2.2 <i>Moment of Inertia</i>	19
3.3 DYNAMIC PROPERTIES OF CONCRETE.....	22

3.4	DYNAMIC PROPERTIES OF REINFORCING STEEL	25
3.5	SUMMARY	29
CHAPTER 4: THEORY: STRUCTURAL RESPONSE OF REINFORCED CONCRETE BEAMS TO BLAST LOADS		30
4.1	MODES OF STRUCTURAL BEHAVIOR.....	30
4.2	DYNAMIC DESIGN OF BEAMS	30
4.2.1	Overview	30
4.2.2	Ultimate Dynamic Moment Capacity.....	31
4.2.3	Reinforcement Ratio.....	31
4.2.3.1	Maximum Flexural Reinforcement	32
4.2.3.2	Minimum Flexural Reinforcement	33
4.2.4	Diagonal Tension	34
4.2.5	Direct Shear	36
4.2.6	Dynamic Analysis	37
4.2.6.1	Overview	37
4.2.6.2	Resistance-Deflection Curve for Design	37
4.2.6.3	Ultimate Resistance	39
4.2.6.4	Plastic Deflection.....	39
4.2.6.5	Support Shears	43
4.2.6.6	Dynamic Design Factors	43
4.2.6.7	Dynamic Analysis	46
4.2.6.8	Prediction of Blast Pressure	50
4.2.6.9	Design for Rebound	52
4.3	STRUCTURE RESPONSE OF REINFORCED CONCRETE BEAMS STRENGTHENED WITH FRP COMPOSITES.....	53
4.3.1	Introduction	53
4.3.2	Methods of Strengthening	54
4.3.3	Mechanical Properties of FRP Composites	54
4.3.4	Partial Safety Factor	56
4.3.5	Failure Modes	56
4.3.6	Flexural Strength	59
4.3.6.1	Overview	59
4.3.6.2	Design Equation.....	59
CHAPTER 5: ILLUSTRATIVE EXAMPLES: REINFORCED CONCRETE SOLID SLAB AND T- BEAM DECK BRIDGES		65

5.1	INTRODUCTION	65
5.2	REINFORCED CONCRETE SOLID SLAB BRIDGE.....	65
5.2.1	<i>Definition of Problem</i>	65
5.2.2	<i>Design Aspect</i>	67
5.2.3	<i>Example Problem</i>	71
5.3	REINFORCED CONCRETE T-BEAM BRIDGE	78
5.3.1	<i>Definition of Problem</i>	78
5.3.2	<i>Design Aspect</i>	80
5.3.3	<i>Example Problem</i>	81
5.4	REINFORCED CONCRETE T-BEAM BRIDGE STRENGTHENED WITH CFRP COMPOSITES.....	91
CHAPTER 6: PARAMETRIC STUDIES AND DISCUSSIONS		101
6.1	INTRODUCTION	101
6.2	CASE STUDIES	101
6.2.1	<i>Case Study 1:</i>	102
6.2.2	<i>Case Study 2:</i>	105
6.2.3	<i>Case Study 3:</i>	109
6.2.4	<i>Case Study 4:</i>	112
6.2.5	<i>Case Study 5:</i>	116
6.2.6	<i>Case Study 6:</i>	118
6.2.7	<i>Case Study 7:</i>	121
6.2.8	<i>Case Study 8:</i>	122
6.3	SUMMARY	124
CHAPTER 7: CONCLUSIONS AND RECOMMENDATIONS		125
7.1	INTRODUCTION	125
7.2	CONCLUSIONS.....	125
7.3	RECOMMENDATIONS AND FUTURE RESEARCH DIRECTIONS	127
REFERENCES.....		128

List of Tables

Table 3.5 Dynamic Increase Factor (DIF) for Design of Reinforced Concrete Elements	29
Table 4.2.3.1 Balanced and Maximum Reinforcement Ratio	34
Table 4.2.6a Ultimate Load Resistance for Beams	41
Table 4.2.6b General and Ultimate Deflections for Beams.....	42
Table 4.2.6c Support Shears for Beams	44
Table 4.2.6d Transformation Factors for Beams	45
Table 4.2.6.7 Elastic, Elasto-Plastic and Equivalent Elastic Stiffness for Beams	49
Table 4.3.3a Typical mechanical properties of GFRP, CFRP and AFRP composites (Head 1996)	55
Table 4.3.3b Measured parameters of the different composite material (Tepfers et al. 1994)	55
Table 4.3.4 Partial Safety Factors for Concrete, Steel, and FRP	56
Table 6.2.1 Simply supported solid slab	102
Table 6.2.2 Simply supported T-beam	106
Table 6.2.3 Solid slab with fixed ends.....	109
Table 6.2.4 T-Beam with fixed ends	113
Table 6.2.5a Solid-slab with fixed ends.....	116
Table 6.2.5b Simply supported solid-slab	117
Table 6.2.6a T-Beam with fixed ends	119
Table 6.2.6b Simply supported T-beam	119
Table 6.2.7 Comparison between boundary conditions for T-Beam strengthened with CFRP	121
Table 6.2.8 Simply supported T-Beam with and without CFRP	122

Table of Figures

Figure 2.2	September 11, 2001 World Trade Center Attacks.....	5
Figure 2.3a	A Section of The Collapsed Bridge on The Barge.....	7
Figure 2.3b	Buckling of I-95 Due to Tanker Fire.	8
Figure 2.3c	Collapse of an Overpass in San Francisco.....	9
Figure 2.4.1	FRP being installed for strengthening.	15
Figures 3.2.2a	Coefficient, F for Calculation of Moment of Inertia of Cracked Section with Tensile Reinforcement.....	20
Figures 3.2.2b	Coefficient, F Calculation of Moment of Inertia of Cracked Section with Reinforcement on both Tension and Compression Faces.....	21
Figure 3.3a	Stress- Strain Curve for Concrete.....	22
Figure 3.3b	Design Curve for DIF for Yield Stress of ASTM A615 Grade 60 Reinforcing Steel.....	23
Figure 3.3c	Dynamic increase factor for peak stress of concrete.....	24
Figure 3.4a	Stress- Strain Curve for Steel.....	25
Figure 3.4b	Design Curve for DIF for Yield Stress of ASTM A615 Grade 60 Reinforcing Steel.....	27
Figure 3.4c	Proposed DIF for ASTM A615 Grade 40, 60 and 75 Steel Rebar...	28
Figure 4.2.6.2	Resistance-Deflection Curve of Beams.....	38
Figure 4.2.6.4a	Rotation at the support for a beam.....	39
Figure 4.2.6.4b	Response Chart.....	40
Figure 4.2.6.7a	Equivalent System.....	46
Figure 4.2.6.7b	Typical Single-Degree-of-Freedom System.....	47
Figure 4.2.6.8	Blast Load.....	50
Figure 4.2.6.9	Blast wave pressure-time history.....	53
Figure 4.3.2	RC beam bonded with FRP soffit plate.....	54
Figure 4.3.5	Failure modes of FRP-plated RC beams.....	58
Figure 4.3.6.2a	Stress-strain curve for concrete (Kong and Evans, Teng et al.).	59
Figure 4.3.6.2b	Strain and stress over beam depth.....	60
Figure 5.2.1a	Solid Slab Bridge Cross Section (Barker 2007).....	66

Figure 5.2.1b The Perspective & Elevation View of The Model Bridge.....	66
Figure 5.2.2a Live-load placement for maximum shear force: (a) truck, (b) lane, and (c) tandem (Barker 2007).....	69
Figure 5.2.2b Live-load placement for maximum bending:(a) truck, (b) lane, and (c) tandem (Barker 2007)	70
Figure 5.3.1a T-Beam Bridge Cross Section (Barker 2007).	78
Figure 5.3.1b T- Beam Cross Section.....	79
Figure 5.3.1c The Perspective & Elevation View of The Model Bridge.....	79
Figure 5.4.1 Cross section in a T-Beam.....	91
Figure 6.2.1a Span Vs Rotation.....	103
Figure 6.2.1b Span Vs Ultimate resistance.....	103
Figure 6.2.1c Span Vs Elastic and Maximum deflection.....	104
Figure 6.2.1d Span Vs Elastic stiffness, k_E and natural period, T_N	104
Figure 6.2.2a Span Vs Rotation.....	106
Figure 6.2.2b Span Vs Ultimate resistance.....	107
Figure 6.2.2c Span Vs Elastic deflection and Maximum deflection	107
Figure 6.2.2d Span Vs Equivalent elastic stiffness, k_E and Natural period, T_N ..	108
Figure 6.2.3a Span Vs Rotation.....	110
Figure 6.2.3b Span Vs Ultimate resistance.....	110
Figure 6.2.3c Span Vs Elastic and Maximum deflection.....	111
Figure 6.2.3d Span Vs Elastic deflection, k_E and natural period, T_N	111
Figure 6.2.4a Span Vs Rotation.....	113
Figure 6.2.4b Span Vs Ultimate resistance.....	114
Figure 6.2.4c Span Vs Elastic and Maximum deflection.....	114
Figure 6.2.4d Span Vs Elastic stiffness, k_E and natural period, T_N	115
Figure 6.2.5a Fixed ends solid slab	117
Figure 6.2.5b Simply supported solid slab	118
Figure 6.2.6a Concrete compressive strength Vs Rotation and ultimate resistance.....	119
Figure 6.2.6b Concrete compressive strength Vs Rotation and ultimate resistance.....	120
Figure 6.3 Span Vs Rotation (comparison)	123

Chapter 1: Introduction

1.1 Background

Among surface transportation's modal systems, the nation's highway infrastructure is relatively robust and redundant. Nevertheless, the consequences of a terrorist attack on critical links could be significant. There are certain points across the United States in which the loss of key links could have major economic and mobility impacts and result in immediate loss of life. Furthermore, as demonstrated in September 11, 2001, highway systems can play a vital role in response to terrorist incidents via their evacuation and emergency access roles. Moreover, according to the National Bridge Inventory Database, as of 2002, the average age of bridge structures is 40 years, and 41 percent of the bridges are at least 40 years old; therefore, a strengthening method should be considered to keep those bridges functioning.

1.2 Objective

The design of bridges and other highway facilities is often governed by the possibility of loading or conditions from extreme events including earthquakes, hurricanes, and ship collisions. Current research efforts are focused on studying the effects of blast loading from terrorist attack and any other incident event such as fuel tank explosion.

The objective of this research is to develop design guidance for improving the structural performance and resistance to intermediate and moderate explosive effects of new and existing bridges.

Tasks necessary to achieve these objectives include:

1. Perform a search of the existing literature review to collect information on past performance of bridges and other structures during and subsequent to extreme events, and the availability of simplified methods of analysis.
2. Work on enhancing those methods and generalize them to be applied on the current research.
3. Describe procedures of implementing the analytical method and present illustrative examples of bridges subjected to blast loads.

1.3 Approach

This study includes analytical investigations of reinforced concrete solid slab and T-Beam bridges to withstand an abnormal type of loading such as explosion. NAVFAC is used as a source in the formulations and a general spreadsheet generated to analyze solid slab and T-Beam deck bridges for both simply supported and fixed ends boundary conditions.

1.4 Scope

The available literature search on blast/damage on structures, the severity of damage on structures and possible way to reduce the vulnerability are being reviewed on Chapter 2. Methods for estimating the

blast load and structural response, and the characteristic of the steel and concrete at high strain rates are discussed. Effect of strengthening of reinforced concrete T-beam bridge using CFRP is also discussed. Chapter 3 presents the material behavior at high strain rates. Chapter 4 presents the details of the structural response of reinforced concrete to blast loads. Chapter 5 presents illustrative examples for reinforced concrete solid slab and T-Beam deck bridges. An example for a T-Beam deck bridge strengthened with CFRP is also included. Comprehensive parametric studies are carried out in Chapter 6. The conclusions and recommendations for future research are presented in Chapter 7.

Chapter 2: Literature Review

2.1 Introduction

This chapter presents a literature review including past research and examples of blast/damage to structures. The severity of damage in bridges due to blast are discussed along with the vulnerability reduction for bridges. Different methods are discussed to estimate blast loads and structural response. Moreover, steel and concrete characteristics at high strain-rate are presented along with the dynamic increase factor. Effect of strengthening of reinforced concrete using Fiber Reinforced Polymer/Plastic (FRP) composites is also reviewed in this study.

2.2 Importance of Study

Among the 600,000 bridges in the United States, preliminary studies indicate that there are approximately 1,000 bridges where substantial casualties, economic disruption, and other societal ramifications will result from isolated attacks as per "*Preliminary Estimate*, NCHRP Project 20-59(5).

The Blue Ribbon Panel BRP recommends prioritization of these bridge assets, followed by risk assessment as a guide for allocating federal and state funds to address security concerns, and then implementation of cost-effective operational security measures and

engineering design standards to reduce the vulnerability of high priority bridges to terrorist attacks.

The panel considered the nature of the bridge components of the highway system and lessons learned from natural disasters, the effects of transportation-related consequences of the September 11 attack (**Figure 2.2**), and the recent barge collision in Oklahoma, where the collision caused destruction of 150 meters of the busy interstate highway. The panel has determined that loss of a critical bridge at one of the numerous “choke points” in the highway system could result in hundreds or thousands of casualties, billions of dollars worth of direct reconstruction costs, and even greater socio-economic costs.



Figure 2.2 September 11, 2001 World Trade Center Attacks

2.3 Blast/Damage to Structures

In recent years, there have been several significant incidents from terrorist bomb attacks both within the US and overseas. These incidents include the World Trade Center bombing in 1993; the Murrah Federal Building bombing in Oklahoma City; US Embassies in Nairobi, Kenya, and Dar-essalem, Tanzania,; World Trade Center attacks; and many more. As a result of these incidents and the continued threat of more terrorist bombing attacks, there has been an extensively increased need for engineers trained in blast resistant design procedures.

A Blue Ribbon Panel (BRP) of bridge experts from professional practice, academia, federal and state agencies and toll authorities convened to examine bridge security and to develop strategies and practices for deterring, disrupting, and mitigating potential attacks. The BRP, sponsored jointly by the Federal Highway Administration (FHWA) and the American Association of State Highway and Transportation Officials (AASHTO), acknowledges that the nation's bridges are vulnerable to terrorist attacks. The BRP has published a research paper recommending policies and actions to reduce the probability of catastrophic structural damage that could result in substantial human casualties, economic losses, and socio-political damage.

The American Society of Civil Engineering (ASCE) developed a report entitled "Design of Blast Resistant Buildings in Petrochemical Facilities". This report provides general guidelines to the structural design of blast resistant petrochemical facilities. It provides coverage for Occupational Safety and Health Administration OSHA requirements,

design objectives, siting considerations, and load determination. More detailed coverage is provided for types of construction, dynamic material strengths, allowable response criteria, analysis methods, and design procedures. Typical details and ancillary considerations are given including doors and windows. A discussion on the upgrade of existing buildings is provided for older facilities, which may not meet current needs.

Some of the recent bridge failures due to a blast loading are presented in the following:

i) On May 2002, a barge lost control and collided with a bridge support causing 580 foot section of the I-40 bridge plunging into the Arkansas River **Figure 2.3a**. Due to the location of the accident, fourteen people were killed. Traffic resumed only after two months setting a new national record for such a project.

ii) On March 2004, a bridge on I-95 Bridgeport, Connecticut was partly damaged by the explosion of a tanker truck carrying over 11,900 gallons of fuel oil. **Figure2.3b** shows the beams and significant area of the damaged deck.



Figure 2.3a A Section of The Collapsed Bridge on The Barge

iii) On April 2007, a section of freeway that funnels traffic onto the San Francisco-Oakland Bay Bridge in the State of California collapsed after a gasoline tanker truck overturned and caught fire,(**Figure 2.3c**). The heat from the fire was intense enough to melt part of the freeway and cause the collapse. No injuries were reported except the truck driver who walked away from the scene with second-degree burns.



Figure 2.3b Buckling of I-95 Due to Tanker Fire.

Recent focus is on the loads due to blast effect on bridges, since the bridges are less protected infrastructure compared to other structures such as high-rise buildings, any state offices, and other important structures; However, not much work has been done regarding the bridge vulnerability assessment due to blast loads.



Figure 2.3c Collapse of an Overpass in San Francisco.

Published research on blast loading and blast effects include high-rise buildings, military base, and bridges.

A.K.M. Anwarul (Ph.D. Thesis 2005) assesses the performance of an AASHTO Girder Bridge under blast loading. He investigated 2-span 2-lane bridge with type III (AASHTO) girders. STAD program was used to model the bridge. The model bridge failed under typical blast loads applied over and underneath the bridge. The research was preformed based on the static equivalent effect of the blast load. The research finding concluded that the AASHTO girders, pier cap, columns could not resist typical blast loads. Some of the recommendations for future studies include the effect of carbon fiber wrapped on bridge elements, and future research on other AASHTO girder type bridges, bulb-Tee bridges, and segmental bridges.

The University Transportation Center for Alabama UTCA, (Uddin et al. 2005) discussed vulnerability of concrete bridge piers to withstand loads created by impact or explosion. Retrofitting the piers with continuous-fiber-reinforced thermoplastic polymers could reduce vulnerability to blast loads. Fiber-reinforced thermoset polymers are used to add stiffness and tensile strength to concrete bridge members.

Malvar (2001) carried out research regarding Carbon Fiber Reinforced Plastic Materials. A retrofit design procedure is presented that decreases the vulnerability of a wide variety of reinforced concrete (RC) buildings to terrorist bombings. The design procedure is generically applicable to retrofitting RC columns which have weak lateral resistance. Retrofit design procedures allow conventional RC columns to survive large explosive loads at very close standoffs. The effectiveness of the resulting retrofit designs is demonstrated through high-fidelity physics based on calculations using the PRONTO3D finite element code.

A review paper of the use of composites, for retrofitting key structural components such as columns, beams, and walls subjected to blast loading, was presented by Malvar (2007). According to the paper blast loads can lead to the shearing of main load-bearing columns and result in the collapse of the whole structure.

Longinow (1996) discussed about protection of buildings against vehicle bomb attacks. The objective was to describe damage mechanisms

that are manifested by solid phase explosions and provide suggestions on steps to reduce damage and casualties in buildings subjected to such attacks. They concluded that it is not practical to design conventional buildings against the effects of a close-in-blast. To retrofit existing buildings against blast is even more impractical.

Mendis (2003) suggested some methods to improve the impact resistance of concrete walls, slabs, and the rotation capacity of the beams, columns and joints for collapse prevention. The paper presents a vulnerability assessment procedure based on the analysis of a typical tall building in Australia. The structural stability and integrity of the building was assessed by considering the effects of the failure of some perimeter columns, spandrel beams and floor slabs due to blast overpressure or impact. The criterion of the analysis is to check, if failure of any primary structural member will cause progressive collapse propagating beyond one story level above or below the affected member. The overall stability of the structure will rely on continuity and ductility of these elements to redistribute forces within the structure.

Gui (2006) discussed blast resistant analysis for a tunnel beneath the Taipei Shongsan airport. The overall analysis is presented to obtain the maximum lining thrust caused by a bomb explosion for use in the lining design. Since there have not been any established common standards governing the design of such a structure, a series of parametric studies have been carried out in order to evaluate the significance and sensitivity

of several parameters on the lining thrust. The parameters evaluated are: intensity of blast loading, size of crater, dynamic undrained shear strength, dynamic Young's modulus, and soil-damping ratio.

Mendis (2007) reported blast loading and blast loading effects on structures. Due to the threat from such extreme loading conditions "explosion" efforts have been made during the past three decades to develop methods of structural analysis and design to resist blast loads. The analysis and design of structures subjected to blast loads require a detailed understanding of blast phenomena and the dynamic response of various structural elements. An explanation of the nature of explosions and the mechanism of blast waves in free air is given. Moreover, this paper introduces different methods to estimate blast loads and structural response. Material behavior at high strain-rate was discussed along with dynamic increase factors.

Sechin (1991) presented a survey of the behavior of reinforced concrete subjected to dynamic loading. Realistic methods of design should take into consideration the strain-rate-dependent properties of reinforced concrete in order to accurately predict the behavior of a reinforced concrete structure subjected to dynamic loads. Concrete compressive strength, steel yield strength, and flexural capacity of reinforced concrete member also increase with increase in loading rate. The increase in flexural capacity of individual members as a result of high strain rates may

shift the failure mode of a structure from a preferred ductile manner to a less desirable brittle mode.

Mahin (1981) reported the response of reinforced concrete members under seismic loading rate. They observed that (i) high strain rates increased the initial yield resistance, but caused small differences in either stiffness or resistance in subsequent cycles at the same displacement amplitudes; (ii) strain rate effect on resistance diminished with increased deformation in a strain-hardening range; and (iii) no substantial changes were observed in ductility and overall energy absorption capacity.

Otani (Otani et al.) had done experimental study on four pairs of cantilever beam specimens; one specimen in each pair was tested under static loading and the other under dynamic loading. Based on the experimental study on flexure dominant specimens with comparable shear strength to some conclusions were derived: (i) increase in the flexural resistance of beams by 7-20% over the strength under static loading because of the strain rate increase; (ii) crack patterns of companion specimens were similar under static and dynamic loading; (iii) for specimens having similar ratio of shear strength of flexural yielding resistance, slender specimen developed largest deformation capacity under static loading. However, specimen with heavy lateral reinforcement developed largest deformation capacity under dynamic loading.

Malvar (1998) presented a paper on high strain rates in the steel reinforcing bars; at high strain rates, the reinforcing bars yield stress can increase by 100%, or more, depending on the grade of steel used. The dynamic increase factor (DIF) is normally reported as function of strain rate. Knowledge of the DIF is of significant importance in the design and analysis of structures for explosives safety. They made a literature review of the effects of high strain rates on the properties of steel reinforcing bars. Static and dynamic properties were reported which satisfy ASTM A615, A15, A432, A431, and A706, with yield stresses ranging from 42 to 103 ksi (290 to 710). The data indicated that the DIF decreases for higher rebar yield stress, and that the DIF is higher for yield stress than for ultimate stress.

Crawford (2006) described methods for designing and implementing protective technologies for improving the blast and impact resistance of buildings. The paper briefly described some design concepts to improve the protection of buildings against explosives and impacts that have both high performance and reasonably good aesthetics. Contrast between these concepts and other more conventional ones are made to distinguish and highlight the features thought to be of most benefit for improving impact and blast resistance. As a conclusion for this paper, blast resistance of new and existing buildings can markedly be enhanced with products and concepts available today. Their design, however, requires expertise, which is not widely available.

2.4 Flexural Strengthening of Beams Using Externally Bonded Composite Materials

2.4.1 Overview

FRP, Fiber Reinforced Polymer, is non-metallic, non-magnetic material; it has high strength, chemical resistance and lightweight. Numerous researches have been done on composite materials. Therefore, it is widely important to incorporate some of those researches in the literature search herein. **Figure 2.4.1** shows FRP being installed for strengthening.



Figure 2.4.1 FRP being installed for strengthening.

2.4.2 Importance of FRP Composites

According to FHWA "Federal Highway Administration" there are about 30% of 600,000 bridges being classified as either functionally obsolete or structural deficient, which means that they require some type of maintenance or major rehabilitation to restore them to their original condition or to their original load carrying capacity. Therefore, using FRP composites will be one of the best options because of the ease of the installation and the practical consideration which was mentioned earlier.

According to Tang (2003) when structural member is being repaired using FRP composites, it will be much stronger than it is original undamaged condition. The FHWA tested to failure a repaired Type-II AASHTO prestressed concrete girder. The repair was hand-wrapped using CFRP fabric and epoxy adhesive system. The repaired beam was 130% stronger than its original design.

Chajes et al. (1995) tested a series of reinforced beams to determine the ability of externally bonded composite reinforcement to improve the beams, flexural and shear capacity. A unidirectional carbon-fiber-reinforced laminate was used. According to Chajes, the composite reinforcement led to an increase in flexural stiffness ranging from 103 percent to 178 percent, and increases in the ultimate beam capacity ranging from 158 to 292 percent. Moreover, a simple formulas were used to predict the ultimate capacity of the externally reinforced beams along

with the test results. Some of those formulas were adopted to be used in this research.

Kolsch (H. Kolsch) presented a method for upgrading existing buildings. Experiments with upgraded concrete beams and masonry wall with flexural loading have been carried out. Moreover, modeling and numerical simulation of the experiments with the finite element method have been done.

Pham (2004) conducted a finite element modeling of debonding failure of rectangular reinforced-concrete beams strengthened with externally bonded Carbon Fiber Reinforced Polymer (CFRP) fabrics under bending. Smeared crack models were used to simulate concrete cracking. Interface element were used to model the bond between concrete and reinforcement. The model proved to be able to simulate the beams' behavior, predicting the failure modes, the failure loads and the reinforcement strain distributions relatively well.

Chapter 3: Material Behavior at High Strain Rates

3.1 Overview

A structural element subjected to a blast loading exhibits a higher strength than a similar element subjected to static loading. Blast loads typically produce very high strain rates. Both the concrete and reinforcing steel exhibit greater strength under rapid strain rates; in reinforced concrete structures subjected to blast effect, the strength of concrete and steel reinforcing bars can increase significantly due to strain rate effects. The increased strength of material due to strain rate is described by the dynamic increase factor, DIF. The DIF is equal to the ratio of the dynamic to static stress, e.g., " f_{dy} / f_y " and f'_{dc} / f'_c . The dynamic increase factor, DIF, depends on the material and the applied strain rate. Knowledge of DIF is of significant importance in the design and analysis of structures to ensure safety against explosion.

3.2 Properties of Concrete and Reinforcing Steel Under Static Loads

3.2.1 Modulus of Elasticity

3.2.1.1 Concrete

The modulus of elasticity of concrete E_c is given by:

$$E_c = w_c^{1.5} 33 \sqrt{f'_c} \quad \text{For } 90 \leq w_c \leq 155 \text{ lb/ft}^3 \quad (3.1)$$

Where: w_c is the unit weight of concrete that is normally equal to 150 lb/ft³

3.2.1.2 Reinforcing Steel

The modulus of elasticity of reinforcing steel E_s is taken as

$$E_s = 29 \times 10^6 \text{ psi}$$

3.2.1.3 Modular Ratio

The ratio of the modulus of elasticity of steel to that of concrete, is modular ratio given by

$$n = \frac{E_s}{E_c} \quad (3.2)$$

3.2.2 Moment of Inertia

As cracking progresses, the effective moment of inertia of the cross section along the element changes continually. Therefore, the determination of the deflection of a reinforced concrete member in the elastic and elasto-plastic ranges is more complex. According to the NAVFAC, the average moment of inertia I_a should be used in all deflection calculations and is given by:

$$I_a = \frac{I_g + I_c}{2} \quad (3.3)$$

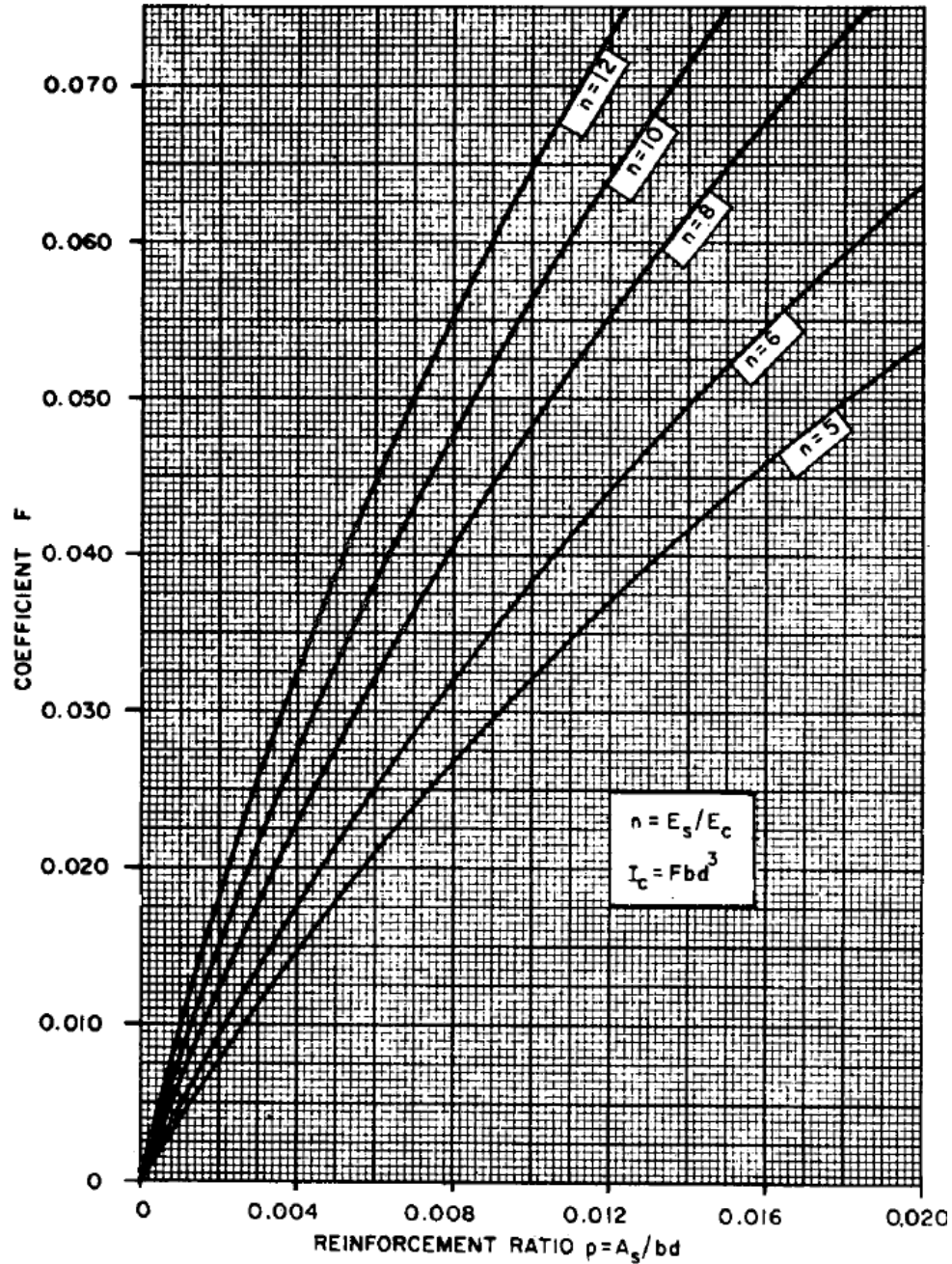
Where

$$I_g = \frac{bd^3}{12}$$

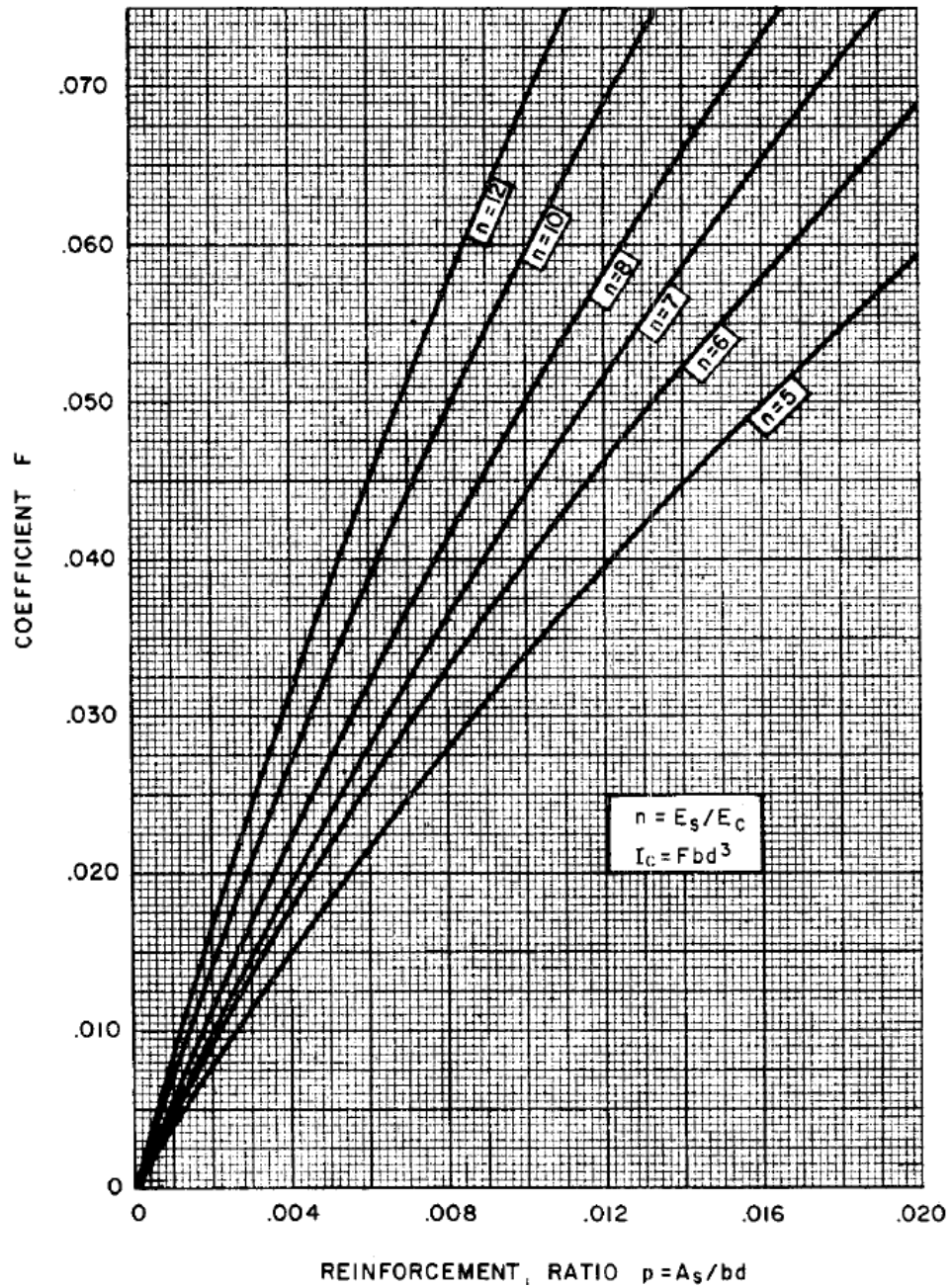
$$I_c = \text{Cracked moment of inertia} \quad I_c = Fbd^3$$

Where the values of F are given in **Figures 3.2.2a** and **3.2.2b**

In the elasto-plastic and plastic ranges, the structural member will exhibit cracks.



Figures 3.2.2a Coefficient, F for Calculation of Moment of Inertia of Cracked Section with Tensile Reinforcement



Figures 3.2.2b Coefficient, F Calculation of Moment of Inertia of Cracked Section with Reinforcement on both Tension and Compression Faces.

3.3 Dynamic Properties of Concrete

The mechanical properties of concrete under dynamic loading conditions can be quite different from that under static loading condition.

Figure 3.3a shows the relationship between the stress and the strain of concrete under ASTM strain rate "static load" and the rapid strain rate that is normally due to dynamic load.

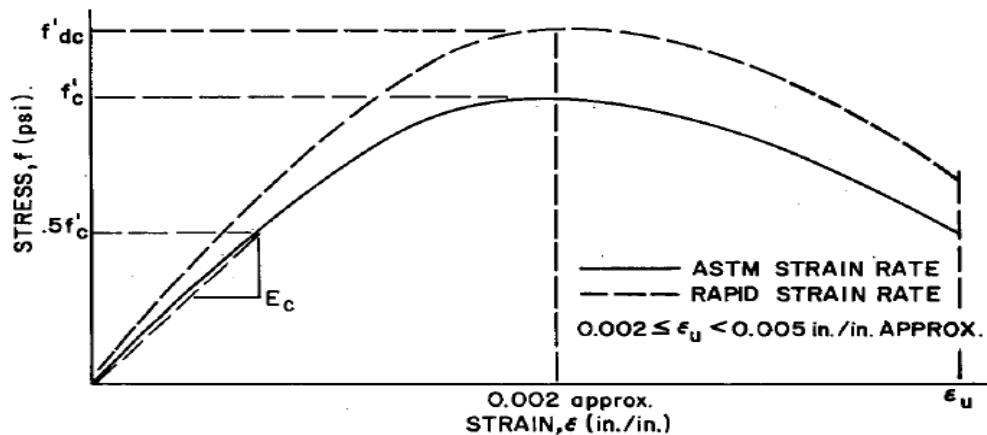


Figure 3.3a Stress- Strain Curve for Concrete

As discussed in previous section, the increased strength of material due to the increased strain rate is described by the dynamic increase factor, DIF.

$$DIF = f'_{dc} / f'_c \quad (3.4)$$

The curve shown in **Figure 3.3b** was derived from test data having a maximum strain rate of 10×10^{-3} in./in./msec.

Values of DIF will vary between the members in the far design range and the members in the close-in design range. Due to the increase in the magnitude of the blast loads, which will lead to the increase in the strain rate, elements subjected to close-in detonation have higher dynamic increase factor than elements subjected to far effect explosions.

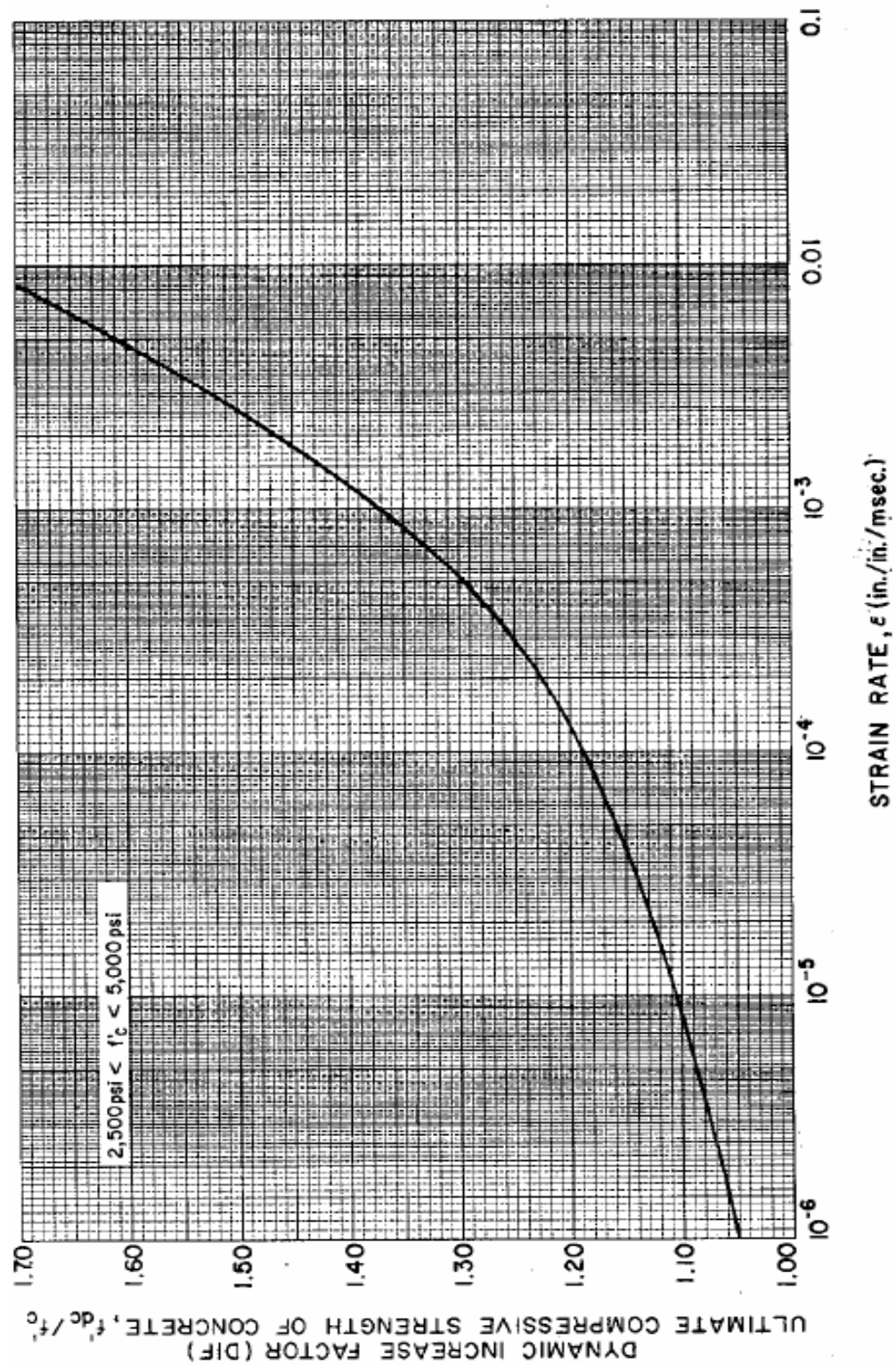


Figure 3.3b Design Curve for DIF for Yield Stress of ASTM A615 Grade 60 Reinforcing Steel

Another method presented by CEB-FIP is presented below. For the increase in the peak compressive stress (f'_c) a Dynamic Increase Factor is introduced in the **CEB-FIP (1990)** model for strain-rate enhancement of concrete (**Figure3.3c**)

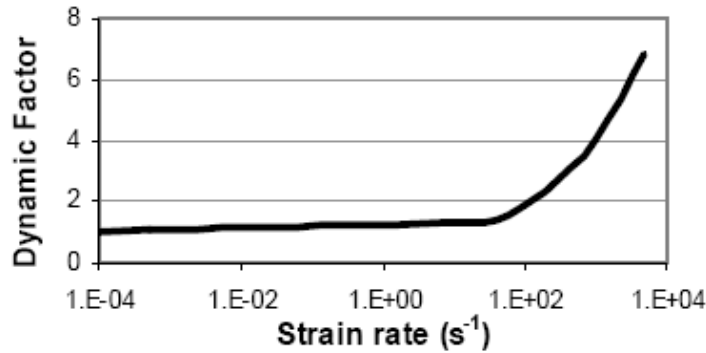


Figure 3.3c Dynamic increase factor for peak stress of concrete

$$\text{DIF} = (\varepsilon' / \varepsilon'_s)^{1.026\alpha} \quad \text{for } \varepsilon' \leq 30 \text{ sec}^{-1} \quad (3.5)$$

$$\text{DIF} = (\varepsilon' / \varepsilon'_s)^{1/3} \quad \text{for } \varepsilon' > 30 \text{ sec}^{-1} \quad (3.6)$$

Where:

ε' = Strain rate (The rate of change of strain with time)

ε'_s = $30 \times 10^{-6} \text{ sec}^{-1}$ (quasi-static strain rate)

$$\log \gamma = 6.156\alpha - 2$$

$$\alpha = 1 / (5 + 9 f'_c / f_{co})$$

$$f_{co} = 10 \text{ MPa} = 1450 \text{ psi}$$

The original CEB-FIB Model Code of 1978 had a considerable impact on the national design codes in many countries. In particular, it has been used extensively for the harmonization of national design codes. Euro

Code 2 used Model Code 1978 as its basic reference document. Model Code 1990 has more detailed guidelines and explanations than national codes and can be used as a basis for them. It has already influenced the codification work that is being carried out both nationally and internationally and will continue to do so.

3.4 Dynamic Properties of Reinforcing Steel

Due to the isotropic properties of metallic materials, their elastic and inelastic response to dynamic loading can easily be monitored and assessed. **Figure 3.4a** shows the relationship between the stress and the strain of the steel under ASTM strain rate "static load" and the rapid strain rate that is normally due to dynamic load.

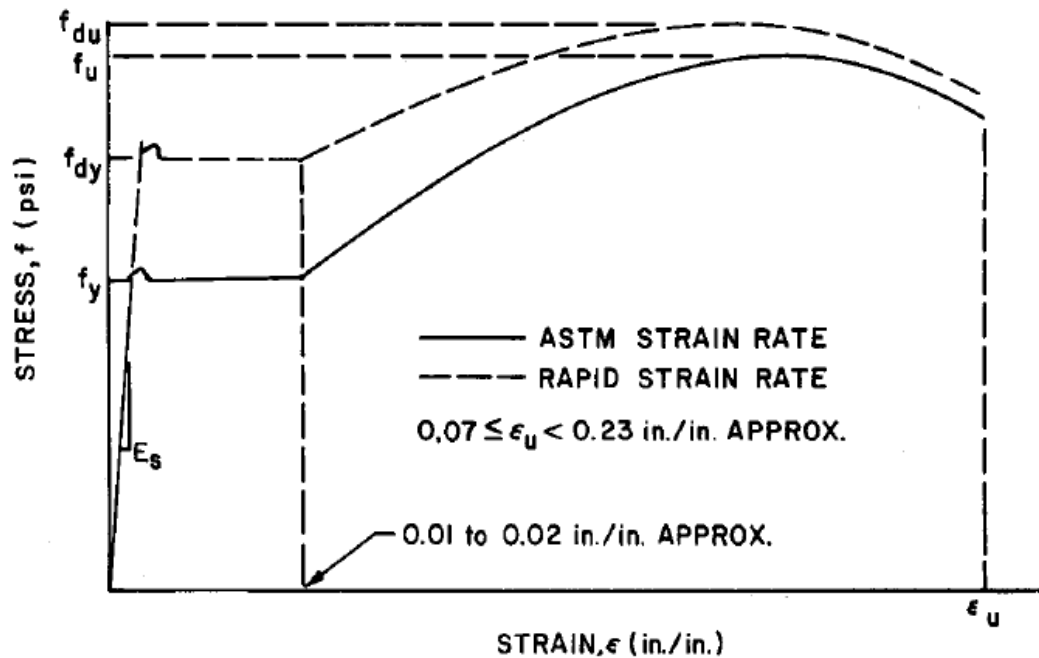


Figure 3.4a Stress- Strain Curve for Steel

For reinforced concrete structures subjected to blast effects, response at very high strain rates (up to 1000 s^{-1}) is often sought. At these high strain rates, the reinforcing bars yield stress can increase by 100%, or more, depending on the grade of steel used.

The increase in strength of steel due to the increased strain rate is described by the dynamic increase factor, DIF, and $\text{DIF} = f_{dy} / f_y$ (**Figure 3.4b.**).

Malvar and Crawford (1989) proposed a formulation for DIF for steel. It was assumed that the DIF data can be approximated by a straight line from a plot of logarithm of the dynamic increase factor versus logarithm of strain rate. The adopted DIF formulation was, for both yield and ultimate stress:

$$\text{DIF} = (\dot{\epsilon}' / 10^{-4})^{\alpha} \quad (3.7)$$

Wherein

For the yield stress, $\alpha = \alpha_{fy} = 0.074 - 0.04 f_y / 60$

And for the ultimate stress, $\alpha = \alpha_{fu} = 0.0194 - 0.009 f_y / 60$

$\dot{\epsilon}'$ in s^{-1} and f_y in ksi (if f_y in MPa, then 60 in the denominator should be replaced by 414).

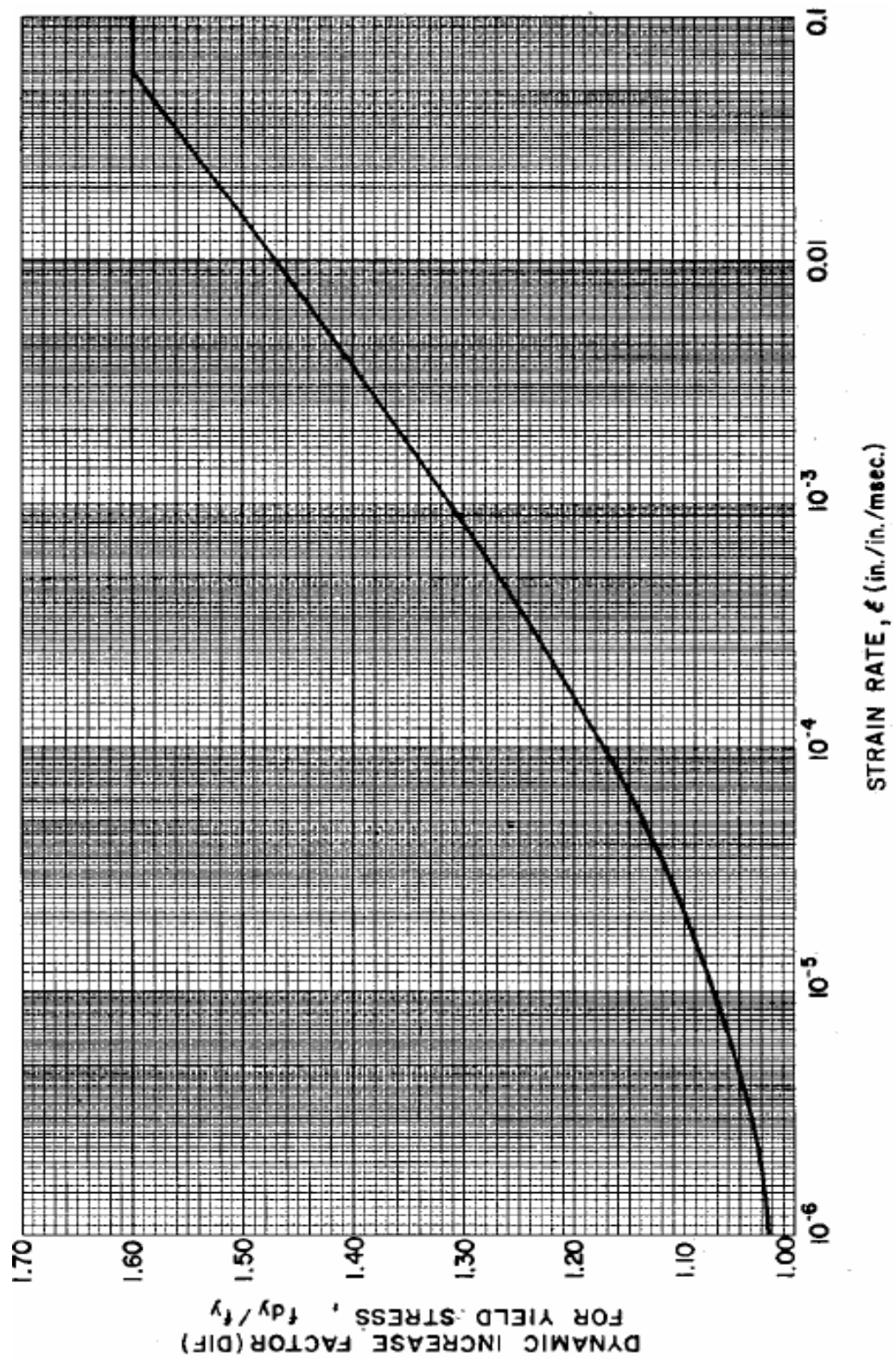


Figure 3.4b Design Curve for DIF for Yield Stress of ASTM A615 Grade 60 Reinforcing Steel

Figure 3.4c shows a plot of the proposed formulation for the DIF, for grade 40, 60, and 75 bars, assuming mean yield stresses of 48, 69, and 87 ksi (330, 475, 600 MPa), respectively

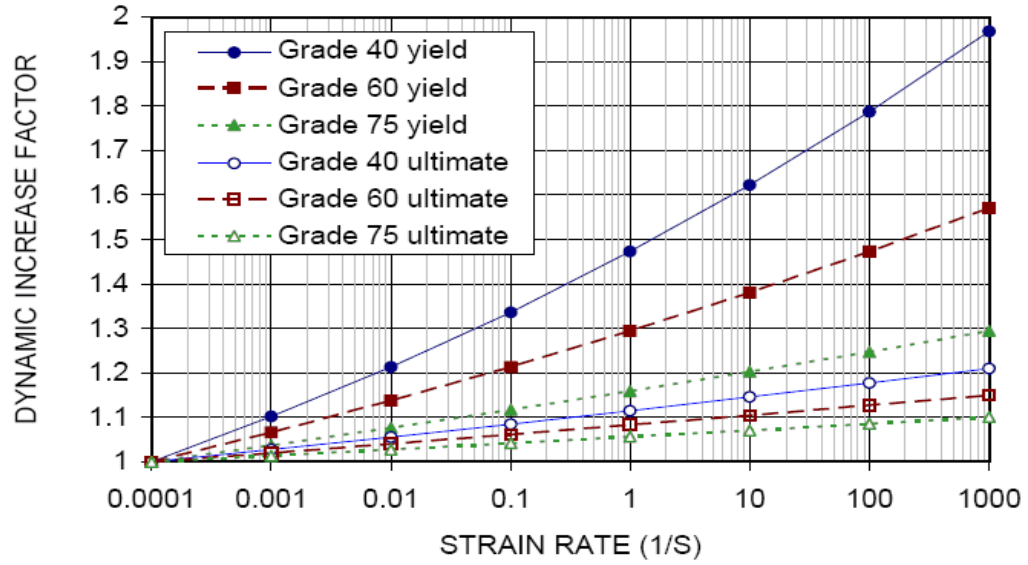


Figure 3.4c Proposed DIF for ASTM A615 Grade 40, 60 and 75 Steel Rebar

3.5 Summary

It is clear that increase in the rate of loading will result in increases in strength and stiffness of concrete, yield strength of steel. A literature review was conducted to determine static and dynamic characteristics of concrete as well as steel reinforcing bars.

However, the DIF values can significantly affect the final design of certain members, and the extra calculations required to obtain the actual DIF values are fully warranted. The actual DIF values are usually higher than the design values of **Table 3.5** shows the values of DIF for design.

Table 3.5 Dynamic Increase Factor (DIF) for Design of Reinforced Concrete Elements

TYPE OF STRESS	FAR DESIGN RANGE			CLOSE-IN DESIGN RANGE		
	Reinforcing Bars		Concrete	Reinforcing Bars		Concrete
	f_{dy}/f_y	f_{du}/f_u	f'_{dc}/f'_c	f_{dy}/f_y	f_{du}/f_u	f'_{dc}/f'_c
Bending	1.17	1.05	1.19	1.23	1.05	1.25
Diagonal Tension	1.00	—	1.00	1.10	1.00	1.00
Direct Shear	1.10	1.00	1.10	1.10	1.00	1.10
Bond	1.17	1.05	1.00	1.23	1.05	1.00
Compression	1.10	—	1.12	1.13	—	1.16

Chapter 4: Theory: Structural Response of Reinforced Concrete Beams to Blast Loads

4.1 Modes of Structural Behavior

Ductile and brittle types of failure are the two modes of structural failure for the reinforced concrete beams. These structural elements may attain large inelastic deflections without complete collapse in the ductile mode, while partial failure or complete collapse of the element may occur in the brittle mode. In the case of blast loads, the magnitude and the duration of the blast have an important influence on the behavior of the structural elements.

4.2 Dynamic Design of Beams

4.2.1 Overview

Beams are primary support members where large plastic deformations are generally not permitted. According to the "NAVFAC" the ultimate support rotation of beams is limited to 2° . Consequently, the maximum stress developed by the reinforcement will be within its yield range.

4.2.2 Ultimate Dynamic Moment Capacity

The ultimate dynamic moment capacity of a reinforced concrete rectangular beam section of width, b and effective depth, d , with tension reinforcement is given by

$$M_u = A_s f_{dy} \left(d - \frac{a}{2} \right) \quad (4.1)$$

$$a = \frac{A_s f_{dy}}{0.85 b f'_{dc}} \quad (4.2)$$

Where:

M_u = ultimate moment capacity, in-lb

A_s = total area of tension reinforcement within the beam, in²

f_{dy} = dynamic yield stress of reinforcement, psi

f'_{dc} = dynamic ultimate compressive strength of concrete, psi

a = depth of equivalent rectangular compression block, in

d = distance from the extreme compression fiber to centroid of tension reinforcement, in

b = width of beam, in

4.2.3 Reinforcement Ratio

At any section of a reinforced concrete structural member, the ratio of the effective area of the reinforcement to the effective area of the concrete ρ is defined as:

$$\rho = \frac{A_s}{bd} \quad (4.3)$$

4.2.3.1 Maximum Flexural Reinforcement

There is a unique amount of reinforcement that will cause the tension steel to reach the minimum net tensile strain $\epsilon_{t_{\min}}$ just as the extreme concrete fiber in compression reaches a strain of ϵ_{cu} of 0.003. Using basic principles, the reinforcement ratio ρ corresponding to this condition is given by:

$$\rho(\epsilon_t = 0.004) = \frac{0.003 + \epsilon_y}{0.007} \rho_b = \rho_{\max} \quad (4.4)$$

where

ρ_b = the reinforcement ratio in the balanced strain condition, which is given by

$$\rho_b = \frac{0.85 f'_c}{f_y} \beta_1 \left(\frac{87000}{87000 + f_y} \right) \quad (4.5)$$

in which f'_c and f_y are in psi.

$$\rho_{\max} = \frac{0.003 + \epsilon_y}{0.007} \rho_b \quad (4.6)$$

This value represents the maximum reinforcement ratio ρ_{\max} that ensures a minimum net tensile steel strain of 0.004 and provides an indirect, but practical, way to satisfy the minimum tensile steel strain requirement.

Table 4.2.3.1 shows the balanced and maximum reinforcement ratio for different values of f'_c , f_y and β_1

4.2.3.2 Minimum Flexural Reinforcement

Since a ductile failure mode is desired, the smallest amount of steel permitted should be the amount that would equal the strength of an under-reinforced section. The minimum reinforcement for T-Sections having slab in compression ranges from

$$A_{s\min} = \frac{2.4\sqrt{f'_c}}{f_y} b_w d \quad \text{to} \quad A_{s\min} = \frac{3.2\sqrt{f'_c}}{f_y} b_w d \quad (4.7)$$

For rectangular sections

$$A_{s\min} = \frac{1.6\sqrt{f'_c}}{f_y} b_w d \quad \text{to} \quad A_{s\min} = \frac{2.1\sqrt{f'_c}}{f_y} b_w d \quad (4.8)$$

ACI 1995 gives formula for the minimum reinforcement as

$$A_{s\min} = \frac{3\sqrt{f'_c}}{f_y} b_w d \quad (4.9)$$

But not less than

$$A_{s\min} = \frac{200}{f_y} b_w d \quad (4.10)$$

For T-Sections having slab in tension, the minimum reinforcement ranges from

$$A_{s\min} = \frac{5.6\sqrt{f'_c}}{f_y} b_w d \quad \text{to} \quad A_{s\min} = \frac{7.4\sqrt{f'_c}}{f_y} b_w d \quad (4.11)$$

ACI 1995 states that minimum reinforcement for statically determinate members with a flange in tension is to be computed using ACI formula

except that b_w is replaced by either $2b_w$ or the width of the flange, whichever is smaller.

Table 4.2.3.1 Balanced and Maximum Reinforcement Ratio

f_y psi		$f'_c=3000$ psi	$f'_c=3500$ psi	$f'_c=4000$ psi	$f'_c=5000$ psi	$f'_c=6000$ psi
		$\beta_1=0.85$	$\beta_1=0.85$	$\beta_1=0.85$	$\beta_1=0.80$	$\beta_1=0.75$
40000		$\rho_b=0.0371$	$\rho_b=0.0433$	$\rho_b=0.0495$	$\rho_b=0.0582$	$\rho_b=0.0655$
	$\rho_{max}=$	$0.626*\rho_b=0.0232$	$0.626*\rho_b=0.0271$	$0.626*\rho_b=0.0310$	$0.626*\rho_b=0.0365$	$0.626*\rho_b=0.0410$
50000		$\rho_b=0.0275$	$\rho_b=0.0321$	$\rho_b=0.0367$	$\rho_b=0.0432$	$\rho_b=0.0486$
	$\rho_{max}=$	$0.675*\rho_b=0.0186$	$0.675*\rho_b=0.0217$	$0.675*\rho_b=0.0248$	$0.675*\rho_b=0.0291$	$0.675*\rho_b=0.0328$
60000		$\rho_b=0.0214$	$\rho_b=0.0249$	$\rho_b=0.0285$	$\rho_b=0.0335$	$\rho_b=0.0377$
	$\rho_{max}=$	$0.724*\rho_b=0.0155$	$0.724*\rho_b=0.0181$	$0.724*\rho_b=0.0206$	$0.724*\rho_b=0.0243$	$0.724*\rho_b=0.0273$

4.2.4 Diagonal Tension

The occurrence of the first inclined crack determines the shear strength of a beam without web reinforcement. Because crack development is a function of the tensile strength of the concrete in the beam web, knowledge of the principal stress in the critical sections is necessary. The controlling principal stress in concrete is the result of the shearing stress v_u due to the external factored shear V_u and the horizontal flexural stress f_t due to the external factored bending moment M_u .

The nominal shear stress v_u as a measure of diagonal tension is computed from

$$v_u = \frac{V_u}{bd} \quad (4.12)$$

Where

v_u = nominal shear stress, psi

V_u = total shear at critical section, lb

The critical section is taken at a distance, d , from the face of the support for those members that cause compression in their supports. For members that cause tension in their supports, the critical section is at the face of the supports.

The shear stress permitted in an unreinforced web of a beam subjected to flexure only is limited to

$$v_c = \Phi(1.9\sqrt{f'_c} + 2500\rho) \leq 2.28\Phi\sqrt{f'_c} \quad (4.13)$$

where

v_c = maximum shear capacity of an unreinforced web, psi

ρ = reinforcement ratio of the tension reinforcement at the support

Φ = capacity reduction factor = 0.85

Shear reinforcement must be provided whenever the nominal shear stress, v_u , exceeds the shear capacity, v_c , of the concrete.

Closed ties placed perpendicular to the flexural reinforcement must be used to provide the additional shear capacity. Open stirrups, either single or double leg, are not permitted. The required area of shear reinforcement is calculated using

$$A_v = \frac{(v_u - v_c)bs_s}{\Phi f_y} \quad (4.14)$$

where

A_v = total area of stirrups, in²

$v_u - v_c$ = excess shear stress, psi

s_s = spacing of stirrups in the direction parallel to the longitudinal reinforcement, in.

Φ = capacity reduction factor = 0.85

Limitations:

i) $(v_u - v_c) \geq v_c$

ii) $v_u \leq 10\Phi\sqrt{f'_c}$

iii) $A_v \geq 0.0015bs_s$ and should be determined at the critical section, and should be distributed uniformly throughout the member.

iv) $s_{s \max} \begin{cases} \frac{d}{2} & \text{when } (v_u - v_c) \leq 4\Phi\sqrt{f'_c} \\ \frac{d}{4} & \text{when } (v_u - v_c) < 4\Phi\sqrt{f'_c} \end{cases}$

4.2.5 Direct Shear

Direct shear failure of a member is described by the rapid propagation of a vertical crack through the depth of the member. This crack is usually located at the supports where the maximum shear stresses occur. It is important to point out that direct shear failure is possible even in members reinforced for diagonal tension.

The magnitude of the ultimate direct shear force, V_d which can be resisted by a beam, is limited to

$$V_d = 0.18f'_{dc}bd \quad (4.15)$$

The total support shear produced by the applied loading may not exceed V_d . If the support shear exceeds V_d , the depth or width of the beam or both must be increased since the use of diagonal bars is not recommended.

4.2.6 Dynamic Analysis

4.2.6.1 Overview

The dynamic analysis of beams is performed in the same manner as that given in the NAVAC P-397 for slabs. The most significant difference in the design procedure is that in the case of a slab, the resistance is based on load per unit area (psi), whereas for a beam, the resistance is based on load per unit length of the beam.

4.2.6.2 Resistance-Deflection Curve for Design

The resistance deflection function for design takes the form shown in **Figure 4.2.6.2**. One, two, and three step Elasto-Plastic System.

The maximum deflection x_m , of a beam within the elastic, elasto-plastic, and limited plastic ranges. One and two-step systems are generally used for beams. A three-step function is possible but only for fixed ended beams with unequal negative moment capacities. It is important to mention that the response charts are prepared for one-step systems.

The variables in **Figure 4.2.6.2** are as follows:

k_E = equivalent elastic deflection

k_e = elastic stiffness

x_e = elastic deflection

x_{ep} = elasto-plastic deflection

x_p = plastic deflection

x_m = maximum deflection

x_E = equivalent elastic deflection

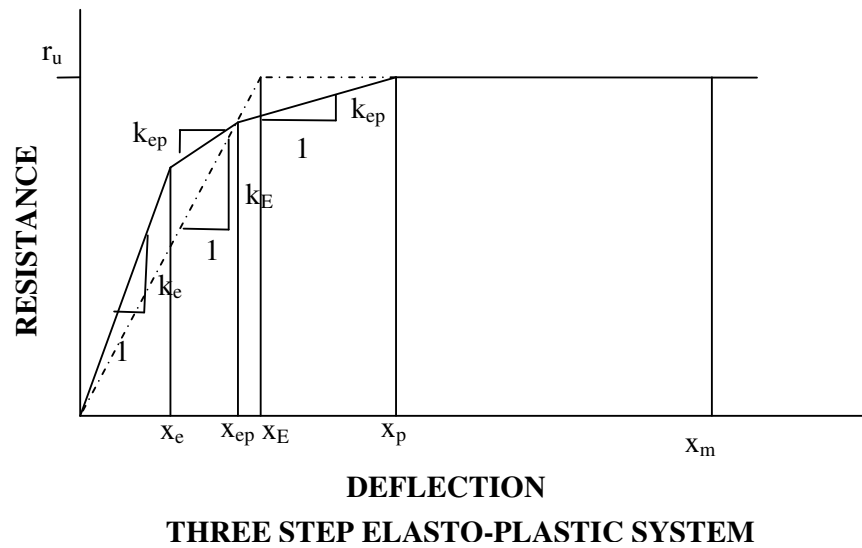
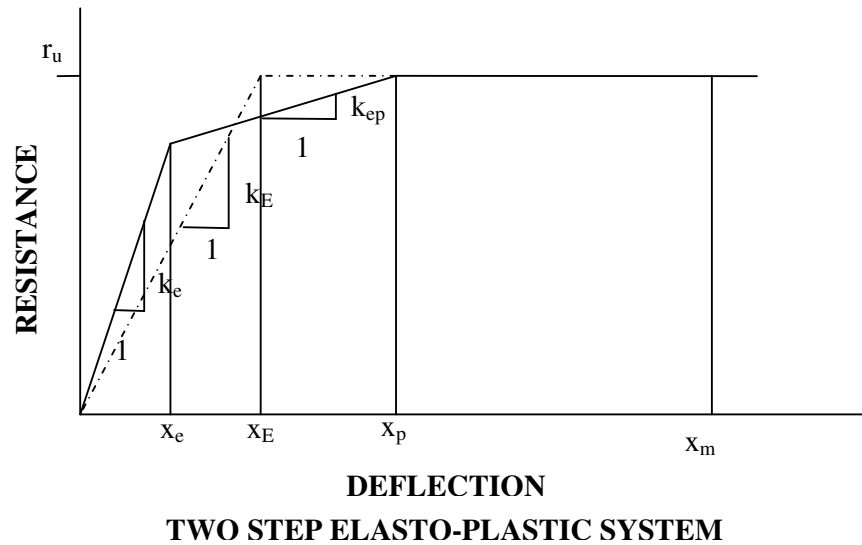
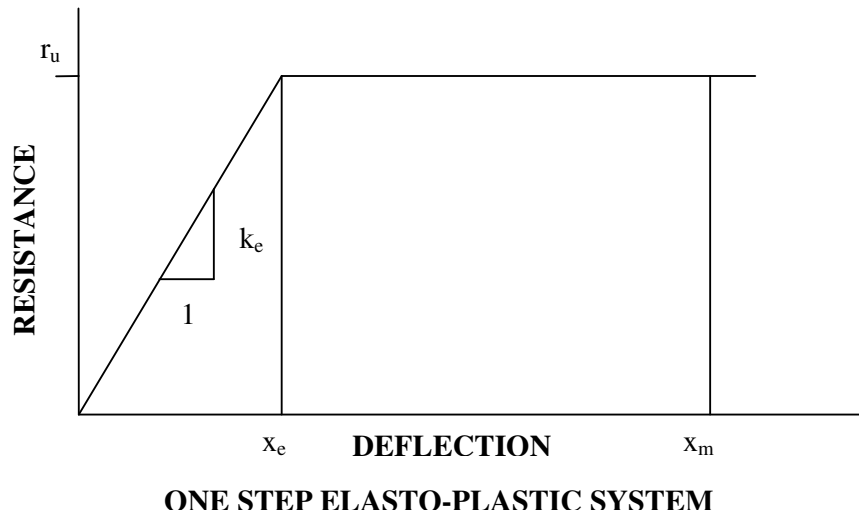


Figure 4.2.6.2 Resistance-Deflection Curve of Beams

4.2.6.3 Ultimate Resistance

Table 4.2-6a shows the ultimate load resistance of beams. It has been constructed in a way that covers various loading conditions. r_u is the ultimate load that the beam can take; M_p , and M_n are the positive and negative moment respectively. r_u , and R_u are the ultimate load resistance for uniform and concentrated load respectively.

4.2.6.4 Plastic Deflection

Table 4.2.6b shows the maximum plastic deflection and the ultimate deflection for beams with various loading and support conditions. The deflection is given as a function of the support rotation.

Figure 4.2.6.4a shows the support rotation, θ and maximum deflection x_m .

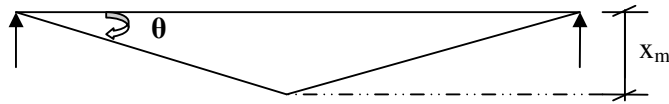


Figure 4.2.6.4a Rotation at the support for a beam

For θ in the range of $0 - 2^\circ$, the concrete is effective in resisting moment and the concrete cover on both surfaces of the element remains intact and the ultimate support rotation of beams is limited to 2 degrees. It has been proved by experiments that reinforced concrete members lose their structural integrity after support rotations of 2° have been reached. In order to be able to find the support rotation, the maximum deflection, x_m should be calculated. It can be calculated from the ductility ratio, which is given in

Figure 4.2.6.4b. The use of this chart is discussed in Chapter 5.

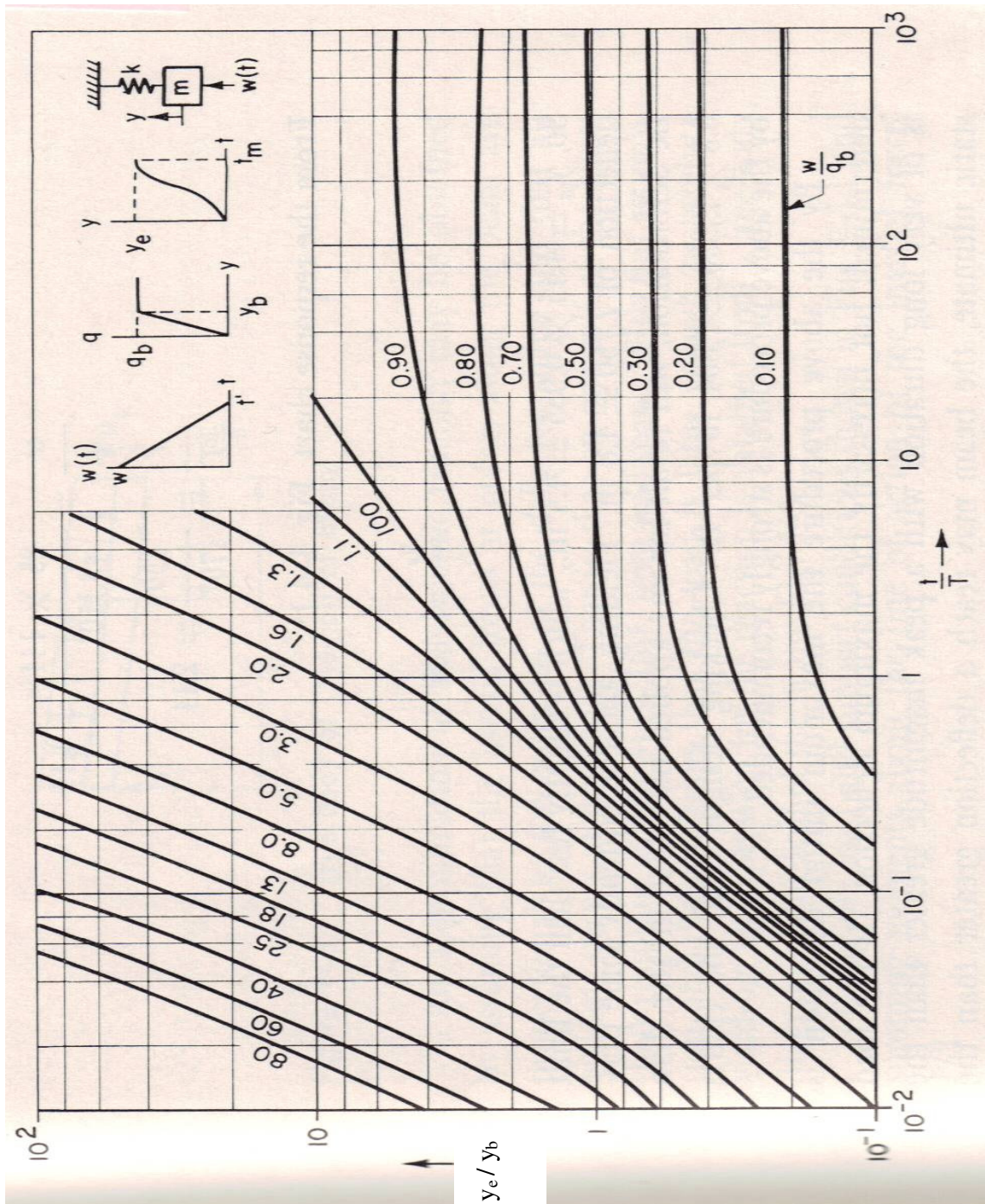


Figure 4.2.6.4b Response Chart

Table 4.2.6a Ultimate Load Resistance for Beams

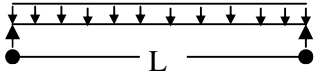
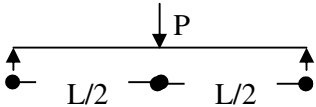
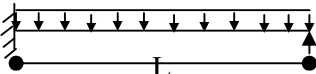
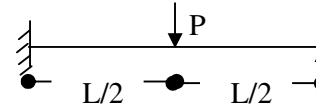
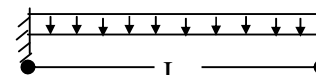
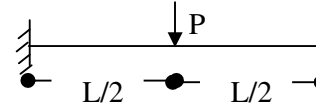
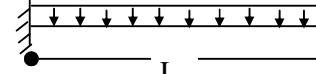

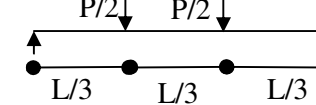
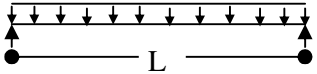
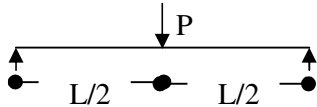
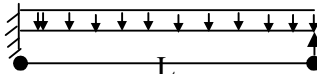
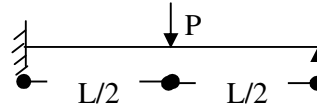
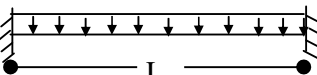
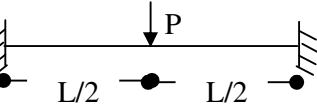
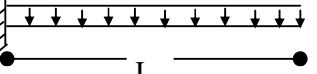
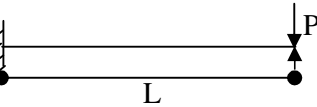
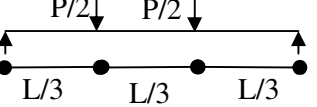
End conditions and Loading Diagrams	Ultimate Load Resistance
	$r_u = \frac{8M_p}{L^2}$
	$R_u = \frac{4M_p}{L}$
	$r_u = \frac{4(M_N + 2M_p)}{L^2}$
	$R_u = \frac{2(M_N + 2M_p)}{L}$
	$r_u = \frac{8(M_N + M_p)}{L^2}$
	$R_u = \frac{4(M_N + M_p)}{L}$
	$r_u = \frac{2M_N}{L^2}$
	$R_u = \frac{M_N}{L}$
	$R_u = \frac{6M_p}{L}$

Table 4.2.6b General and Ultimate Deflections for Beams

End conditions and Loading Diagrams	Maximum Deflection, x_m	Ultimate Deflection, x_u
	$\frac{L}{2} \tan \theta$	$\frac{L}{2} \tan \theta_{\max}$
	$\frac{L}{2} \tan \theta$	$\frac{L}{2} \tan \theta_{\max}$
	$\frac{L}{2} \tan \theta$	$\frac{L}{2} \tan \theta_{\max}$
	$\frac{L}{2} \tan \theta$	$\frac{L}{2} \tan \theta_{\max}$
	$\frac{L}{2} \tan \theta$	$\frac{L}{2} \tan \theta_{\max}$
	$\frac{L}{2} \tan \theta$	$\frac{L}{2} \tan \theta_{\max}$
	$L \tan \theta$	$L \tan \theta_{\max}$
	$L \tan \theta$	$L \tan \theta_{\max}$
	$\frac{L}{3} \tan \theta$	$\frac{L}{3} \tan \theta_{\max}$

4.2.6.5 Support Shears

Table 4.2.6c shows the support reactions for beams with various support and loading conditions. r_u , and R_u are the ultimate uniform and concentrated loads respectively.

4.2.6.6 Dynamic Design Factors

Table 4.2.6d shows transformation factors, which are load factors, mass factors, and the load-mass factors for the Elastic, Elasto-Plastic, and Plastic ranges of behavior. As per the NAVFAC p-397, the load mass factor is used for majority of design cases while the load and mass factors are essential for more complicated design cases.

Table 4.2.6c Support Shears for Beams

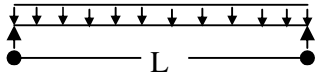
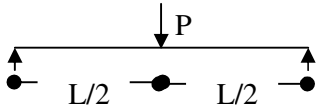
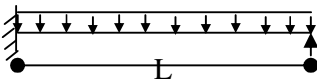
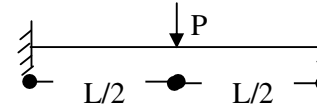
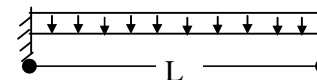
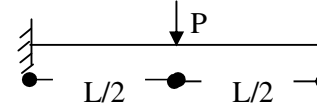
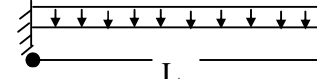
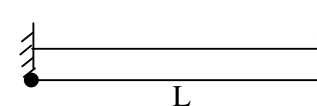
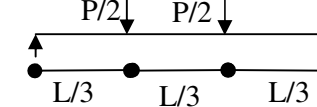
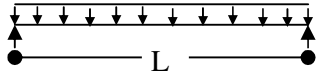
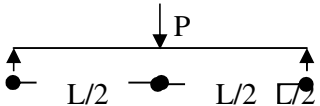
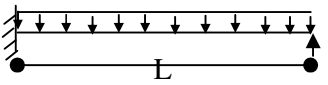
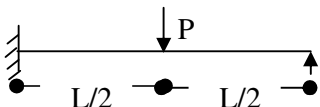
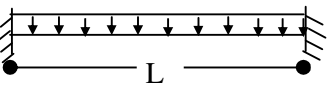
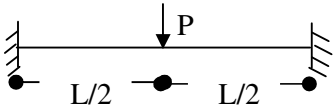
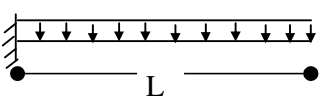
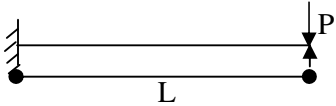
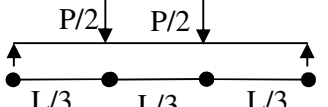
End conditions and Loading Diagrams	Support Reactions, V_s
	$\frac{r_u L}{2}$
	$\frac{R_u}{2}$
	Left $\frac{5r_u L}{8}$ Right $\frac{3r_u L}{8}$
	Left $\frac{11R_u}{16}$ Right $\frac{5R_u}{16}$
	$\frac{r_u L}{2}$
	$\frac{R_u}{2}$
	$r_u L$
	R_u
	$\frac{R_u}{2}$

Table 4.2.6d Transformation Factors for Beams

End conditions and Loading Diagrams	Range of Behavior	Load Factor K_L	Mass Factor K_M	Load-Mass Factor K_{LM}
	Elastic	0.64	0.50	0.78
	Plastic	0.50	0.33	0.66
	Elastic	1.0	0.49	0.49
	Plastic	1.0	0.33	0.33
	Elastic	0.58	0.45	0.78
	Elasto-Plastic	0.64	0.50	0.78
	Plastic	0.50	0.44	0.66
	Elastic	1.0	0.43	0.43
	Elasto-Plastic	1.0	0.49	0.49
	Plastic	1.0	0.33	0.33
	Elastic	0.53	0.41	0.77
	Elasto-Plastic	0.64	0.50	0.78
	Plastic	0.50	0.33	0.66
	Elastic	1.0	0.37	0.37
	Plastic	1.0	0.33	0.33
	Elastic	0.40	0.26	0.65
	Plastic	0.50	0.33	0.66
	Elastic	1.0	0.24	0.24
	Plastic	1.0	0.33	0.33
	Elastic	0.87	0.52	0.60
	Plastic	1.0	0.56	0.56

4.2.6.7 Dynamic Analysis

The solid slab and T-beam bridges are modeled as a single-degree of freedom system. To find the response of the solid slab and T-beam due to blast load, it is based on the observation that under blast load the mid-span deflection of a beam is similar to that of a spring-mass system. In the analogy, the beam is replaced by a lumped mass on a spring **Figure 4.2.6.7a**. The resistance of the spring represents the stiffness of the uniformly loaded beam, the load becomes the total load on the beam, and the weight of the mass becomes the weight of the beam times the load-mass factor.

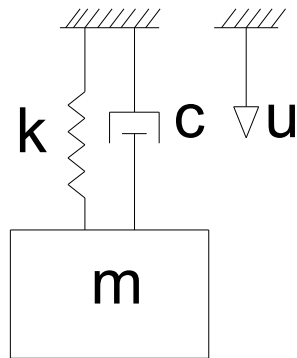


Figure 4.2.6.7a Equivalent System

The equivalent system is defined in terms of its ultimate resistance r_u , equivalent elastic deflection x_E , and natural period of vibration T_N .

Figure 4.2.6.7b shows a typical undamped single degree of freedom system "SDOF". It is important to emphasize that although all structures possess many degrees of freedom, one mode usually predominates the response to short duration loads. Therefore, for all practical purposes, this

one mode may be considered to define the behavior of the structure, and thus, the problem can be simplified by considering a single degree of freedom system whose properties are those of the fundamental mode of the structures. The SDOF system is defined as one in which only one type of motion is possible or, in other words, only one coordinate is required to define its motion. The equation of motion for such a system is given as

$$ma = F - R \quad (4.16)$$

$$m \frac{d^2 y}{dt^2} = w(t) - q(y) \quad \text{or} \quad m \frac{d^2 y}{dt^2} = p - r_u \quad (4.17)$$

where:

$$m \frac{d^2 y}{dt^2} = ma = \text{Mass times acceleration}$$

$$w(t) = p = \text{Load, a function of time}$$

$$q(y) = r_u = \text{Resistance of the structure}$$

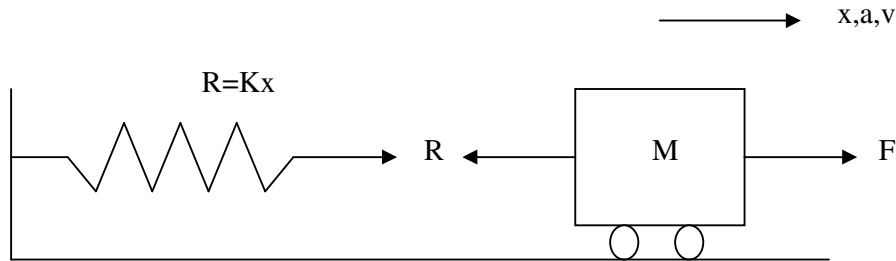


Figure 4.2.6.7b Typical Single-Degree-of-Freedom System

4.2.6.7.1 Period of Vibration and Effective Mass

In order to solve the equation of motion, natural frequency and fundamental period are required, and are given by the following Equations

$$\omega = \sqrt{\frac{k_E}{K_{LM}m}} \text{ And } T_N = 2\pi \sqrt{\frac{K_{LM}m}{k_E}} \quad (4.18)$$

where

ω, T_N are natural frequency and fundamental period respectively.

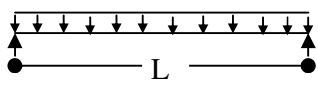
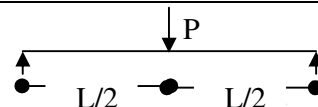
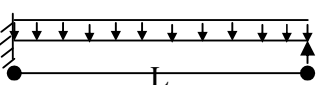
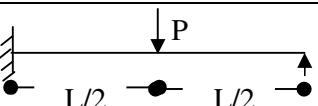
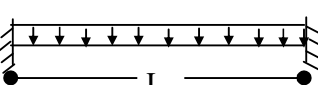
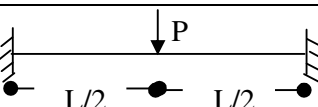
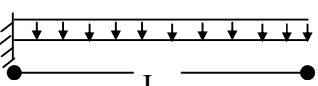

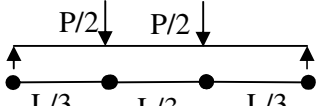
K_E = equivalent stiffness of the structure" **Table 4.2.6.7**

m = unit mass of the structure.

K_{LM} = Load-Mass factor "**Table 4.2.6d**"

Structural elements in general have a uniformly distributed mass; therefore, a load mass factor is applied to the actual mass of the element to reduce it to an equivalent single degree of freedom system.

Table 4.2.6.7 Elastic, Elasto-Plastic and Equivalent Elastic Stiffness for Beams

End conditions and Loading Diagrams	Elastic Stiffness, K_e	Elasto-Plastic Stiffness, K_{ep}	Equivalent Elastic Stiffness, K_E
	$\frac{384EI}{5L^4}$	-----	$\frac{384EI}{5L^4}$
	$\frac{48EI}{L^3}$	-----	$\frac{48EI}{L^3}$
	$\frac{185EI}{L^4}$	$\frac{384EI}{5L^4}$	$\frac{160EI}{L^4}^*$
	$\frac{107EI}{L^3}$	$\frac{48EI}{L^3}$	$\frac{106EI}{L^3}^*$
	$\frac{384EI}{L^4}$	$\frac{384EI}{5L^4}$	$\frac{307EI}{L^4}^*$
	$\frac{192EI}{L^3}$	$\frac{48EI}{L^3}^{**}$	$\frac{192EI}{L^3}^*$
	$\frac{8EI}{L^4}$	-----	$\frac{8EI}{L^4}$
	$\frac{3EI}{L^3}$	-----	$\frac{3EI}{L^3}$
	$\frac{56.4EI}{L^3}$	-----	$\frac{56.4EI}{L^3}$

- * Valid only if $M_N = M_p$
- ** Valid only if $M_N < M_p$

4.2.6.8 Prediction of Blast Pressure

The blast load may be idealized as a triangular pressure-time function with zero rise time as shown in **Figure 4.2.6.8**.

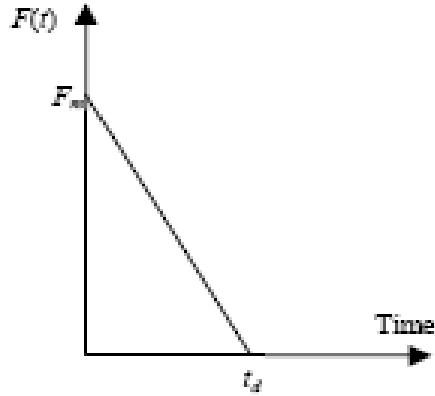


Figure 4.2.6.8 Blast Load

Blast wave parameters for conventional high explosive materials have been used in a number of studies in the past. Estimations of peak overpressure due to spherical blast based on scaled distance, Z are made as follows:

$Z = R/W^{1/3}$ were introduced by Newmark and Hansen as

$$P_{so} = 6784 \frac{W}{R^3} + 93 \left(\frac{W}{R^3} \right)^{1/2} \quad (4.19)$$

Newmark and Hansen (1961) introduced a relationship to calculate the maximum blast overpressure, P_{so} , in bars, for a high explosive, charge detonation at the ground surface.

Another expression of the peak overpressure in KPa is introduced by Mills (1987), in which W is expressed as the equivalent charge weight in kilograms of TNT, and Z is the scaled distance:

$$P_{so} = \frac{1772}{Z^3} - \frac{114}{Z^2} + \frac{108}{Z} \quad (4.20)$$

As the blast wave propagates through the atmosphere, the air behind the shock front is moving outward at lower velocity. The velocity of the air particles, and hence the wind pressure, depends on the peak overpressure of the blast wave. This velocity of the air is associated with dynamic pressure, $q(t)$. The maximum value, q_s , is given by

$$q_s = \frac{5p_{so}^2}{2(p_{so} + 7p_o)} \quad (4.21)$$

if the blast encounters an obstacle perpendicular to the direction of propagation, reflection increases the overpressure to a maximum reflected pressure P_r as:

$$P_r = 2p_{so} \left(\frac{7p_o + 4p_{so}}{7p_o + p_{so}} \right) \quad (4.22)$$

A full discussion and extensive charts for predicting blast pressures and blast durations are given by Mays and Smith (1995) and TM5-1300(1990). Some representative numerical values of peak reflected overpressure are given in the Table below:

$\begin{matrix} \text{W} \\ \text{R} \end{matrix}$	100 kg TNT	500 kg TNT	1000 kg TNT	2000 kg TNT
1 m	165.8	354.5	464.5	602.9
2.5 m	34.2	89.4	130.8	188.4
5 m	6.65	24.8	39.5	60.19
10 m	0.85	4.25	8.15	14.7
15 m	0.27	1.25	2.53	5.01
20 m	0.14	0.54	1.06	2.13

Applied Research Associates, Inc (ARA, Inc) developed a computer program named AT Blast to calculate the blast loads for known values of charge weight and stand off distance. The AT Blast software is widely used and recommended by the professionals to determine the equivalent blast pressure due to an explosion.

AT Blast is a software program that estimates the blast loads that develop during an open-air explosion. Using the program, the user could input the minimum and maximum range, explosive charge weight, angle of incidence, and TNT equivalent factor. From this information, AT Blast calculates the following output: velocity (ft/msec), time of arrival (msec), pressure (psi), impulse (psi-msec), and load duration (msec). Moreover, Pressure Vs Range, and Impulse Vs Range curves are displayed in the output. The outputs were compared to the calculated numbers from the preceding formulas. Therefore, use of AT Blast software to determine the blast load is acceptable.

4.2.6.9 Design for Rebound

Rebound of negative deflection is a negative phase where a partial vacuum is created and air is sucked in. It occurs after the maximum positive deflection has been reached. It is not as critical as the positive phase pressure wise but it is acting upward where the beam hasn't been designed for this loading case; therefore, beams should be designed to resist this type of loading. **(Figure 4.2.6.9)**

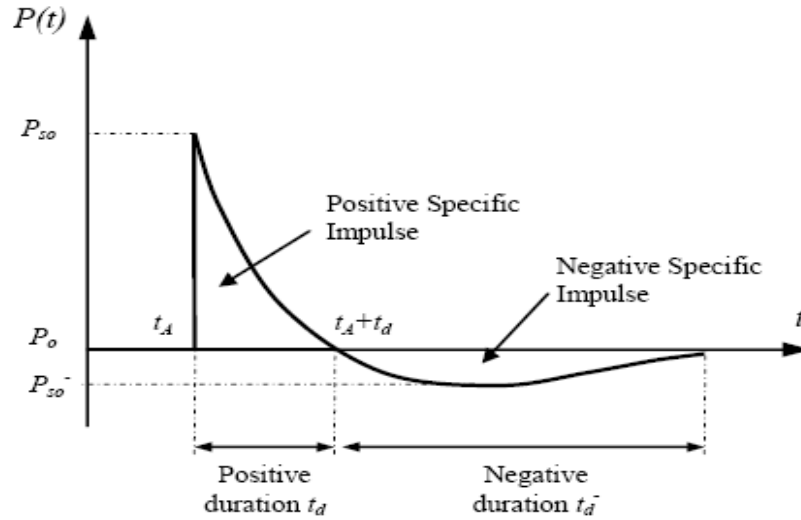


Figure 4.2.6.9 Blast wave pressure-time history

4.3 Structure Response of Reinforced Concrete Beams Strengthened with FRP Composites

4.3.1 Introduction

Fiber reinforced polymer/plastic (FRP) composites comprise fibers of high strength within a polymer matrix. The fibers are generally carbon or glass, in a matrix such as vinyl ester or epoxy. These materials are preformed to form plates under factory conditions.

The FRP composites are lightweight, and have the merits of ease of installation, minimal labor costs and site constraints, high strength-to-weight and stiffness-to-weight ratios, and durability, and therefore, FRP strengthening is highly recommended.

4.3.2 Methods of Strengthening

According to (Teng et al. 2002), flexural strengthening is to be bond an FRP plate to the soffit of the beam. Prior to the former application, the weak surface layer of the soffit should be removed, and the concrete aggregate should be exposed to improve the bond with the FRP, and provide an even surface. It should be noted that number of variations of the basic procedure are available including prestressing of the plate as well as providing anchors such as U strips at the end of the plate to reduce the de-bonding risk. However, RC beams strengthened with unstressed plates without mechanical anchors are more common in practical applications.

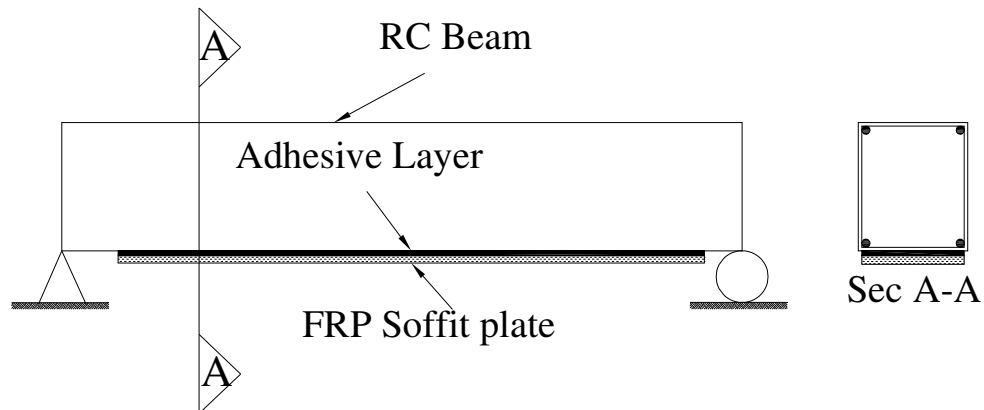


Figure 4.3.2 RC beam bonded with FRP soffit plate

4.3.3 Mechanical Properties of FRP Composites

Depending on the fiber used, FRP composites are classified into three types: glass-fiber-reinforced polymer (GFRP) composites; carbon-fiber-reinforced polymer (CFRP) composites; and aramid-fiber-reinforced polymer (AFRP) composites. ACI 440R-96 (1996) presents a general

background on the composition of these materials. The preceding three types of composites have been used for strengthening reinforced concrete structures. **Table 4.3.3a** (Head, 1996) presents the mechanical properties of FRP with unidirectional fibers.

It should be noted that ranges given in this table are indicative, and a particular product may have properties outside the ranges given herein, especially when the fiber content is different for the ranges considered.

Table 4.3.3a Typical mechanical properties of GFRP, CFRP and AFRP composites (Head 1996)

Unidirectional advanced composite materials	Fiber content (%by weight)	Density (Kg/m ³)	Longitudinal tensile modulus (GPa)	Tensile strength (MPa)
Glass fiber/ Polyester GFRP laminate	50 – 80	1600 – 2000	20 – 55	400 – 1800
Carbon/epoxy CFRP laminate	65 – 75	1600 – 1900	120 – 250	1200 – 2250
Aramid/epoxy AFRP laminate	60 – 70	1050 – 1250	40 – 125	1000 – 1800

Table4.3.3b Measured parameters of the different composite material (Tepfers el al. 1994)

Material	μ Fibers Volume%	f_u MPa	ϵ_u MPa	E_{measured} GPa	$\frac{f_u}{f_{u \text{ carbon}}}$	$\frac{\epsilon_u}{\epsilon_{u \text{ carbon}}}$
Carbon	40	1320	1.15	118	1.00	1.00
Aramid	42	1120	3.20	55	0.85	2.78
Polypropylene	60	220	3.50	9	0.17	3.07

4.3.4 Partial Safety Factor

According to Kong (Kong et al. 1987), partial safety factor, γ is intended to cover those variations in loading, in design or in construction that are likely to occur.

Table 4.3.4 Partial Safety Factors for Concrete, Steel, and FRP

Strength	Partial Safety Factor
Concrete in flexure or in axial compression, γ_c	1.50
Steel reinforcement, γ_s	1.05
FRP tensile strength, γ_{frp}	1.25
FRP-to- concrete bond strength, γ_b	1.25

4.3.5 Failure Modes

A number of failure modes for RC beams bonded with FRP soffit plates have been observed in numerous experimental studies to date (Ritchie et al. 1991, Saadatmanesh and Ehsani 1991, Triantafillou and Plevris 1992, Chajes et al. 1994, Shrif et al. 1994, Arduini and Nanni 1997, Garden et al. 1997, Ross et al. 1999, Rahimi and Hutchinson 2001).

Typical failure modes were as shown in **Figure 4.3.5**. according to Teng (Teng et al.2002); the failure modes are classified into seven main categories.

- Flexural Failure: the ultimate flexural capacity of the beam is reached when either the FRP plate fails by tensile rupture (**Figure 4.3.5 a**) or the concrete is crushed (**Figure 4.3.5 b**)
- Shear Failure: Normal reinforced concrete beams are designed to fail in flexure rather than in shear, which is a brittle mode while the strengthened beam can fail abruptly in shear (Buyukozturk and Hearing 1998, Lopez et al. 1999) (**Figure 4.3.5 c**)
- Plate – end Debonding Failures: separation of the concrete cover has been the most commonly mode of debonding in experimental studies (**Figure 4.3.5 d**).
- Intermediate Crack – induced Interfacial Debonding: Debonding may initiate at a flexural or a mixed flexural shear crack away from the plate ends and then propagates towards one of the plate ends as in (**Figure 4.3.5 f** and **Figure 4.3.5g**).

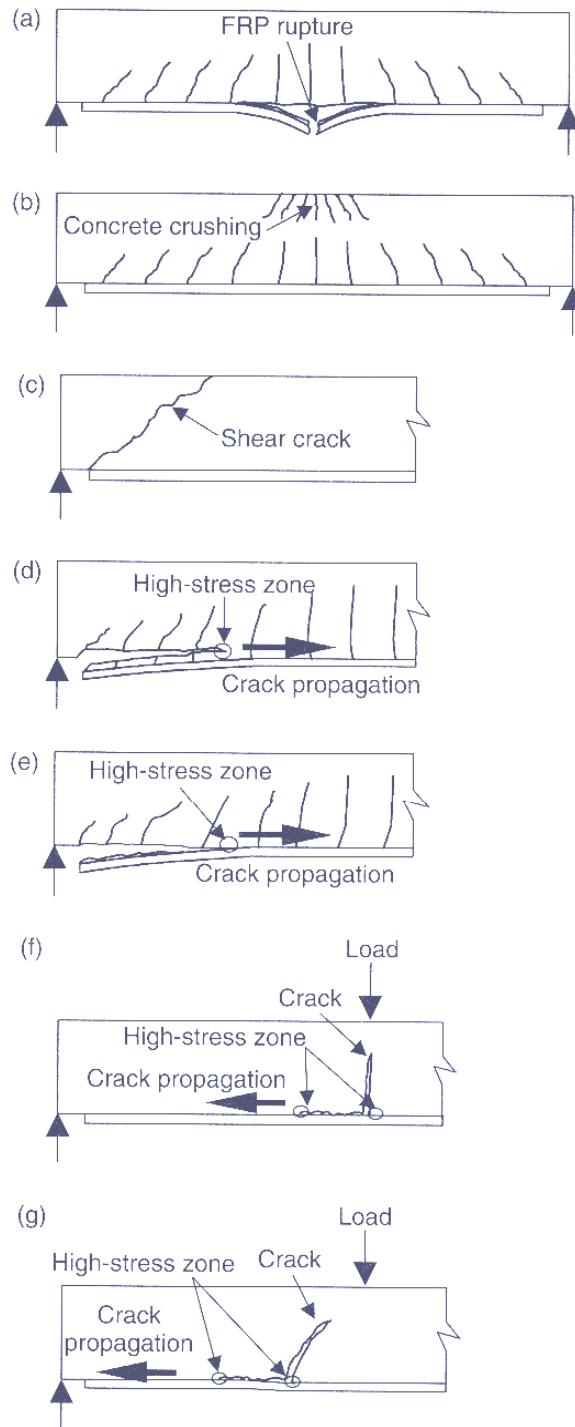


Figure 4.3.5 Failure modes of FRP-plated RC beams: (a) FRP rupture; (b) crushing of compressive concrete; (c) shear failure; (d) concrete cover separation; (e) plate-end interfacial debonding; (f) intermediate flexural crack-induced interfacial debonding; (g) intermediate flexural shear crack-induced interfacial debonding

4.3.6 Flexural Strength

4.3.6.1 Overview

Existing research suggests that the ultimate flexural strength of FRP – strengthened RC beams can be predicted using existing RC beam design approaches with appropriate modifications to account for the brittle nature of FRP's. (Chajes el al. 1994). The following presentation is based on the work of (Teng el al. 2000)

4.3.6.2 Design Equation

The following design procedure is presented by Teng (Teng el al. 2002)

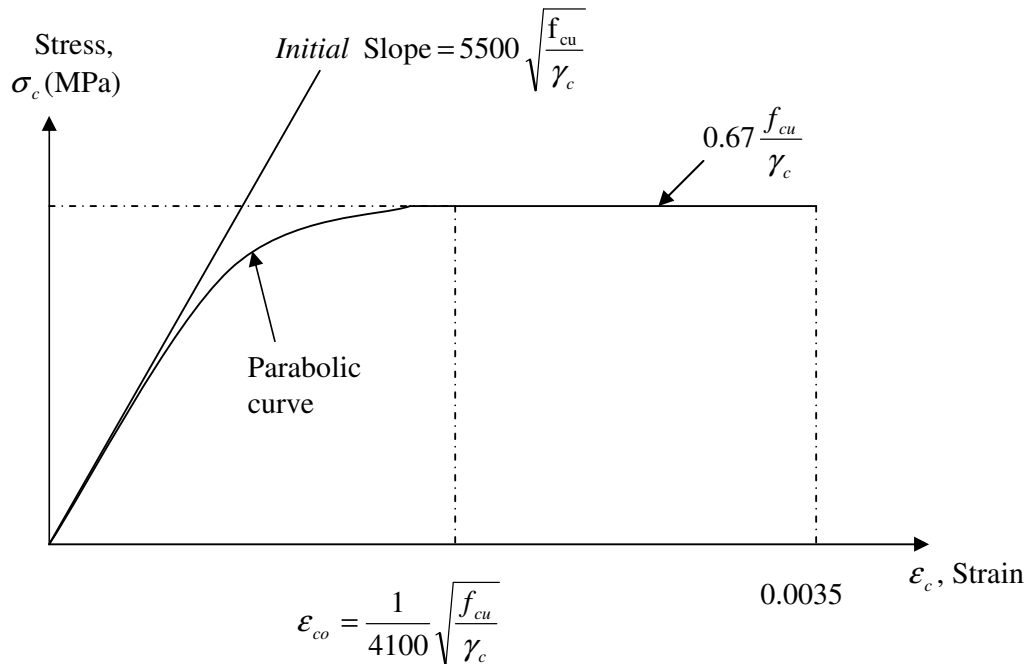


Figure 4.3.6.2a Stress-strain curve for concrete (Kong and Evans, Teng el al.)

Following BS 8110 (1997), the ultimate strain at the extreme concrete compression fiber is taken to be 0.0035. The stress-strain curve of concrete as in Kong and Evans (Kong et al. 1987) is given in **Figure 4.3.6.2a**. The ultimate strain of concrete may not have been reached when the FRP ruptures because the behavior of the FRP composites is brittle. Therefore, the simplified rectangular stress block of the code (BS 8110 1997) for the compression concrete is no longer valid. The strains and stress over the depth of a plated beam are shown in **Figure 4.3.6.2b**. (Teng et al. 2002).

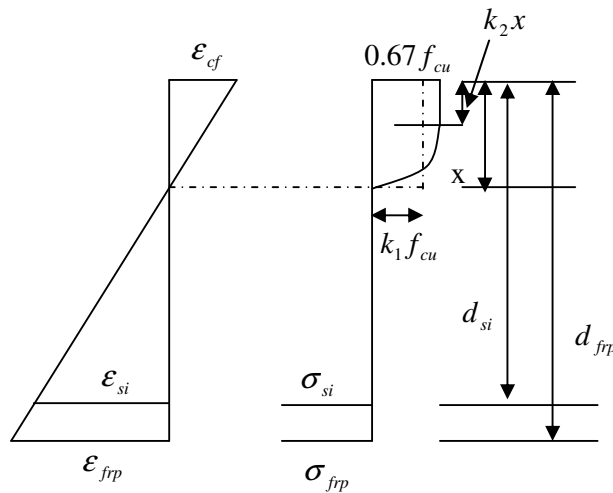


Figure 4.3.6.2b Strain and stress over beam depth

Compressive strains are taken to be positive here, so the strains in the compression concrete are positive, while the strains in the FRP are negative. Strains in the FRP, ϵ_{frp} , and in the steel bars, ϵ_{si} are related to the extreme compression fiber strain of concrete, ϵ_{cf} as follows:

$$\varepsilon_{frp} = \varepsilon_{cf} \frac{x - d_{frp}}{x} \quad (4.23)$$

$$\varepsilon_{si} = \varepsilon_{cf} \frac{x - d_{si}}{x} \quad (4.24)$$

Where: x, d_{si}, d_{frp} are distances from the extreme concrete compression fiber to the natural axis, to the centroid of steel bars, and to the centroid of the FRP respectively. Likewise, when the strain in the FRP, ε_{frp} is known, the value of ε_{cf} can be found as

$$\varepsilon_{cf} = \varepsilon_{frp} \frac{x}{x - d_{frp}} \quad (4.25)$$

According to the stress-strain curve of **Figure 4.3.6.2a**, compressive stresses in the concrete are given by (Kong and Evans 1987)

$$\sigma_c = 5500 \left(\sqrt{\frac{f_{cu}}{\gamma_c}} \varepsilon_c - \frac{4100}{2} \varepsilon_c^2 \right) \quad \text{if } 0 \leq \varepsilon_c \leq \varepsilon_{co} \quad (4.26)$$

and

$$\sigma_c = 0.67 \frac{f_{cu}}{\gamma_c} \quad \text{if } \varepsilon_{co} \leq \varepsilon_c \leq 0.0035 \quad (4.27)$$

Where

σ_c is the compressive concrete stress

ε_{co} is the compressive concrete strain

$$\varepsilon_{co} = \frac{1}{4100} \sqrt{\frac{f_{cu}}{\gamma_c}} \quad (4.28)$$

f_{cu} is the cube compressive strength of concrete = $1.25 f'_c$

Where

f'_c is the concrete cylinder strength

γ_c is the partial safety factor for concrete.

C is the total concrete compressive force for any given ϵ_{cf}

$$C = k_1 \frac{f_{cu}}{\gamma_c} b_c x \quad (4.29)$$

Where

b_c is the beam width and k_1 is the mean stress factor defined by

$$k_1 = \frac{\int_0^{\epsilon_{cf}} \sigma_c d\epsilon_c}{(f_{cu} / \gamma_c) \epsilon_{cf}} \quad (4.30)$$

Substituting 4.26 and 4.27 into Equation 4.30 gives

$$k_1 = 0.67 \left(\frac{\epsilon_{cf}}{\epsilon_{co}} - \frac{\epsilon_{cf}^2}{3\epsilon_{co}^2} \right) \quad \text{if} \quad 0 \leq \epsilon_{cf} \leq \epsilon_{co} \quad (4.31)$$

and

$$k_1 = 0.67 \left(1 - \frac{\epsilon_{co}}{3\epsilon_{cf}} \right) \quad \text{if} \quad \epsilon_{co} \leq \epsilon_{cf} \leq 0.0035 \quad (4.32)$$

By solving Equation 4.33, the depth of the neutral axis x will be determined

$$k_1 \frac{f_{cu}}{\gamma_c} b_c x + \sum_{i=1}^n \sigma_{si} A_{si} + \sigma_{frp} A_{frp} = 0 \quad (4.33)$$

Where σ_{si} and σ_{frp} are the stresses in the steel bars and the FRP

respectively, A_{si} is the total area of steel in layer i , n is the total number of

steel layers, and A_{frp} is the area of the FRP. σ_{si} and σ_{frp} are given by

$$\sigma_{si} = E_s \epsilon_{si} \quad \text{if } |\epsilon_{si}| < \frac{f_y}{\gamma_s E_s} \quad (4.34)$$

$$\sigma_{si} = \frac{\epsilon_{si}}{|\epsilon_{si}|} \frac{f_y}{\gamma_s} \quad \text{if } |\epsilon_{si}| \geq \frac{f_y}{\gamma_s E_s} \quad (4.35)$$

And

$$\sigma_{frp} = E_{frp} \epsilon_{frp} \geq \frac{-f_{frp}}{\gamma_{frp}} \quad (4.36)$$

Where

E_s is the modulus of elasticity of the steel bars

E_{frp} is the modulus of elasticity of the FRP

f_y is the yield strength of the steel

f_{frp} is the tensile strength of the FRP

γ_s is the partial safety factor for steel

γ_{frp} is the partial safety factor for FRP

Since f_y and f_{frp} are material properties, they are always positive.

$$D = k_2 x \quad (4.37)$$

Where

D is the distance from the extreme concrete compression fiber to the line of action of concrete compression force, and it determines the location of the concrete compression force C .

K_2 is the centroid factor of the compression force and it is given by

$$k_2 = 1 - \frac{\int_0^{\epsilon_{cf}} \epsilon_c \sigma_c d\epsilon_c}{\epsilon_{cf} \int_0^{\epsilon_{cf}} \sigma_c d\epsilon_c} \quad (4.38)$$

Evaluating the right hand side of Equation 4.38 yields

$$k_2 = \frac{\frac{1}{3} - \frac{\epsilon_{cf}}{12\epsilon_{co}}}{1 - \frac{\epsilon_{cf}}{3\epsilon_{co}}} \quad \text{if } 0 \leq \epsilon_{cf} \leq \epsilon_{co} \quad (4.39)$$

and

$$k_2 = \frac{\frac{\epsilon_{cf}}{2} + \frac{\epsilon_{co}^2}{12\epsilon_{cf}} - \frac{\epsilon_{co}}{3}}{\epsilon_{cf} - \frac{\epsilon_{co}}{3}} \quad \text{if } \epsilon_{co} \leq \epsilon_{cf} \leq 0.0035 \quad (4.40)$$

The moment capacity of the beam M_n is given by

$$M_n = k_1 \frac{f_{cu}}{\gamma_c} b_c x \left(\frac{h}{2} - k_2 x \right) + \sum_{i=1}^n \sigma_{si} A_{si} \left(\frac{h}{2} - d_{si} \right) + \sigma_{frp} A_{frp} \left(\frac{h}{2} - d_{frp} \right) \quad (4.41)$$

Where

h is the depth of the reinforced concrete beam

According to BS8 8110 (1997) and (An el al. 1991), the beam is deemed to have reached failure when either the concrete compression strain attains the maximum strain 0.0035 and/or the FRP reaches its rupture

$$\text{strain } \epsilon_{frp, rup} = f_{frp} / (\gamma_{frp} E_{frp}) \quad (4.42)$$

Chapter 5: Illustrative Examples: Reinforced Concrete Solid Slab and T- Beam Deck Bridges

5.1 Introduction

This chapter presents two illustrative examples: i) reinforced concrete solid slab bridge and ii) reinforced concrete T-Beam bridge. An excel spread sheet is generated to calculate ultimate resistance, equivalent elastic stiffness, equivalent elastic deflection, natural period of the beam, the maximum deflection, and the maximum rotation in the support for a simple span solid slab and T-Beam bridges.

5.2 Reinforced Concrete Solid Slab Bridge

5.2.1 Definition of Problem

The design of a solid slab bridge subjected to blast load is investigated in this section. The superstructure for the solid slab bridge has a 22 in. slab. **Figure 5.2.1a** shows cross section of the solid slab bridge. Clear roadway width of the bridge is shown to be 44 ft. curb to curb consisting of 3 lanes and 12 ft. shoulders, 6ft. in each side. A standard barrier – 32 in. high, 1'-3" wide – was used to have an overall 46.5 ft. width with a barrier on each side.

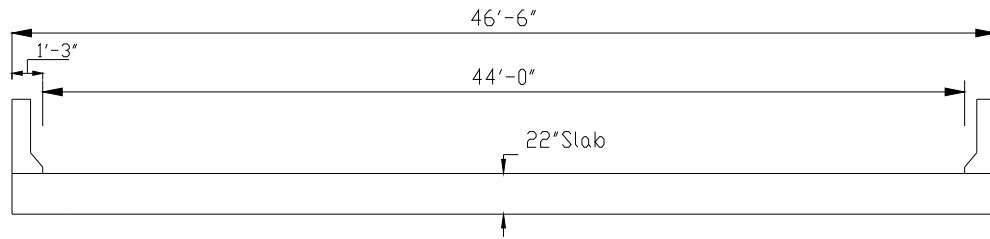


Figure 5.2.1a Solid Slab Bridge Cross Section (Barker 2007).

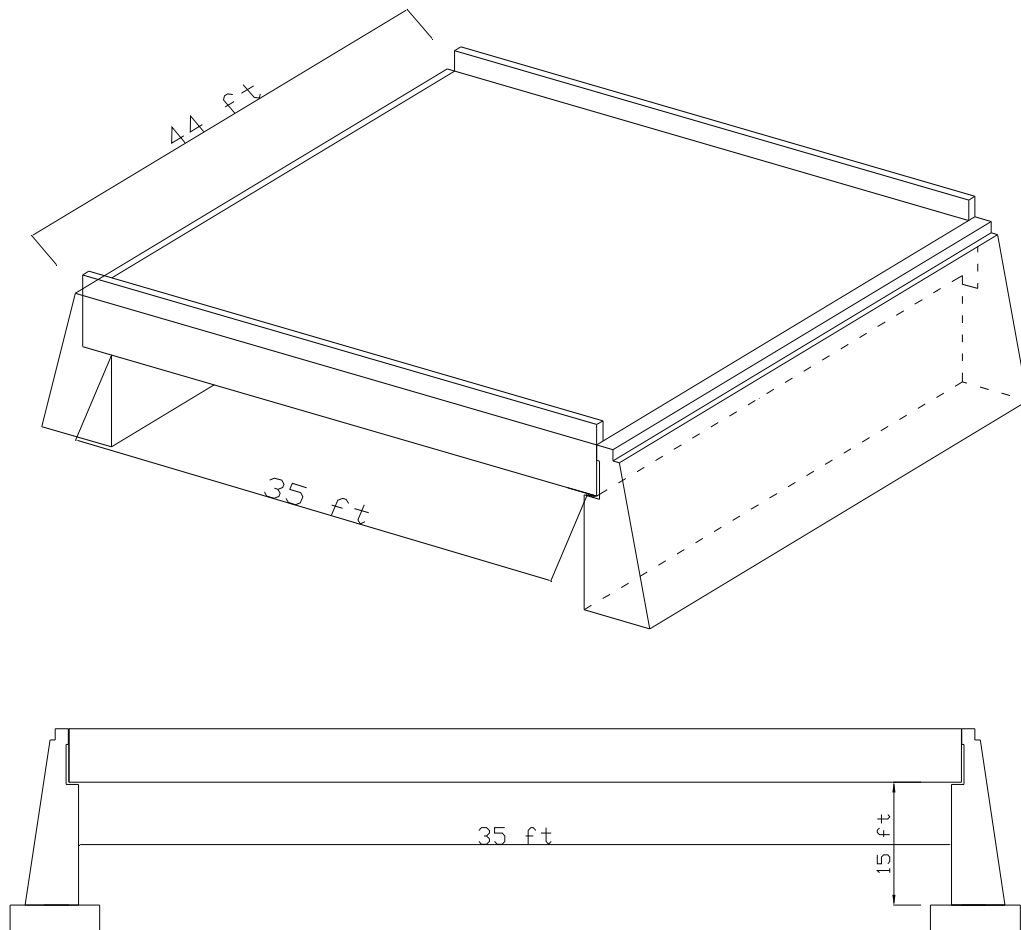


Figure 5.2.1b The Perspective & Elevation View of The Model Bridge.

The perspective and elevation views of the model bridge are shown in **Figure 5.2.1b**. Two abutments at the beginning and the end of the bridge support the bridge span. Selecting the optimal abutment type depends on the site conditions, cost considerations, superstructure geometry, and aesthetics. For this study, a full depth reinforced concrete cantilever abutment is chosen in this example.

5.2.2 Design Aspect

A. Check Minimum Recommended Depth

$$h_{\min} = \frac{1.2(L+10)}{30} \times 12 = 21.6 \text{ in.} \Rightarrow \text{Use } h = 22 \text{ in.}$$

B. Select Applicable Load combinations

Strength I limit State

$$U = 1.0[1.25DC + 1.50DW + 1.75(LL + IM) + 1.0FR + \gamma_{TG}TG]$$

Service I limit State

$$U = 1.0(DC + DW) + 1.0(LL + IM) + 0.3(WL) + 1.0(FR)$$

Fatigue Limit State

$$U = 0.75(LL + IM)$$

Where

DC: dead load of structural components and nonstructural attachments

DW: dead load of wearing surfaces and utilities

LL: vehicle live load

IM: vehicle dynamic load allowance

FR: friction

TG: temperature gradient

WS: wind load on structure

WL: wind on live load

γ_{TG} : load factor

C. Calculate Live Load Force Effects

Slab-type bridges shall be designed for all of the vehicular live loads specified in AASHTO, including the lane load

1. Maximum shear force – axle loads

$$\text{Truck: } V_A^{Tr} = 32(1.0 + 0.6) + 8(0.2) = 52.8 \text{ Kips}$$

$$\text{Lane: } V_A^{Ln} = 0.64(35.0) / 2 = 11.2 \text{ Kips}$$

$$\text{Tandem: } V_A^{Ta} = 25\left(1 + \frac{35 - 4}{35}\right) = 47.1 \text{ Kips}$$

Impact factor = $1 + IM/100$, where $IM = 33\%$

Impact factor = 1.33, not applied to design lane load

$$V_{LL+IM} = 52.8(1.33) + 11.2 = 81.4 \text{ Kips}$$

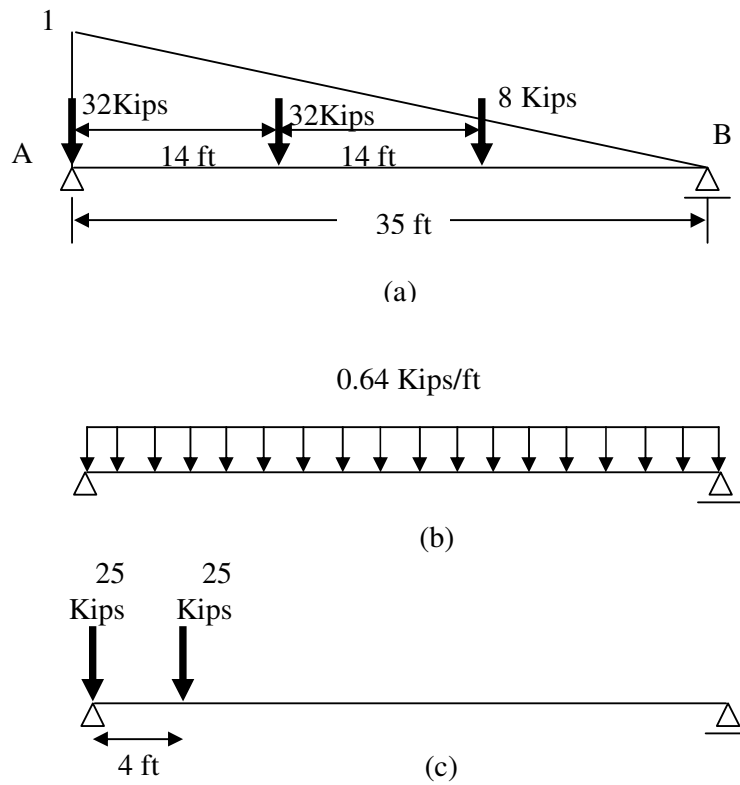
2. Maximum bending moment at mid-span – axle loads

$$\text{Truck: } M_c^{Tr} = 32(8.75 + 1.75) + 8(1.75) = 350 \text{ Kip - ft}$$

$$\text{Lane: } M_c^{Ln} = 0.64(8.75)(35) / 2 = 98.0 \text{ Kip - ft}$$

$$\text{Tandem: } M_c^{Ta} = 25(8.75)(1 + 13.5/17.5) = 387.5 \text{ Kip - ft} \quad \text{governs}$$

$$M_{LL+IM} = 387.5(1.33) + 98.0 = 613.4 \text{ Kip - ft}$$



**Figure 5.2.2a Live-load placement for maximum shear force:
(a) truck, (b) lane, and (c) tandem (Barker 2007)**

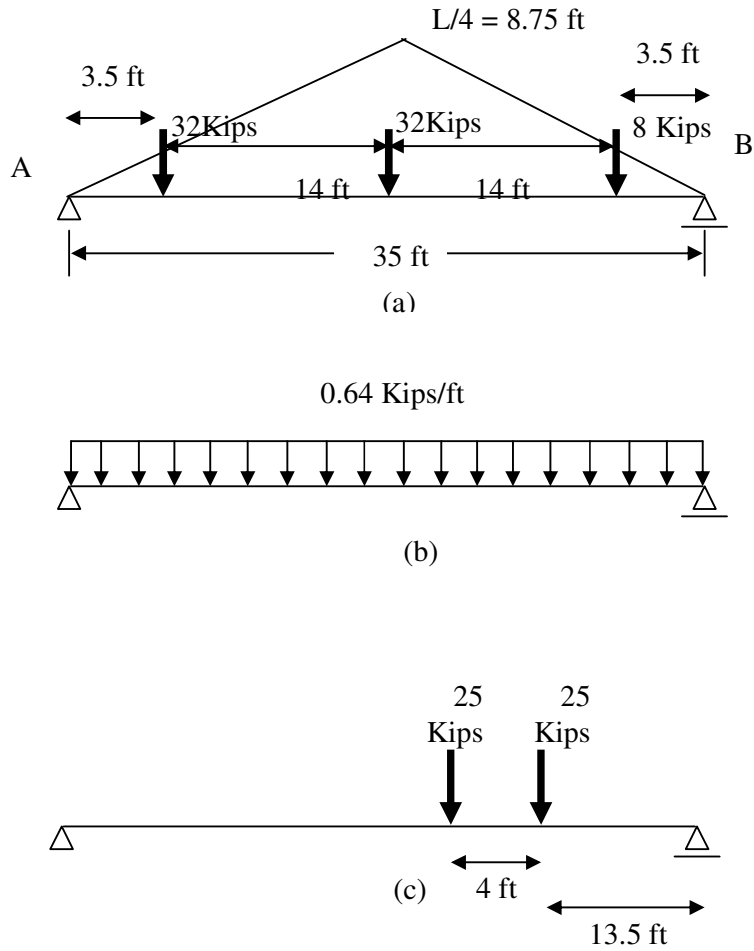


Figure 5.2.2b Live-load placement for maximum bending:(a) truck, (b) lane, and (c) tandem (Barker 2007)

D. Calculate Force Effects from Other Loads

1. interior strip, 1.0 ft wide

$$\rho_{conc} = 0.15 \text{ kcf}$$

$$w_{DC} = 0.150(22.0/12) = 0.275 \text{ ksf}$$

$$V_{DC} = 0.5(0.275)(35) = 4.81 \text{ kips/ft}$$

$$M_{DC} = w_{DC} L^2 / 8 = 0.275(35)^2 / 8 = 42.1 \text{ kip - ft/ft}$$

DW Bituminous wearing surface, 3.0 in. thick

$$\rho_{DW} = 0.14 \text{ kcf}$$

$$w_{DW} = 0.14(3.0/12) = 0.035 \text{ ksf}$$

$$V_{DW} = 0.5(0.035)(35) = 0.613 \text{ kips/ft}$$

$$M_{DW} = 0.035(35)^2 / 8 = 5.36 \text{ kip - ft/ft}$$

2. Edge strip, 1.0 ft wide, barrier = 0.32 kips/ft Assume barrier load spread over width of live-load edge strip of 62.5 in. = 5.21 ft:

$$w_{DC} = 0.275 + 0.320 / 5.21 = 0.336 \text{ ksf}$$

DC $V_{DC} = 0.5(0.336)(35) = 5.89 \text{ kips/ft}$

$$M_{DC} = 0.336(35)^2 / 8 = 51.45 \text{ kip - ft/ft}$$

$$w_{DW} = 0.035(62.5 - 15.0) / 62.5 = 0.025 \text{ ksf}$$

DW $V_{DW} = 0.5(0.025)(35) = 0.438 \text{ kips/ft}$

$$M_{DW} = 0.025(35)^2 / 8 = 3.83 \text{ kip - ft/ft}$$

E. Investigate Limit States

Service limit state governs. (According to Barker 2007) Use No. 9 at 6 in.

5.2.3 Example Problem

Analyze a simply supported solid slab bridge of **Figure 5.2.1a** with a span length of 35ft center to center of bearings for a 20 lb TNT blast load.

Given:

1. Structural configuration is shown in **Figures 5.2.1a and 5.2.1b**
2. Maximum support rotation of one degree.
3. Yield stress of reinforcing steel, $f_y = 60000 \text{ psi}$ and concrete compressive strength, $f'_c = 4000 \text{ psi}$
4. Weight of concrete, $w = 150 \text{ lbs/ft}^3$

Solution:

1. Find the DIF from **Table 3.5**, for close-in-range case

f'_c "psi"	f_y "psi"	Concrete, DIF		Steel, DIF
		Bending	Direct Shear	Bending
4000	60000	1.25	1.1	1.23

The dynamic strength of concrete as well as that of steel are given by

$$f'_{dc} = DIF \cdot f'_c \text{ and } f_{dy} = DIF \cdot f_y$$

Concrete		Steel
Bending, f'_{dc}	Direct Shear, f'_{dc}	f_{dy}
5000	4400	73800

2. For A_s of 2 No. 9 bars

Tension Reinforcement		
Bars size	No. of bars	A_s "in ² "
9	2	1.988

3. Calculate "effective depth, d , " for negative, d_N , "support" and positive, d_P , " mid-span"

Section Dimensions		Bottom	Top	d_P	d_N
b "in"	h "in"	cover "in"	cover "in"		
12	22	1	2.5	20.4375	18.9375

Where d_P , d_N are positive and negative effective depths respectively.

4. From Equation $\rho = \frac{A_s}{bd}$

$$\rho_p = \frac{1.988}{12 * 20.44} \quad \text{and} \quad \rho_N = \frac{1.988}{12 * 18.94}$$

ρ_{\max} and ρ_{\min} are calculated using Equations **4.9**, **4.10** and **Table**

4.2.3.1

$$\rho_{\max} = 0.724\rho_b \quad \text{where} \quad \rho_b = 0.0285 \quad \rho_{\min} = 3 * \frac{\sqrt{f'_c}}{f_y} \geq \frac{200}{f_y}$$

ρ_p	ρ_N	ρ_{\max}	ρ_{\min}
0.00811	0.00875	0.02064	0.00333

5. Moment Capacity of the beam is calculated from Equations **4.1** and

4.2

a_p "in."	a_N "in."	M_{up} "in-lb"	M_{uN} "in-lb"
2.87681	2.87681	2787495.68	2567419.75

Where M_{up} , M_{uN} are the ultimate moment capacity at the mid-span and at the support respectively.

From **Table 4.2.6a** the ultimate resistance of uniformly loaded beam with both ends fixed is given by

$$r_u = \frac{8(M_{uN} + M_{up})}{L^2}$$

Ultimate Resistance, r_u "lb/in"
For both ends fixed with uniform load, (r_u) "lb/in"
242.8533079

6. The average moment of inertia is calculated using Equation **3.3** and

Figure 3.2.2a

Concrete modulus of elasticity E_c "psi"	Steel modulus of Elasticity E_s "psi"	Modular Ratio n
3.83E+06	29000000	
From Figure 3.4-2b		7.56
F_N	F_p	
0.041	0.038	

The cracked moment of inertia is calculated as follows:

$I_c = F \cdot b \cdot d^3$	I_{cN} "in ⁴ "	I_{cp} "in ⁴ "	$I_{c\text{ ave}}$ "in ⁴ "	I_g "in ⁴ "	I_a "in ⁴ "
	3341.435	3892.675	4617.055	10648	7132.528

7. The equivalent elastic system K_E of a uniformly loaded beam with fixed ends, from **Table 4.2.6.7** is given by

$$K_E = \frac{307 E_c I_a}{L^4}$$

Equivalent Elastic Stiffness, K_E
For both ends fixed with uniform load, (K_E)
269.8146 lb/in/in

8. The equivalent elastic deflection is

$$x_E = \frac{r_u}{K_E}$$

Equivalent Elastic Deflection x_E "in"
For both ends fixed with uniform load, (x_E)
0.900074643

9. Load-mass factor from **Table 4.2.6d**

For a beam with uniformly distributed load, the load mass factor for the plastic range is:

Load Mass Factor K_{LM}	
For both ends fixed with uniform load (K_{LM})	
Elastic	0.77
Elasto-Plastic	0.78
Plastic	0.66

K_{LM} for the plastic range case is given as

$$K_{LM} = \frac{K_{LM}(elastic) + K_{LM}(Elasto - plastic)}{4} + \frac{K_{LM}(plastic)}{2}$$

K_{LM} For Plastic Mode
0.7175

10. Natural period T_N can be calculated from the following formula

$$T_N = 2\pi \sqrt{\frac{K_{LM} m}{k_E}} \quad (4.18)$$

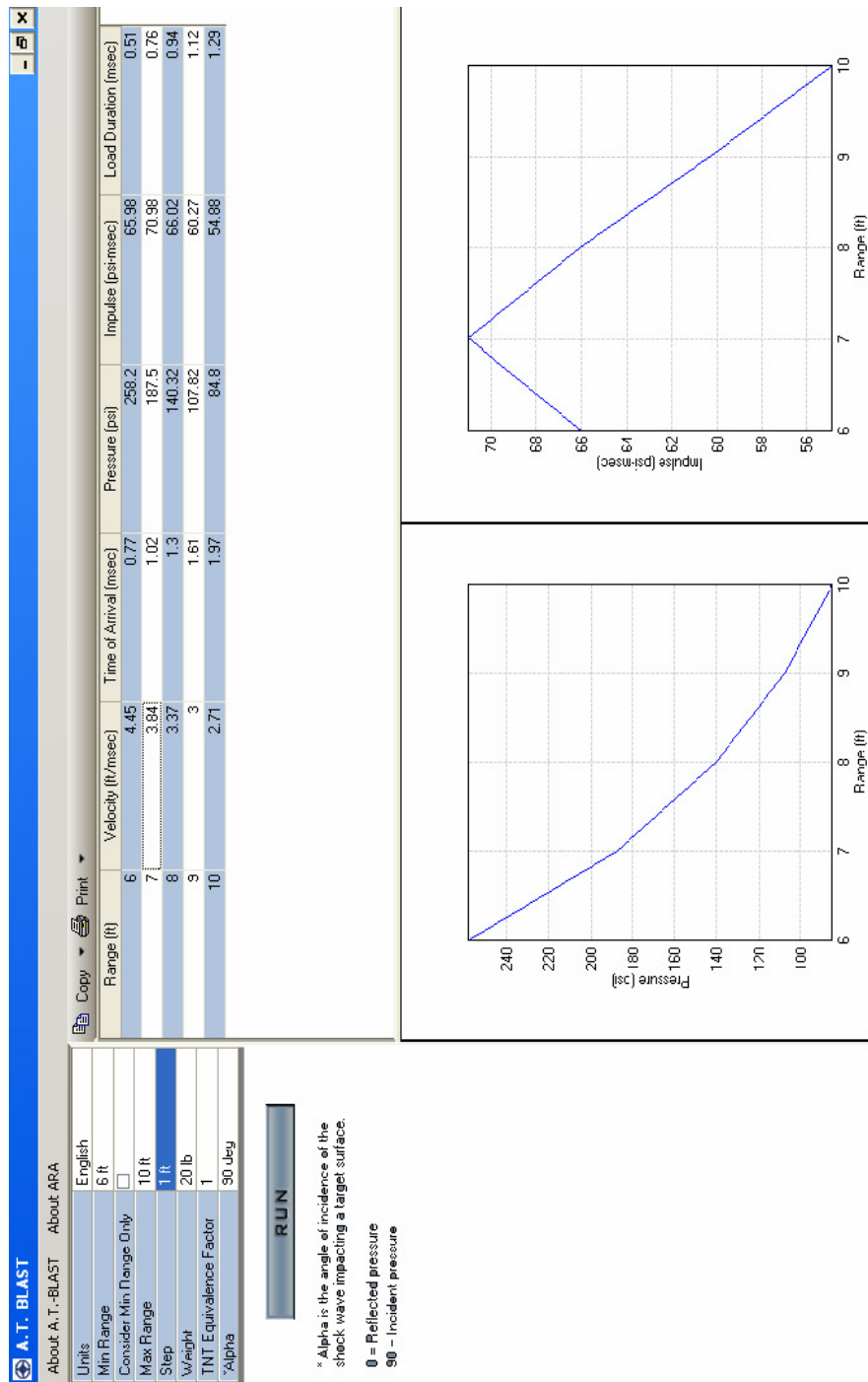
where

m = the mass of the beam $m = \frac{w}{g}$

$$m = [(22) \times 12] \times \frac{150}{12^3} \times \frac{1000^2}{32.2 \times 12} = 59308.144 \frac{\text{lb} \cdot \text{ms}^2}{\text{in}^2}$$

$$T_N = 2\pi \sqrt{\frac{0.7175 \times 59308.144}{269.8146}} = 78.91 \text{ ms}$$

11. Using AT Blast program, the loading pressure and the duration are as follows:



It is assumed that a 20 lb TNT weight explodes at 6 ft height above the bridge deck. Therefore, for 6 ft stand-off distance, $P = w = 258$ psi; "incident pressure".

12. The ductility ratio is determined from **Figure 4.2.6.4b**.

w, q_b, y_b, y_e, t in **Figure 4.2.6.4b**, correspond to P, r_u, x_E, x_m, T in the calculation.

$$\frac{T}{T_N} = \frac{0.51}{78.91} \approx 0.01 = \frac{t}{T_N}$$

$$\frac{r_u}{P \text{ times tributary width}} = \frac{242.853}{258 \times 12} = 0.07844 \Rightarrow \frac{p \text{ times tributary width}}{r_u} = 12.75 = \frac{w}{q_b}$$

$$\Rightarrow \text{From the Figure } \frac{y_e}{y_b} = 0.41 = \frac{x_m}{x_E}$$

13. From **Table 4.2.6b**

$$x_m = \frac{L * \tan \theta}{2}$$

$$x_m = \frac{x_m}{x_E} x_E = 0.369 \Rightarrow \tan \theta = \frac{2x_m}{L} \Rightarrow \theta = 0.1 < \theta_{\max} = 1 \quad \text{ok}$$

14. Shear calculation

Direct shear check, from **Table 4.2.6c**

$$V_s = \frac{r_u L}{2} = \frac{242.853 * 420}{2} = 50999.195 \text{ lb}$$

Section capacity in direct shear, as per the NAVAC code

$$V_d = 0.18 f'_{dc} b d$$

According to Edward G. Nawy (2005), "shear strength is more difficult to determine experimentally because of difficulty in isolating shear from other stresses. This is one reason for the large variation in shear-strength

values, varying from 20% of the compressive strength in normal loading to a considerably higher percentage of up to 85% of the compressive strength in cases where direct shear exists in combination with compression."

$$V_d = 0.18 \times 4400 \times 12 \times 18.9375 = 179982 \text{ lbs} > V_s = 50999.195 \text{ lbs} \quad \text{OK.}$$

5.3 Reinforced Concrete T-Beam Bridge

5.3.1 Definition of Problem

A T-Beam bridge subjected to blast load is illustrated in this section. The superstructure for the T-Beam Bridge consists of six girders spaced at 8 ft. centers. As an integral part of the 8-in. deck slab, a 0.5 in. wearing surface is considered. **Figures 5.3.1a and 5.3.1b** show respectively cross section for T-Beam Bridge and a typical cross section for T-Beam. Clear roadway width of the bridge was selected to be 44 ft. curb to curb consisting of 3 lanes and 12 ft. shoulders, 6ft. in each side. A standard barrier – 32 in. high, 1'-3" wide – was used to have an overall 46.5 ft. width with a barrier on each side.

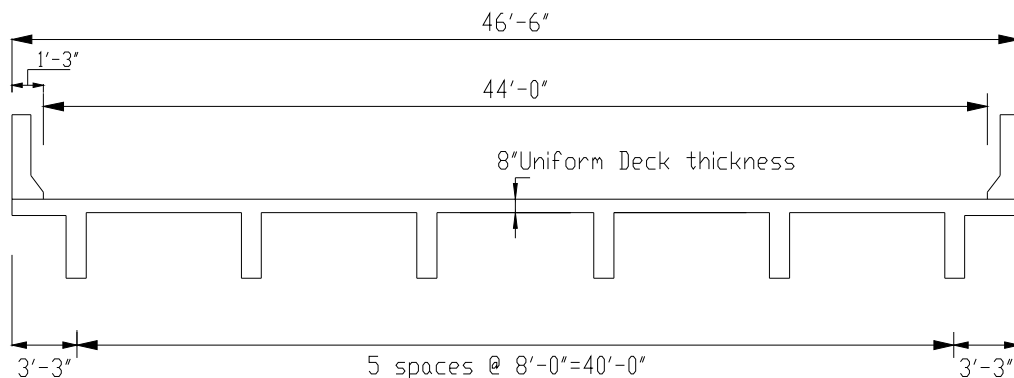


Figure 5.3.1a T-Beam Bridge Cross Section (Barker 2007).

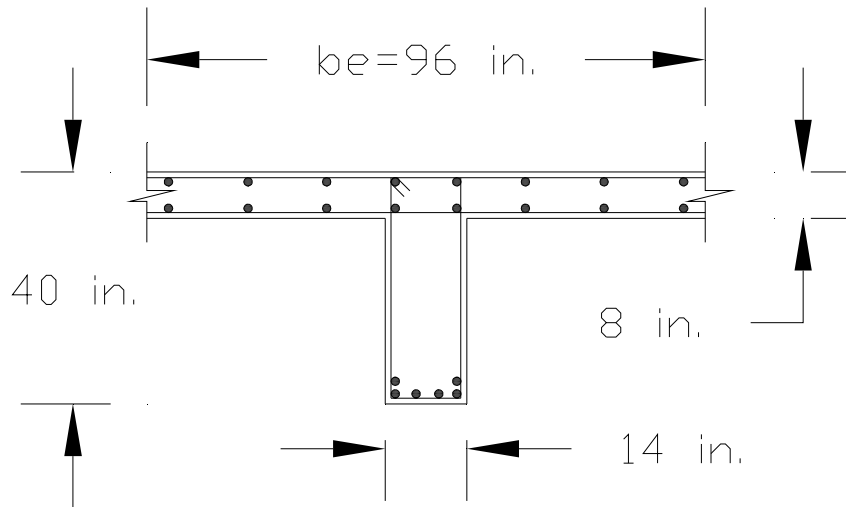


Figure 5.3.1b T- Beam Cross Section

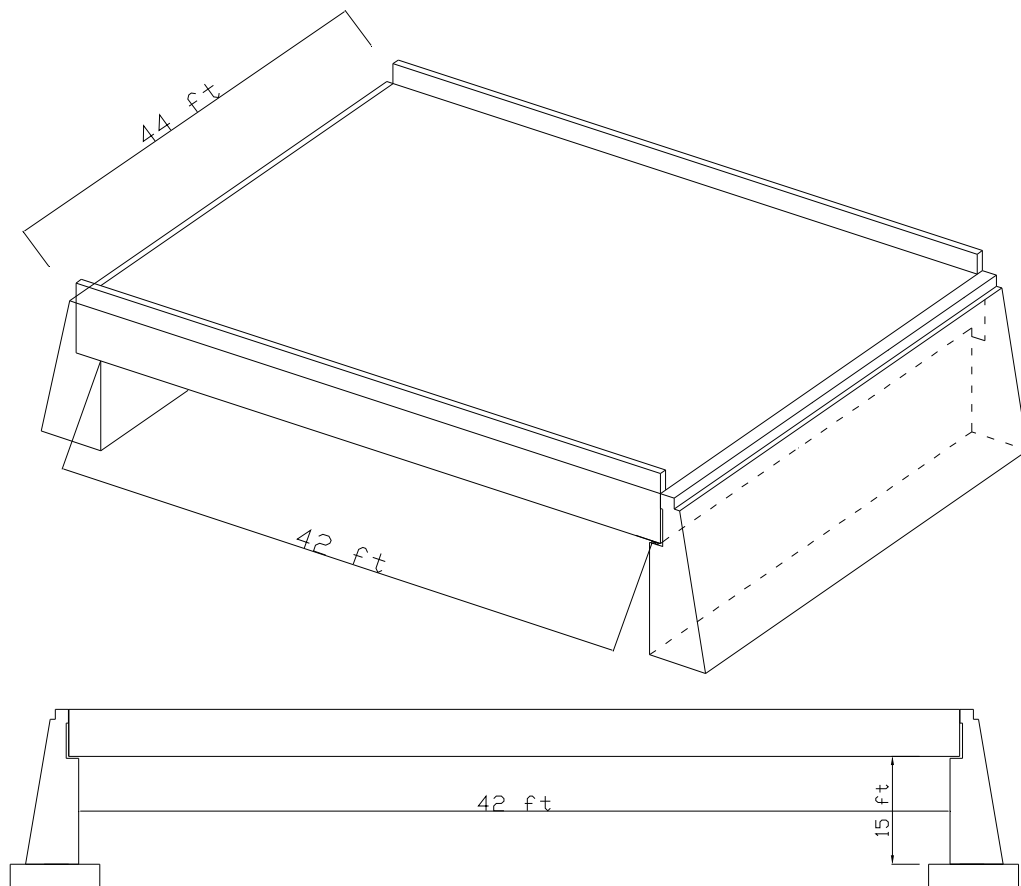


Figure 5.3.1c The Perspective & Elevation View of The Model Bridge.

The perspective and elevation view of the model bridge are shown in **Figure 5.3.1c**. Two bents at the beginning and the end of the bridge support the bridge span. Selecting the optimal abutment type depends on the site conditions, cost considerations, superstructure geometry, and aesthetics. For this study, a full depth reinforced concrete cantilever abutment is chosen.

The following data are used: *slab thickness* = 8 in., $b_w = 14$ in. and *overall depth* = 40 in. The area of reinforcement A_s , that was needed for the T-Beam section was 6 in² (6 No. 9).

5.3.2 Design Aspect

A. Develop Typical Section and Design Basis

Top flange thickness: from deck design, structural thickness = 7.5 in.

Web thickness:

Assume 3 No.11 are needed

$$b_{\min} = 2(2) + 3d_b + 2(2.5d_b) = 12.5 \text{ in.}$$

Where 2 in. external cover is needed and d_b is the bar diameter

To give a little extra room for bars, use $b_w = 14 \text{ in.}$

Structure depth: minimum depth = 0.067 L

$$h_{\min} = 0.67(42 * 12) = 34 \text{ in. Use } h = 40 \text{ in.}$$

B. Design Conventionally Reinforced Concrete Slab

C. Select Applicable Load Combinations

Strength I Limit State

$$U = 1.25DC + 1.50sDW + 1.75(LL + IM) + 1.0(WA + FR)$$

Service I Limit State

$$U = 1.0(DC + DW) + 1.0(LL + IM) + 1.0WA + 0.3(Ws + FR)$$

Fatigue Limit State

$$U = 0.75(LL + IM)$$

D. Calculate Live Load Force Effects and Force Effects from Other Loads

Live load force effects and force effect from other loads are determined following the same procedure as in **sec. 5.2.2 C and D**

F. Investigate Limit States

Service limit state governs. (According to Barker 2007) Use 6 No. 9.

5.3.3 Example Problem

Analyze an interior T-Beam of the T-Beam Bridge, of **Figure 5.3.1a** for a 20 lb TNT blast load.

Given:

1. Structural configuration is shown in **Figures 5.3.1a,b and c**
2. Maximum support rotation of one degree.
3. Yield stress of reinforcing steel, $f_y = 60000\text{ psi}$ and concrete compressive strength, $f'_c = 4000\text{ psi}$
4. Weight of concrete, $w = 150\text{ lbs/ft}^3$

Solution:

1. Find the DIF from **Table 3.5**, for close-in-range case

f'_c "psi"	f_y "psi"	Concrete, DIF		Steel, DIF
		Bending	Direct Shear	Bending
4000	60000	1.25	1.1	1.23

The dynamic strength of concrete as well as that of steel are given by

$$f'_{dc} = DIF \text{ times } f'_c \text{ and } f_{dy} = DIF \text{ times } f_y$$

Concrete		Steel
Bending, f'_{dc}	Direct Shear, f'_{dc}	f_{dy}
5000	4400	73800

2. For A_s (6 No. 9 bars)

Tension Reinforcement		
Bars size	No. of bars	A_s "in ² "
9	6	5.964

3. Calculate "effective depth, d , " for negative "support" d_N and positive" mid-span" d_p

Section Dimensions		Bottom	Top	Diameter	d_p	d_N
b "in"	h "in"	cover "in"	cover "in"	of Tie		
14	40	2	2.5	0.5	36.9375	36.4375

Where d_p , d_N are positive and negative effective depths respectively.

4. From Equation $\rho = \frac{A_s}{bd}$

$$\rho_p = \frac{5.964}{14 \times 36.94}$$

$$\rho_N = \frac{5.964}{14 \times 36.44}$$

ρ_{\max} and ρ_{\min} are calculated using Equations **4.9**, **4.10** and **Table**

4.2.3.1

$$\rho_{\max} = 0.724\rho_b$$

where

$$\rho_b = 0.0285 \quad \rho_{\min} = 3x \frac{\sqrt{f'_c}}{f_y} \geq \frac{200}{f_y}$$

ρ_p	ρ_N	ρ_{\max}	ρ_{\min}
0.01153	0.01169	0.02064	0.00333

5. Moment Capacity of the beam is calculated based on Equations **4.1** and **4.2**

a_p "in."	a_N "in."	M_{up} "in-lb"	M_{uN} "in-lb"
7.39751	7.3975102	14630095.29	14410019.4

Where M_{up} , M_{uN} are the ultimate moment capacity at the mid-span and at the support respectively.

From **Table 4.2.6a** the ultimate resistance of uniformly loaded beam with both ends fixed

$$r_u = \frac{8(M_{uN} + M_{up})}{L^2}$$

Ultimate Resistance, r_u "lb/in"
For both ends fixed with uniform load (r_u) "lb/in"
914.5916684

6. The average moment of inertia is calculated using Equation **3.3** and

Figure 3.2.2a

Concrete modulus of elasticity E_c "psi"	Steel modulus of Elasticity E_s "psi"	Modular Ratio n
3.83E+06	29000000	
From Figure 3.4-2b		7.563401821
F_N	F_p	
0.0542	0.0542	

The cracked moment of inertia is calculated as follows:

$I_c = Fbd^3$	I_{cN} "in ⁴ "	I_{cp} "in ⁴ "	$I_{c\text{ ave}}$ "in ⁴ "	I_g "in ⁴ "	I_a "in ⁴ "
	36709.04	38241.05	37475.05	74666.667	56070.86

7. The equivalent elastic system K_E of a uniformly loaded beam with fixed ends, from **Table 4.2.6.7**:

$$K_E = \frac{307E_c I_a}{L^4}$$

Equivalent Elastic Stiffness, K_E
For both ends fixed with uniform load, (K_E)
1022.902505 lb/in/in

8. The equivalent elastic deflection is

$$x_E = \frac{r_u}{k_E}$$

Equivalent Elastic Deflection x_E "in"
For both ends fixed with uniform load, (x_E)
0.894114213

9. Load-mass factor from **Table 4.2.6d**

For a beam with fixed ends with uniformly distributed load, the load mass factor for the plastic range is:

Load Mass Factor K_{LM}	
For both ends fixed with uniform load, (K_{LM})	
Elastic	0.77
Elasto-Plastic	0.78
Plastic	0.66

K_{LM} for the plastic range case is given as

$$K_{LM} = \frac{K_{LM} (elastic) + K_{LM} (Elasto - plastic)}{4} + \frac{K_{LM} (plastic)}{2}$$

K_{LM} For Plastic Mode
0.7175

10. Natural period T_N can be calculated from the following formula

$$T_N = 2\pi \sqrt{\frac{K_{LM} m}{k_E}} \quad (4.18)$$

Where

m = the mass of the beam plus the effective width of the flange

The effective width of the flange is the smallest of

$$\frac{L}{4} = \frac{42 \times 12}{4} = 126 \text{ in.}$$

$$b + 16h_f = 14 + 15 \times 8 = 142 \text{ in.}$$

Center to center spacing of beams = 96 in.

Therefore, the effective flange width, $b_e = 96$ in.

$$m = \frac{w}{g} \Rightarrow m = [(40 - 8) \times 14 + 96 \times 8] \times \frac{150}{12^3} \times \frac{1000^2}{32.2 \times 12} = 273176.9 \frac{\text{lb} \cdot \text{ms}^2}{\text{in}^2}$$

$$T_N = 2\pi \sqrt{\frac{0.7175 \times 273176.9}{1022.9025}} = 86.975 \text{ ms}$$

11. Using ATBlast program, the loading pressure and the duration will be as follows:

It is assumed that a 20 lb TNT weight explodes at 6 ft height above the bridge deck. Therefore, for 6 ft stand-off distance, $P = w = 258$ psi; "incident pressure"

12. The ductility ratio is determined from **Figure 4.2.6.4b**.

w, q_b, y_b, y_e, t in **Figure 4.2.6.4b**, correspond to P, r_u, x_E, x_m, T in the calculation.

$$\frac{T}{T_N} = \frac{0.51}{86.975} = 0.01 = \frac{t}{T_N}$$

$$\frac{r_u}{P \text{ times tributary width}} = \frac{914.592}{258 \times 96} = 0.0369$$

$$\Rightarrow \frac{p \text{ times tributary width}}{r_u} = 27.1 = \frac{w}{q_b}$$

$$\Rightarrow \text{From the Figure } \frac{y_e}{y_b} = 1 = \frac{x_m}{x_E}$$

13. From **Table 4.2.6b**

$$x_m = \frac{L \tan \theta}{2}$$

$$x_m = \frac{x_m}{x_E} x_E = 0.894 \Rightarrow \tan \theta = \frac{2x_m}{L} \Rightarrow \theta = 0.203 < \theta_{\max} = 1 \quad \text{ok}$$

14. Shear calculation

Direct shear check, from **Table 4.2.6c**

$$V_s = \frac{r_u L}{2} = \frac{914.6 \times 504}{2} = 230477.1 \text{ lb}$$

Section capacity in direct shear, as per the NAVAC code

$$V_d = 0.18 f'_{dc} b d$$

Shear strength is more difficult to determine experimentally because of difficulty in isolating shear from other stresses. This is one reason for the large variation in shear-strength values, varying from 20% of the compressive strength in normal loading to a considerably higher percentage of up to 85% of the compressive strength in cases where direct shear exists in combination with compression. (E. G. Nawy 2005)

$$V_d = 0.18 \times 4400 \times 14 \times 36.44 = 404019 \text{ lbs} > V_s = 230477.1 \text{ lbs} \quad \text{OK.}$$

15. Diagonal tension stress can be found from the following Equation:

$$v_u = \frac{V_u}{bd} < 10\Phi\sqrt{f'_c}$$

V_u , shear at a distance d from the support is

$$V_u = \left(\frac{L}{2} - d \right) r_u = \left(\frac{504}{2} - 36.44 \right) 914.6 = 197151.67 \text{ lbs}$$

$$v_u = \frac{197151.67}{14 \times 36.44} = 386.48 \text{ psi} < 10\Phi\sqrt{f'_c} = 10 \times 0.85 \times \sqrt{4000} = 537.59 \text{ psi} \quad \text{OK}$$

16. Unreinforced web shear stress capacity will be calculated as follows

$$v_c = \phi(1.9\sqrt{f'_c} + 2500\rho) = 0.85(1.9\sqrt{4000} + 2500 \times 0.0117) = 126.99 \text{ psi}$$

$$v_c = \phi(1.9\sqrt{f'_c} + 2500\rho) \leq 3.5\phi\sqrt{f'_c} = 2.28 \times 0.85 \times \sqrt{4000} = 122.57 \text{ psi} \quad \text{Not Good}$$

Therefore, $v_c = 122.57 \text{ psi}$

17. Area of the web reinforcement

$$A_v = \frac{[(v_u - v_c)bs_s]}{\phi f_y} \quad (4.14)$$

Where $(v_u - v_c) \geq v_c \Rightarrow 386.48 - 122.57 = 263.91 \text{ psi} > v_c = 122.57 \text{ psi} \quad \text{OK}$

Assume Spacing of stirrups in the direction parallel to the longitudinal reinforcement, "in"		
$S_s =$	10	in

Therefore,

Area of web reinforcing, A_v "in²"
For both ends fixed with uniform load
0.724451379

Use No. 6 tie $\Rightarrow A_v = 0.88 \text{ in}^2$

Minimum tie reinforcing area

$$A_{v \min} = 0.0015 b s_s = 0.0015 \times 14 \times 10 = 0.21 \text{ in}^2 < 0.88 \text{ in}^2$$

18. Maximum tie spacing

$$4\phi\sqrt{f'_c} = 4 \times 0.85 \times \sqrt{4000} = 215 \text{ psi}$$

$$s_{\max} = \frac{d}{2} = \frac{36.44}{2} = 18.22 \text{ in} > 10 \text{ in} \quad \text{OK}$$

5.4 Reinforced Concrete T-Beam Bridge Strengthened With CFRP Composites

5.4.1 Example Problem

The T-Beam Bridge (**Section 5.3**) strengthened with 9 layers of CFRP is illustrated for a simply supported boundary condition.

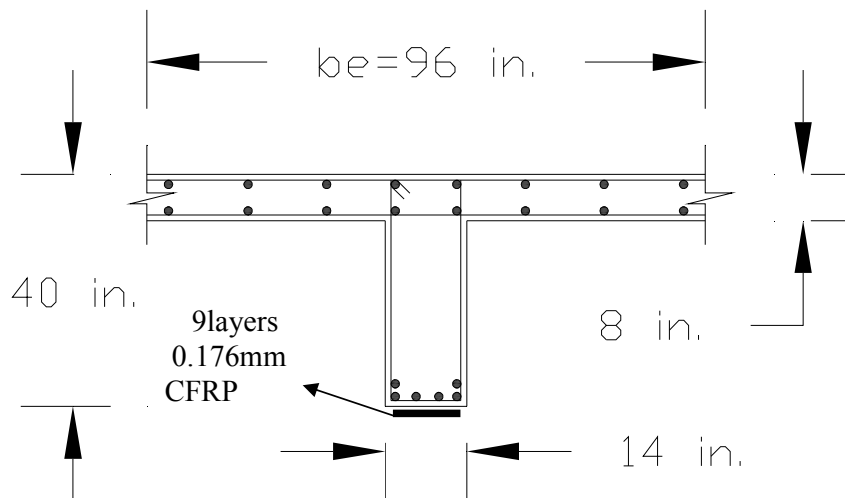


Figure 5.4.1 Cross section in a T-Beam

The illustration of this example is based on the BS8110 (Teng, 2002) which includes formulations involving equations derived based on SI units.

Given:

1. Structural configuration is shown in **Figures 5.3.1a, c** and **Figure 5.4.1**
2. Maximum support rotation of one degree.
3. Yield stress of reinforcing steel, $f_y = 60000 \text{ psi}$, and concrete compressive strength, $f'_c = 4000 \text{ psi}$

4. Weight of concrete, $w = 150 \text{ lbs/ft}^3$

5. 9 layers of FRP is used with thickness of 0.176 mm for each layer. FRP properties are the following: tensile strength

$$f_{frp} = 3800 \text{ N/mm}^2, \text{ modulus of elasticity, } E_{frp} = 208 \text{ GPa} = 208000 \text{ N/mm}^2$$

Solution:

1. Find the DIF from **Table 3.5**, for close-in-range case

f'_c "psi"	f_y "psi"	Concrete, DIF		Steel, DIF
		Bending	Direct Shear	Bending
4000	60000	1.25	1.1	1.23

The dynamic strength of concrete as well as that of steel are given by

$$f'_{dc} = DIF * f'_c \text{ and } f_{dy} = DIF * f_y$$

Concrete	Steel
Bending, f'_{dc} "psi"	f_{dy} "psi"
5000	73800

The above stresses are now converted to SI units as follows:

Concrete	Steel
Bending, f'_{dcu} "N/mm ² "	f_{dy} "N/mm ² "
43.092231	508.8331

Herein f'_{dcu} is the cube strength in N/mm²

2. To find x using Equation 4.23 :

From Equation 4.42 and Table 4.3.4

$$\varepsilon_{frp,rup} = \frac{3800}{1.25 \times 208000} = 1.46 \times 10^{-2}$$

And for $\varepsilon_{cf} = 0.0035$ per the BS 8110 $\Rightarrow x = 196 \text{ mm}$

Use $x = 190 \text{ mm} \Rightarrow$ from Equation 4.25 $\varepsilon_{cf} = 3.36 \times 10^{-3} < 0.0035$

X "mm"	d _{frp} "mm"	d _{si} "mm"
190	1016	938.2125

Where d_{frp} and d_{si} are distances from the extreme concrete compression fiber to the centroid of the FRP and to the centroid of steel bars respectively.

$$\text{From Equation 4.24} \Rightarrow \varepsilon_{si} = 0.0035x \frac{190 - 938.2125}{190} = -0.013783$$

3. Find the compressive concrete strain, ε_{co} from Equation 4.28

$$\varepsilon_{co} = \frac{1}{4100} \sqrt{\frac{43.092}{1.5}} = 0.0013073$$

4. Find the mean stress factor, k_1

$$\varepsilon_{co} \leq \varepsilon_{cf} \leq 0.0035 \Rightarrow \text{from Equation 4.32}$$

$$k_1 = 0.67x(1 - \frac{0.0013073}{3 \times 0.00336}) = 0.5831071$$

5. Find the centroid factor of the compression force, k_2

$$\varepsilon_{co} \leq \varepsilon_{cf} \leq 0.0035 \Rightarrow \text{from Equation 4.40}$$

$$k_2 = \frac{\frac{0.00336}{2} + \frac{0.0013073^2}{12 \times 0.00336} - \frac{0.0013073}{3}}{0.00336 - \frac{0.0013073}{3}} = 0.4399861$$

6. Calculate the stresses in steel, σ_{si}

$$|\epsilon_{si}| \geq \frac{f_y}{\gamma_s x E_s} \Rightarrow \text{from Equation 4.35}$$

$$\sigma_{si} = -484.6029 \text{ N/mm}^2$$

7. Calculate the stresses in FRP, σ_{frp}

$$\sigma_{frp} = E_{frp} \epsilon_{frp} = 208000 \times -1.46 \times 10^{-2} = -3040 \text{ N/mm}^2$$

8. Find the moment capacity of the beam, M_n , from Equation 4.41

$$M_n = 2.139 \times 10^9 \text{ N.mm}$$

$$M_n = 18922692 \text{ lb.in.}$$

9. From **Table 4.2.6a** the ultimate resistance of simply supported beam with uniformly distributed load is given by

$$r_u = \frac{8M_p}{L^2} = \frac{18922692}{504^2} = 595.95 \text{ lb/in}$$

10. The average moment of inertia is calculated using Equation 3.3 and

Figure 3.2.2a

Concrete modulus of elasticity E_c "N/mm ² "	Steel modulus of Elasticity E_s "N/mm ² "
2.64E+04	199948

Modular Ratio n
7.563401821

From Figure 3.4-2b
F
0.0525

The cracked moment of inertia is calculated as follows:

$I_c = F b d^3$	$I_{c \text{ ave}}$ "in ⁴ "	I_g "in ⁴ "	I_a "in ⁴ "
	35557.65	74666.667	55112.16

11. The equivalent elastic system K_E of a uniformly loaded beam with fixed ends, from **Table 4.2.6.7**:

$$k_E = \frac{348E_c I_a}{5L^4}$$

Equivalent Elastic Stiffness, k_E "lb/in/in"
Simply Supported beam with Uniform load (K_E)
251.5169855

12. The equivalent elastic deflection is

$$x_E = \frac{r_u}{k_E}$$

Equivalent Elastic Deflection X_E "in"
Simply Supported beam with Uniform load (X_E)
2.369433389

13. Load-mass factor from **Table 4.2.6d**

For a simply supported beam with uniformly distributed load, the load mass factor for the plastic range is:

Load Mass Factor K_{LM}	
Simply Supported beam with Uniform load (K_{LM})	
Elastic	0.78
Plastic	0.66

K_{LM} for the plastic range case is given as

$$K_{LM} = \frac{K_{LM} (elastic) + K_{LM} (Elasto - plastic)}{4} + \frac{K_{LM} (plastic)}{2}$$

K_{LM} For Plastic Mode
0.525

14. Natural period T_N can be calculated from the following formula

$$T_N = 2\pi \sqrt{\frac{K_{LM} m}{k_E}} \quad (4.18)$$

Where

m = the mass of the beam plus the effective width of the flange

The effective width of the flange is the smallest of

$$\frac{L}{4} = \frac{42 \times 12}{4} = 126 \text{ in.}$$

$$b + 16xh_f = 14 + 15 \times 8 = 142 \text{ in.}$$

Center to center spacing of beams = 96 in.

Therefore, the effective flange width, b_e = 96 in.

$$m = \frac{w}{g} \Rightarrow$$

$$m = [(40 - 8) \times 14 + 96 \times 8] \times \frac{150}{12^3} \times \frac{1000^2}{32.2 \times 12} = 273176.9 \frac{\text{lb} \cdot \text{ms}^2}{\text{in}^2}$$

$$T_N = 2\pi \sqrt{\frac{0.525 \times 273176.9}{251.517}} = 150.037 \text{ ms}$$

15. Using ATBlast program, the loading pressure and the duration will be as follows:

It is assumed that a 20 lb TNT weight explodes at 6 ft height above the bridge deck. Therefore, for 6 ft stand-off distance, $P = w = 258$ psi; "incident pressure"

16. The ductility ratio is determined from **Figure 4.2.6.4b**.

w, q_b, y_b, y_e, t in **Figure 4.2.6.4b**, correspond to P, r_u, x_E, x_m, T in the calculation.

$$\frac{T}{T_N} = \frac{0.51}{150} = 0.0034 = \frac{t}{T_N}$$

$$\frac{r_u}{P \text{ times tributary width}} = \frac{595.95}{258 * 96} = 0.024$$

$$\Rightarrow \frac{p \text{ times tributary width}}{r_u} = 41.56 = \frac{w}{q_b}$$

$$\Rightarrow \text{From the Figure } \frac{y_e}{y_b} = 1.8 = \frac{x_m}{x_E}$$

17. From **Table 4.2.6b**

$$x_m = \frac{L \tan \theta}{2}$$

$$x_m = \frac{x_m}{x_E} x_E = 4.26 \Rightarrow \tan \theta = \frac{2x_m}{L} \Rightarrow \theta = 0.96961 < \theta_{\max} = 1 \quad \text{ok}$$

18. Shear calculation

Direct shear check, from **Table 4.2.6c**

$$V_s = \frac{r_u L}{2} = \frac{595.953 * 504}{2} = 150180.091 \text{ lb}$$

Section capacity in direct shear, as per the NAVAC code

$$V_d = 0.18 f'_{dc} b d$$

Shear strength is more difficult to determine experimentally because of difficulty in isolating shear from other stresses. This is one reason for the

large variation in shear-strength values, varying from 20% of the compressive strength in normal loading to a considerably higher percentage of up to 85% of the compressive strength in cases where direct shear exists in combination with compression. (E. G. Nawy 2005)

$$V_d = 0.18 \times 4400 \times 14 \times 36.44 = 404019 \text{ lbs} > V_s = 150180.091 \text{ lbs} \quad \text{OK.}$$

19. Diagonal tension stress can be found from the following Equation:

$$v_u = \frac{V_u}{bd} < 10\Phi\sqrt{f'_c}$$

V_u , shear at a distance d from the support is

$$V_u = \left(\frac{L}{2} - d \right) r_u = \left(\frac{504}{2} - 36.44 \right) 595.95 = 128465.06 \text{ lbs}$$

$$v_u = \frac{128465.06}{14 \times 36.44} = 251.83 \text{ psi} < 10\Phi\sqrt{f'_c} = 10 \times 0.85 \times \sqrt{4000} = 537.59 \text{ psi} \quad \text{OK}$$

20. Unreinforced web shear stress capacity is calculated as follows

$$v_c = \phi(1.9\sqrt{f'_c} + 2500\rho) = 0.85(1.9\sqrt{4000} + 2500 \times 0.0117) = 126.99 \text{ psi}$$

$$v_c = \phi(1.9\sqrt{f'_c} + 2500\rho) \leq 3.5\phi\sqrt{f'_c} = 2.28 \times 0.85 \times \sqrt{4000} = 122.57 \text{ psi} \quad \text{Not Good}$$

Therefore, $v_c = 122.57 \text{ psi}$

21. Area of the web reinforcement

$$A_v = \frac{[(v_u - v_c) b s_s]}{\phi f_y} \quad (4.14)$$

Where $(v_u - v_c) \geq v_c \Rightarrow 251.83 - 122.57 = 129.26 \text{ psi} > v_c = 122.57 \text{ psi} \quad \text{OK}$

Assume spacing of stirrups in the direction parallel to the longitudinal reinforcement, "in"

$S_s = 10 \text{ in}$

Therefore,

Area of web reinforcing, A_v "in ² "
For a simple beam with uniform load
0.354833227

Use No. 4 tie $\Rightarrow A_v = 0.397in^2$

Minimum tie reinforcing area

$$A_{v\min} = 0.0015bs_s = 0.0015 \times 14 \times 10 = 0.21in^2 < 0.397in^2$$

22. Maximum tie spacing

$$4\phi\sqrt{f'_c} = 4 \times 0.85 \times \sqrt{4000} = 215 psi$$

$$s_{\max} = \frac{d}{2} = \frac{36.44}{2} = 18.22in > 10in \quad \text{OK}$$

Chapter 6: Parametric Studies and Discussions

6.1 Introduction

Comprehensive parametric studies have been done herein. Bridge spans were varied as well as the concrete compressive strength for both simply supported and fixed ends boundary conditions where solid slab and T-Beam bridges are included.

6.2 Case Studies

The case studies are carried out using the generated excel spreadsheet presented in Chapter 5. A 20 lb TNT weight load is applied above the bridge deck at 6 ft stand off distance for all the case studies. The case studies consider the solid slab and T-Beam bridges discussed in Chapter 5. The results for the case studies are presented in the form of tables with the following parameters:

L = Span length

A_s = Area of reinforcement

r_u = Ultimate resistance

K_E = Equivalent elastic stiffness

x_E = Equivalent elastic deflection

T_N = Natural period of the beam

x_m = Maximum deflection of the beam

θ = Rotation of the support

6.2.1 Case Study 1:

A simply supported solid slab bridge is analyzed for different span lengths as shown in **Table 6.2.1**. The area of reinforcement, A_s is determined considering flexure due to dead and live loads. The concrete and steel strengths are the following:

$$f'_c = 4,000 \text{ psi}, f_y = 60,000 \text{ psi}$$

Table 6.2.1 Simply supported solid slab

L in.	A_s in ²	r_u lb /in.	K_E lb/in/in	x_E in.	T_N ms	x_m in.	θ degree
120	2 No. 7= 1.203	970.996	10376	0.09	10.88	0.030	0.029
240	2 No. 8= 1.571	311.765	646.9	0.5	43.59	0.154	0.074
360	2 No. 9= 1.988	172.068	127.5	1.35	98.20	0.499	0.159
480	3 No. 9= 2.982	139.686	40.33	3.5	174.6	2.4	0.562

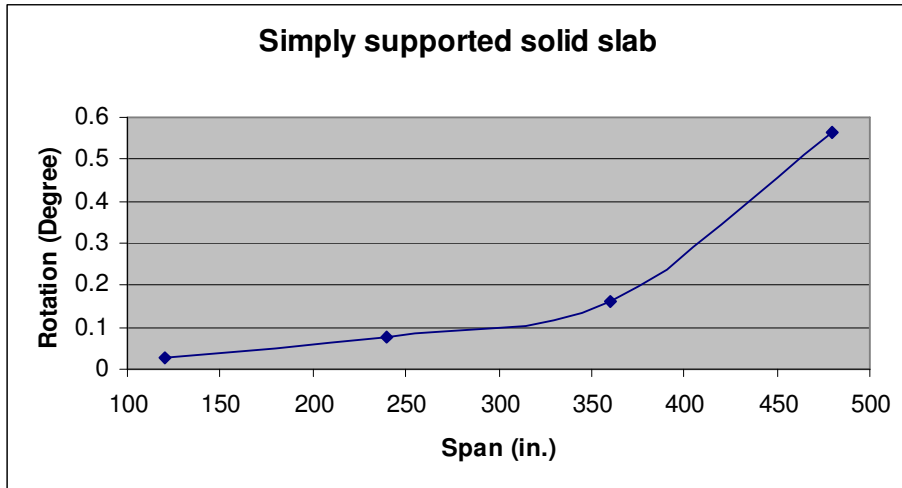


Figure 6.2.1a Span Vs Rotation

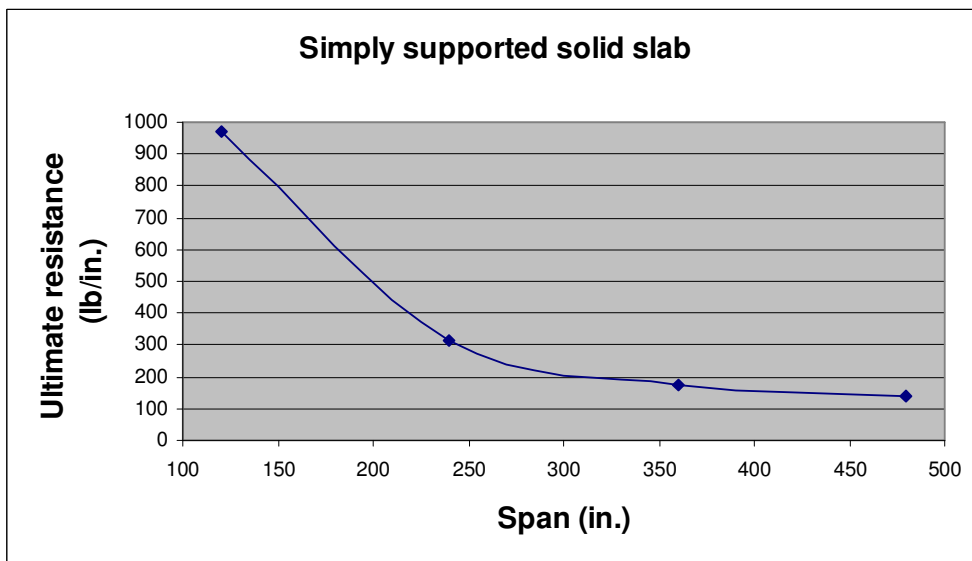


Figure 6.2.1b Span Vs Ultimate resistance

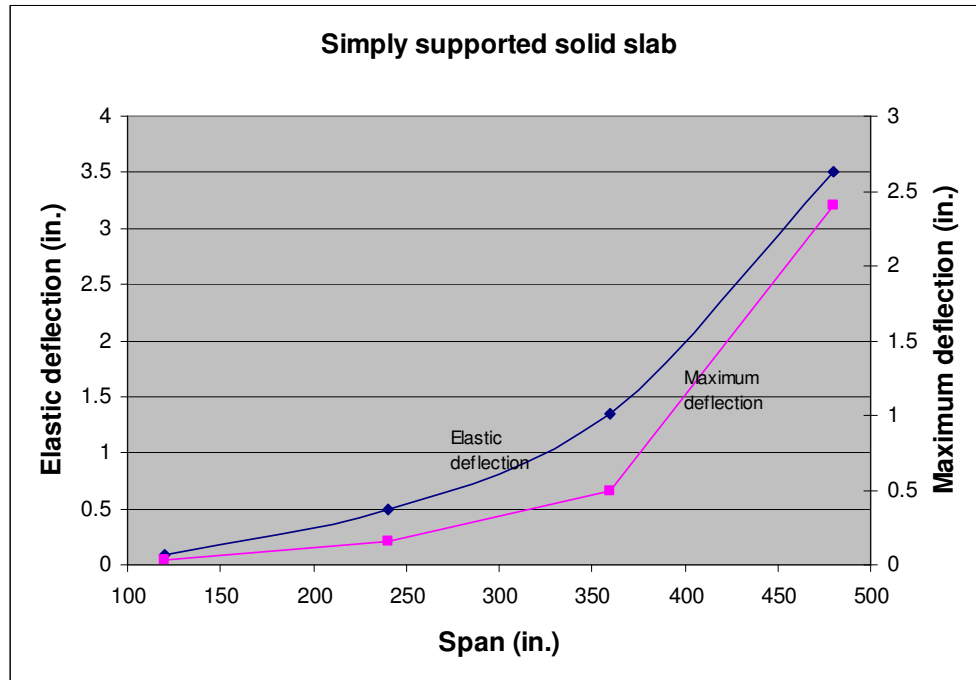


Figure 6.2.1c Span Vs Elastic and Maximum deflection

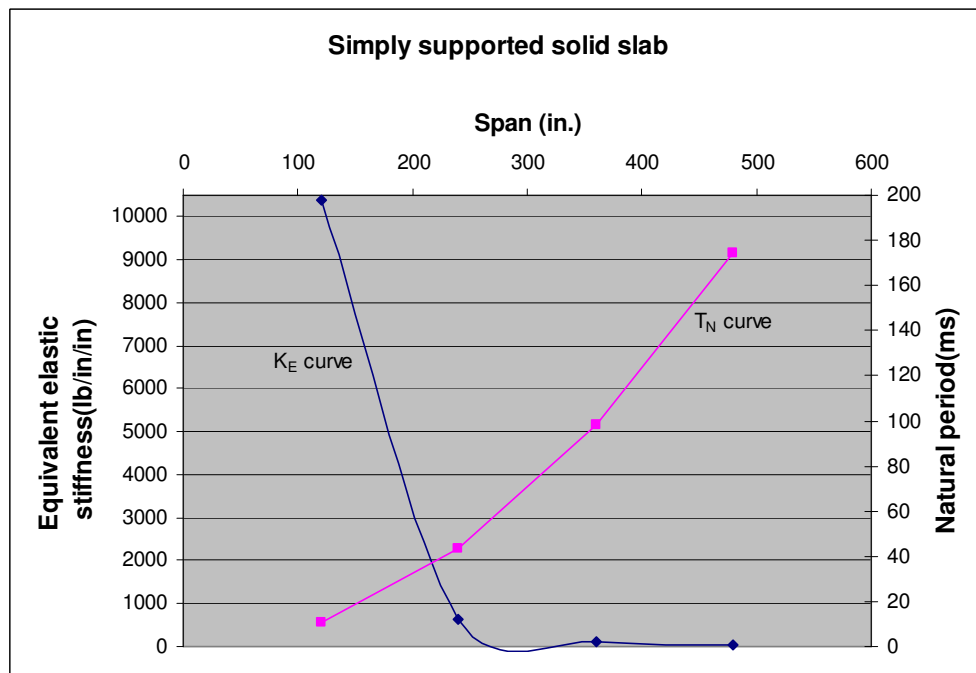


Figure 6.2.1d Span Vs Elastic stiffness, k_E and natural period, T_N

Discussions

As the span length increases, the rotation of the support also increases as can be seen from **Figure 6.2.1a**. The bridge experiences a rotation of 0.562° for a span length of 480 in, it is much smaller than the reported value of 2° that corresponds to the limiting value at failure (NAVFAC); therefore, the bridge is capable of sustaining more than 20 lb TNT weight. **Figure 6.2.1b** shows the relation between the span and the bridge ultimate resistance, where the ultimate resistance is defined as follows: $r_u = \frac{8M_p}{l^2}$. The figure shows a decrease in the ultimate resistance for increasing span lengths that is consistent with the above definition for the ultimate resistance.

Figure 6.2.1c shows the relation between the span and the elastic and maximum deflections. As shown in Chapter 4, the maximum deflection x_m is calculated from the ratio x_m / x_E , which is dependent on the elastic deflection x_E . **Figure 6.2.1d** shows the relation between the span and the equivalent elastic stiffness, k_E and the natural period of the bridge, T_N . For any given increase in the span length, there is a corresponding decrease in the elastic stiffness and increase in the natural period of the bridge.

6.2.2 Case Study 2:

A simply supported T-Beam bridge is analyzed for different spans as shown in **Table 6.2.2**. The area of reinforcement, A_s is estimated

considering the flexure due to dead and live loads. The concrete and steel strengths are the following:

$$f'_c = 4,000 \text{ psi}, f_y = 60,000 \text{ psi}$$

Table 6.2.2 Simply supported T-beam

L in.	A _s in ²	r _u lb /in.	K _E lb/in/in	x _E in.	T _N ms	x _m in.	θ degree
360	8 No. 8= 6.283	947.531	952.9	0.994	75.55	0.994	0.317
480	7 No. 9= 6.958	581.663	301.0	1.932	137.1	2.319	0.554
600	9 No. 9= 8.946	460.536	124.1	3.71	213.6	5.94	1.134
720	8 No. 10= 9.82	344.224	59.37	5.798	308.8	23.19	3.69

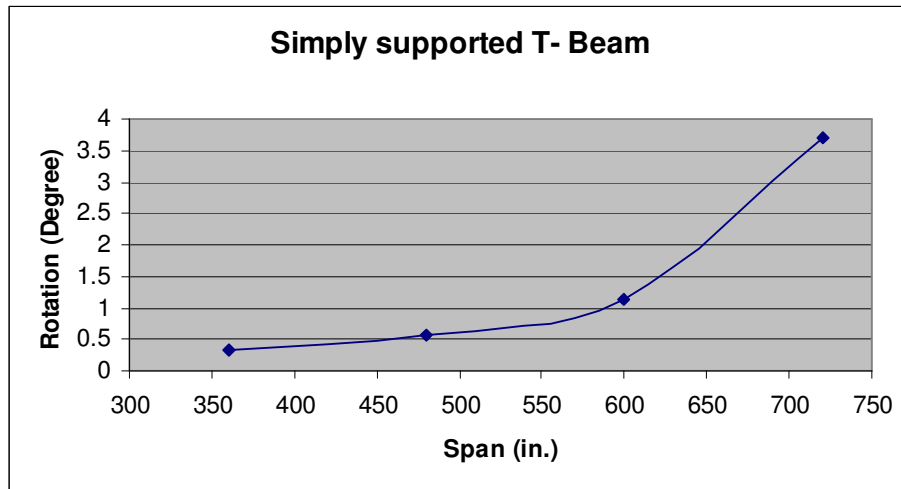


Figure 6.2.2a Span Vs Rotation

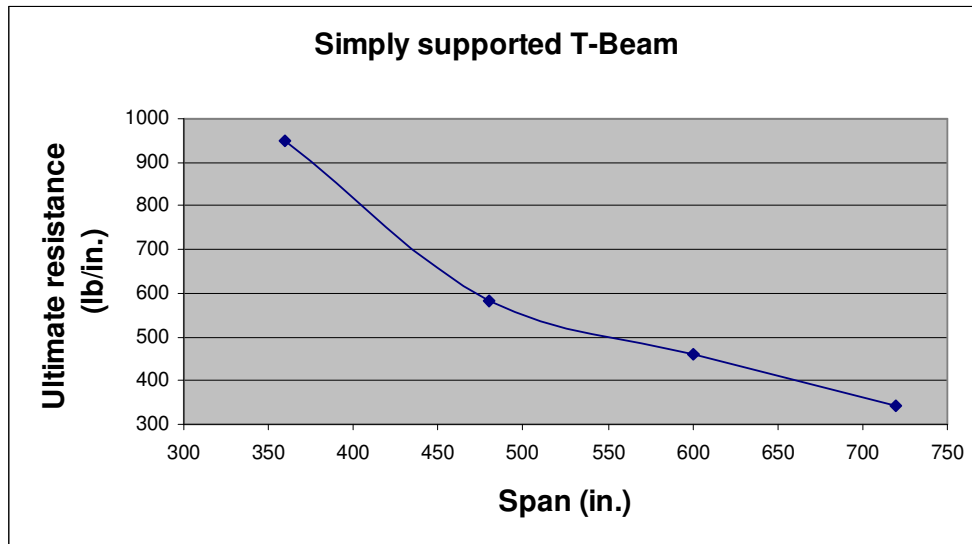


Figure 6.2.2b Span Vs Ultimate resistance

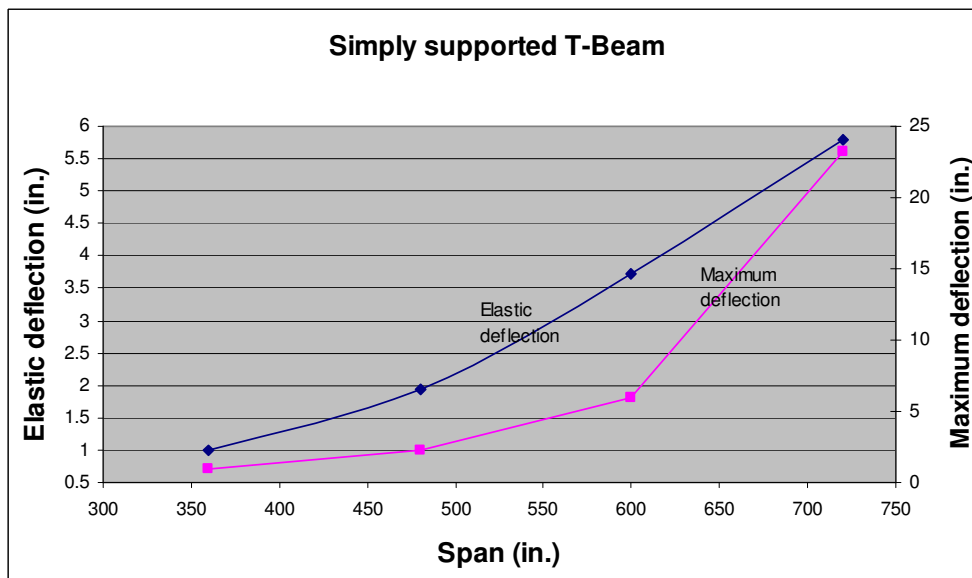


Figure 6.2.2c Span Vs Elastic deflection and Maximum deflection

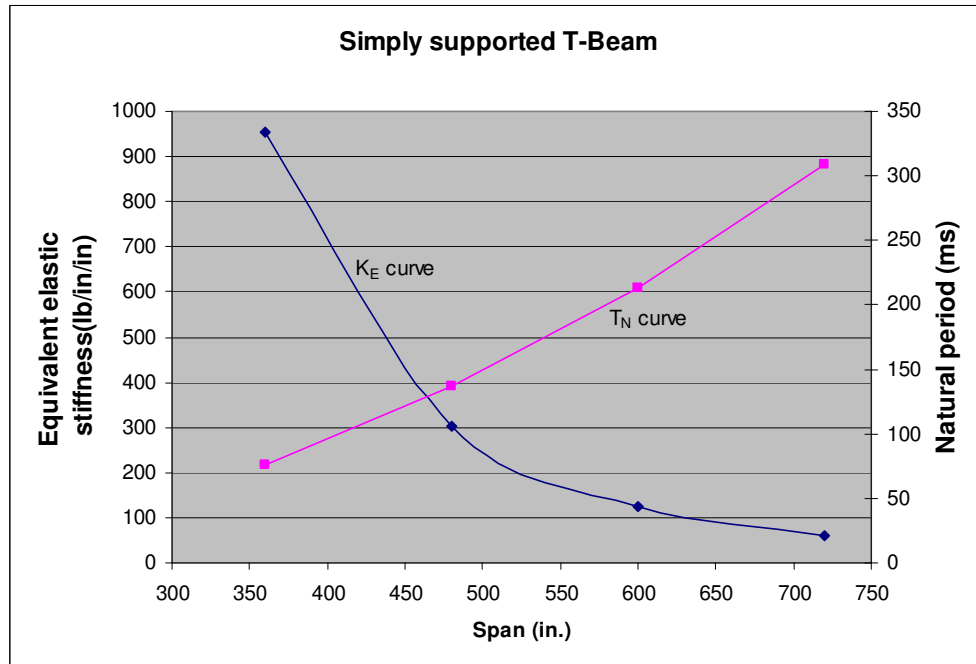


Figure 6.2.2d Span Vs Equivalent elastic stiffness, k_E and Natural period, T_N

Discussions

As the span increases, the support rotation also increases as seen from **Figure 6.2.2a**. The bridge experiences a rotation of 3.69 degrees for a span of 720 in. Earlier researchers have reported that the reinforced concrete members lose their structural integrity when the support rotation reaches a value of 2 degrees. **Figure 6.2.2b** shows the relation between the span and the bridge ultimate resistance, wherein the ultimate resistance is a function of the section capacity and the span length. Thus, the ultimate resistance decreases with the increase in span length.

Figure 6.2.2c shows the relation between the span and the elastic and maximum deflections. As the span length increases, both the elastic

deflection as well as the maximum deflection also increases. It is important to mention that maximum deflection is dependent on the elastic deflection.

Figure 6.2.2d shows the relation between the span and the equivalent elastic stiffness, k_E and the natural period of the bridge, T_N . As the span length increases, the elastic stiffness decreases with a corresponding increase in the natural period of the bridge.

6.2.3 Case Study 3:

A solid slab bridge with fixed ends is analyzed for different spans as shown in **Table 6.2.3**. The area of reinforcement, A_s is estimated considering the flexure due to dead and live loads. The concrete and steel strengths are as the following:

$$f'_c = 4000 \text{ psi}, f_y = 60000 \text{ psi}$$

Table 6.2.3 Solid slab with fixed ends

L in.	A_s in ²	r_u lb /in.	K_E lb/in/in	x_E in.	T_N ms	x_m in.	θ degree
120	2 No. 7= 1.203	1868.03	40744	0.05	6.421	0.02	0.02
240	2 No. 8= 1.571	599.38	2540.3	0.24	25.72	0.13	0.062
360	2 No. 9= 1.988	330.55	500.58	0.66	57.93	0.36	0.107
480	3 No. 9= 2.982	267.91	158.39	1.69	103	0.63	0.149

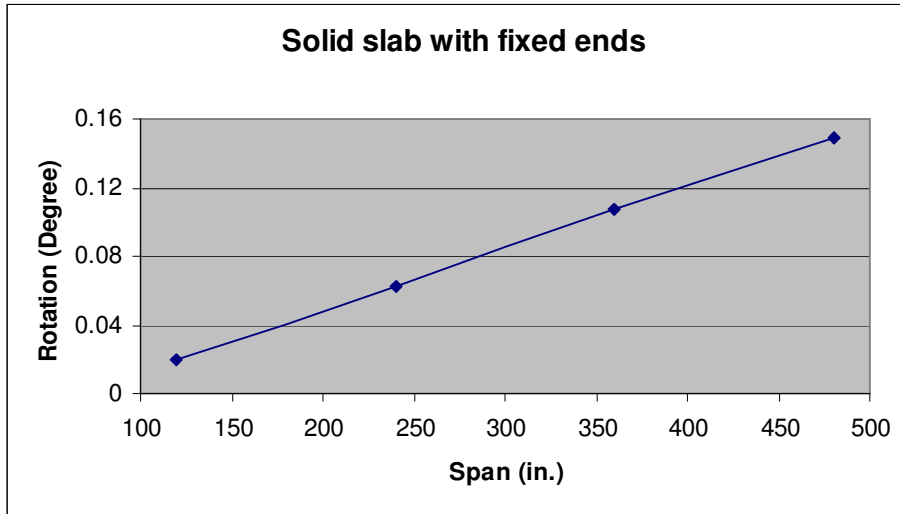


Figure 6.2.3a Span Vs Rotation

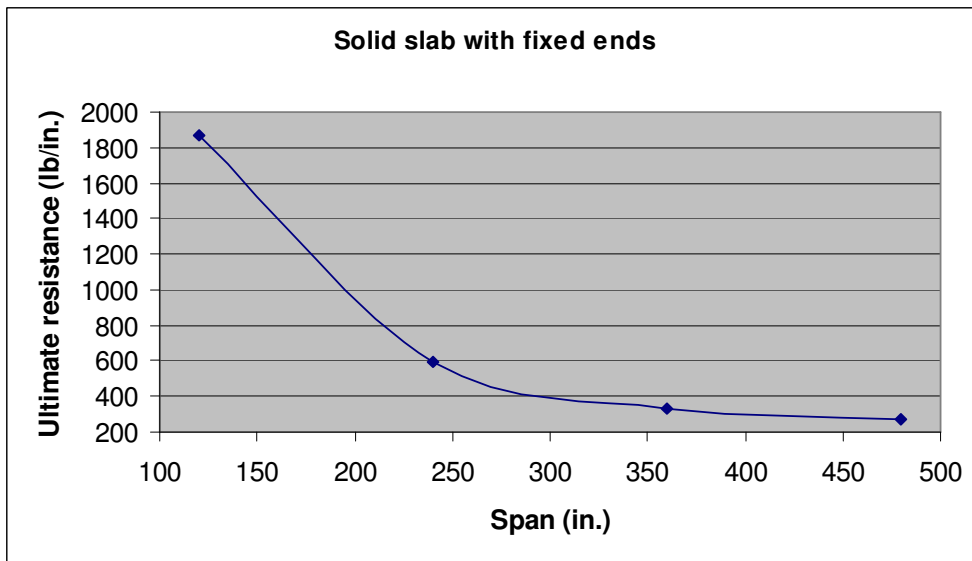


Figure 6.2.3b Span Vs Ultimate resistance



Figure 6.2.3c Span Vs Elastic and Maximum deflection

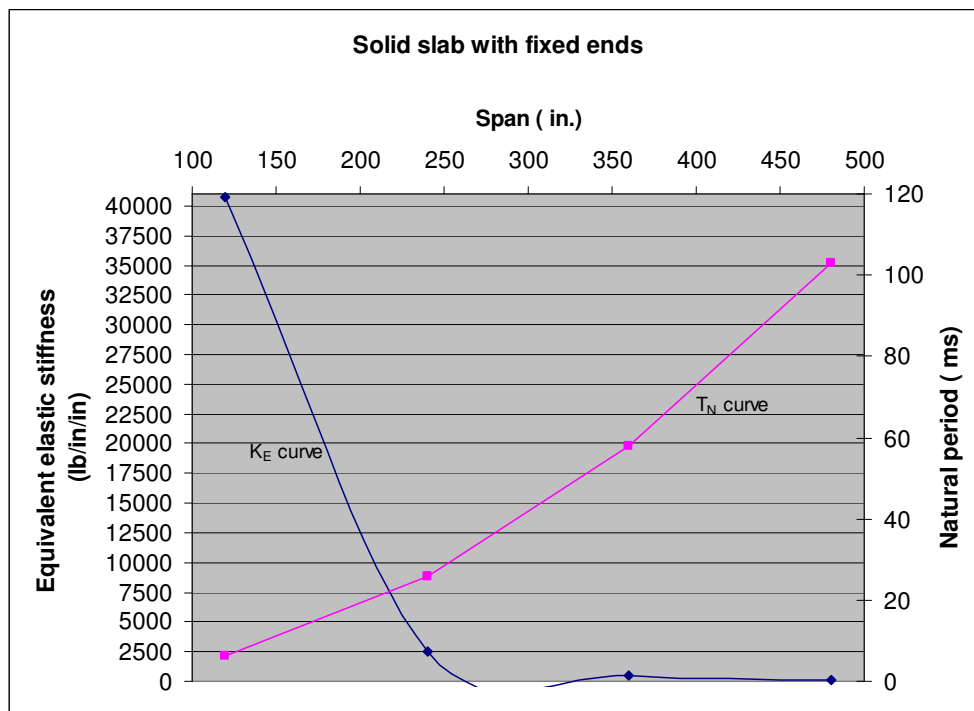


Figure 6.2.3d Span Vs Elastic deflection, k_E and natural period, T_N

Discussions

Figure 6.2.3a shows the relation between the span lengths and the support rotation. It is observed that the rotation at the support for a span length of 480 in. is 0.149° . This rotation is smaller than that of the same structure with simply supported boundary conditions (**Figure 6.2.1a**).

Figure 6.2.3b shows again the importance of the boundary conditions that contributes to an increase in the resistance capacity of the bridge. Comparison of the ultimate resistances from **Figures 6.2.3b** and **6.2.1b** shows the ultimate resistance for the bridge with fixed ends is almost 2 times that for a simply supported bridge.

Figure 6.2.3c shows the relation between the span and the elastic and maximum deflections. An increase in both elastic and maximum deflections can be seen due to the increase in the span length. **Figure 6.2.3d** shows the relation between the span and the equivalent elastic stiffness, k_E and the natural period of the bridge, T_N . Again, it can be observed that the elastic stiffness decreases with a corresponding increase in the natural period of the bridge with increasing span lengths.

6.2.4 Case Study 4:

A T-Beam bridge with fixed ends is analyzed for different spans as shown in **Table 6.2.4**. The area of reinforcement, A_s is estimated considering the flexure due to the dead and live loads. The concrete and steel strengths are the following:

$$f'_c = 4000 \text{ psi}, f_y = 60000 \text{ psi}$$

Table 6.2.4 T-Beam with fixed ends

L	A _s	r _u	K _E	x _E	T _N	x _m	θ
in.	in ²	lb /in.	lb/in/in	in.	ms	in.	degree
360	5 No. 8= 3.927	1227.751	3882.7	0.316	43.75	0.23	0.072
480	5 No. 9= 4.970	855.983	1230.3	0.7	79.31	0.68	0.163
600	7 No. 9= 6.958	738.823	503.94	1.466	123.9	1.47	0.28
720	7 No. 10= 8.59	612.393	242.62	2.524	178.6	2.52	0.402

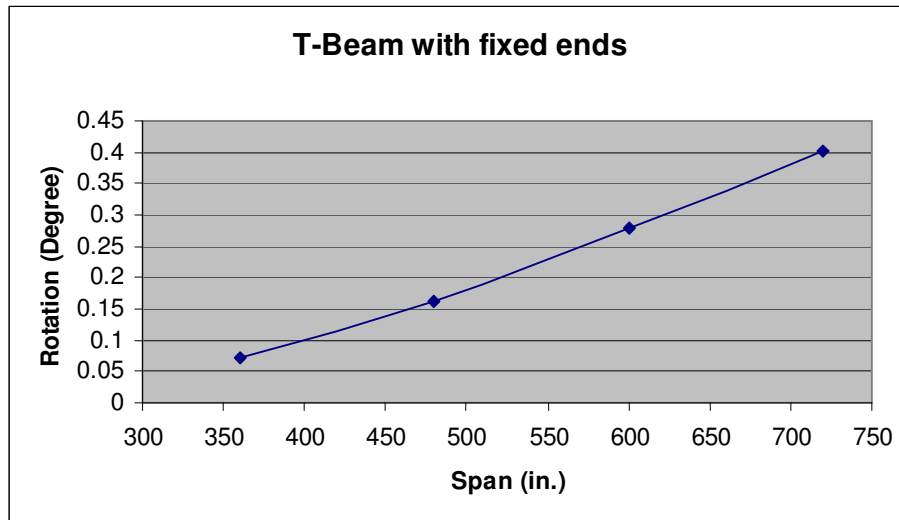


Figure 6.2.4a Span Vs Rotation

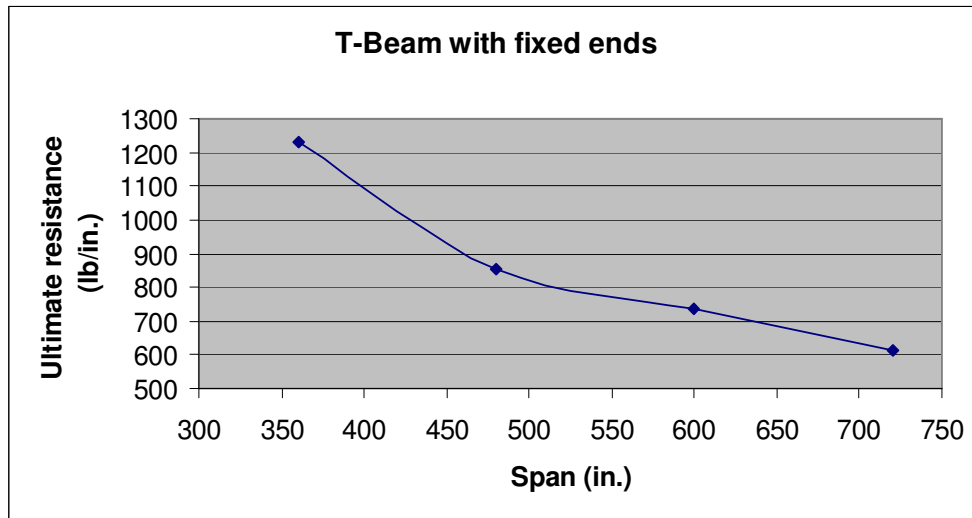


Figure 6.2.4b Span Vs Ultimate resistance

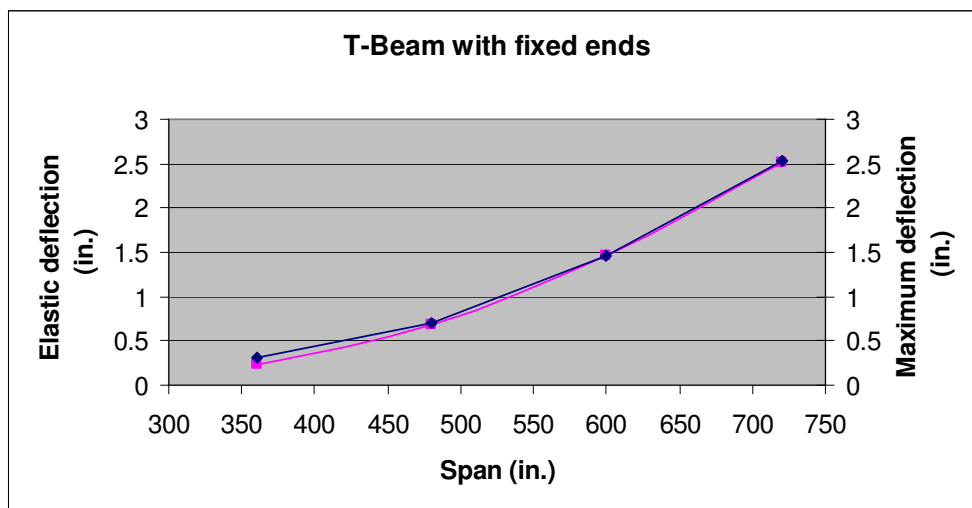


Figure 6.2.4c Span Vs Elastic and Maximum deflection

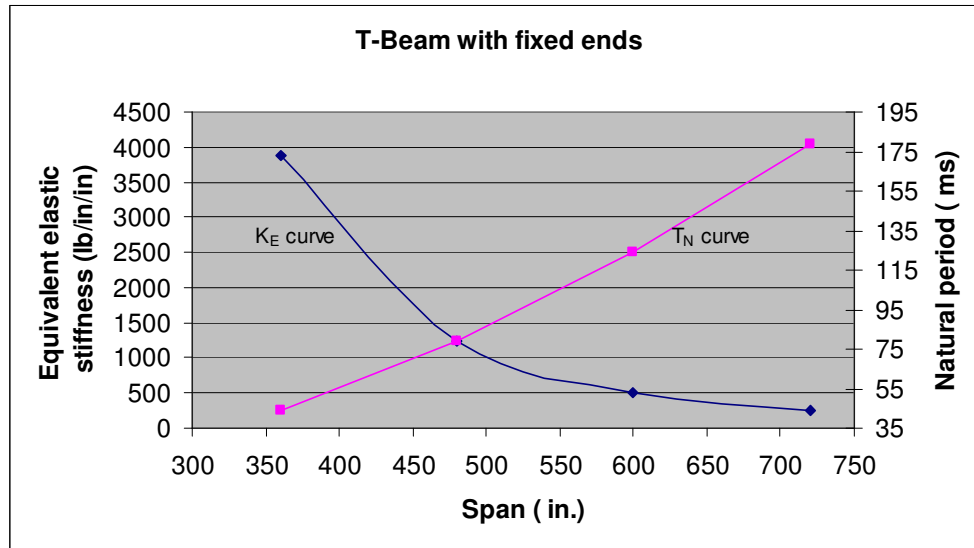


Figure 6.2.4d Span Vs Elastic stiffness, k_E and natural period, T_N

Discussions

Figure 6.2.4a shows the relation between the span increase and the support rotation. As it is seen from the figure, the rotation at the support for 720 in. span length is 0.402° , whereas the same bridge with simply supported boundary conditions exhibits a large rotation of 3.69° (**Figure 6.2.2a**). **Figure 6.2.4b** shows the relation between the span lengths and the ultimate resistance. A comparison with **Figure 6.2.2b**, shows that the bridge with fixed ends boundary conditions will experience an increased in the ultimate resistant to a value of 78%.

Figure 6.2.4c shows the relation between the span and the elastic and maximum deflections. As x_m/x_E was close to one for all the span length, and since the maximum deflection is dependent on the elastic deflection, the elastic and maximum deflections are almost equal. **Figure**

6.2.4d shows the relation between the span and the equivalent elastic stiffness, k_E and the natural period of the bridge, T_N . As the natural period of the bridge increases due to the increase in the span length, a corresponding decrease in the elastic stiffness can be observed.

6.2.5 Case Study 5:

This case study considers a solid slab bridge of span 420 in. for two different boundary conditions: i) fixed ends and ii) simply supported boundary condition. Three different concrete compressive strengths are assumed in this study and the results are shown in **Table 6.2.5a**, and **Table 6.2.5b** respectively.

Table 6.2.5a Solid-slab with fixed ends

f'_c psi	A_s in ²	r_u lb /in.	K_E lb/in/in	x_E in.	T_N ms	x_m in.	θ degree
4000	2 No. 9= 1.988	242.853	269.8	0.90	78.91	0.37	0.101
5000	2 No. 9= 1.988	246.682	295.8	0.83	75.36	0.37	0.100
6000	2 No. 9= 1.988	249.234	318.4	0.78	72.64	0.36	0.098

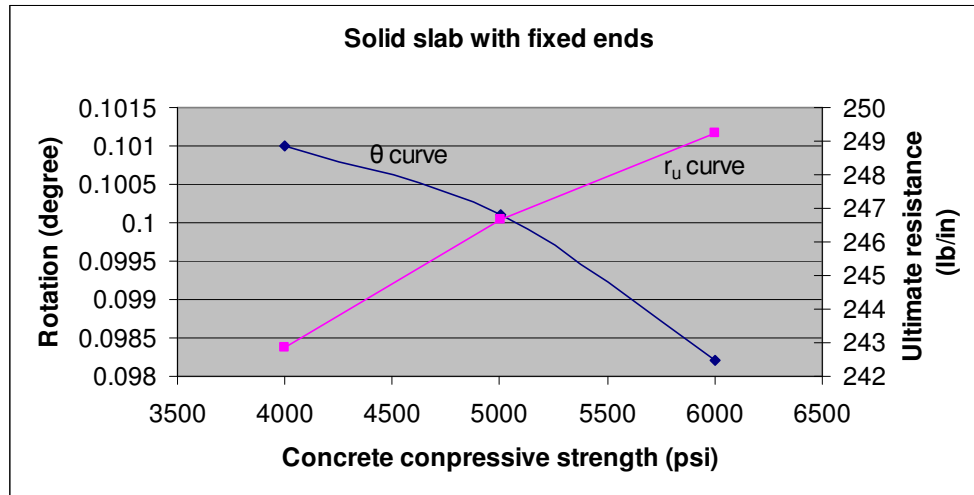


Figure 6.2.5a Fixed ends solid slab

Table 6.2.5b Simply supported solid-slab

f'_c psi	A_s in ²	r_u lb /in.	K_E lb/in/in	x_E in.	T_N ms	x_m in.	θ degree
4000	2 No. 9= 1.988	126.417	68.80	1.84	133.7	1.51	0.411
5000	2 No. 9= 1.988	128.331	75.3	1.70	127.8	1.42	0.386
6000	2 No. 9= 1.988	129.607	81.3	1.59	123	1.23	0.335

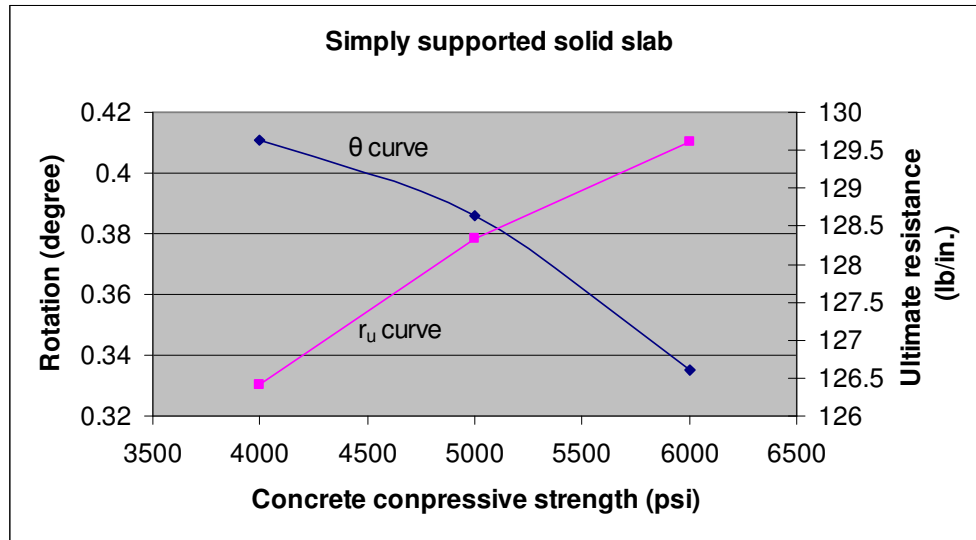


Figure 6.2.5b Simply supported solid slab

Discussions:

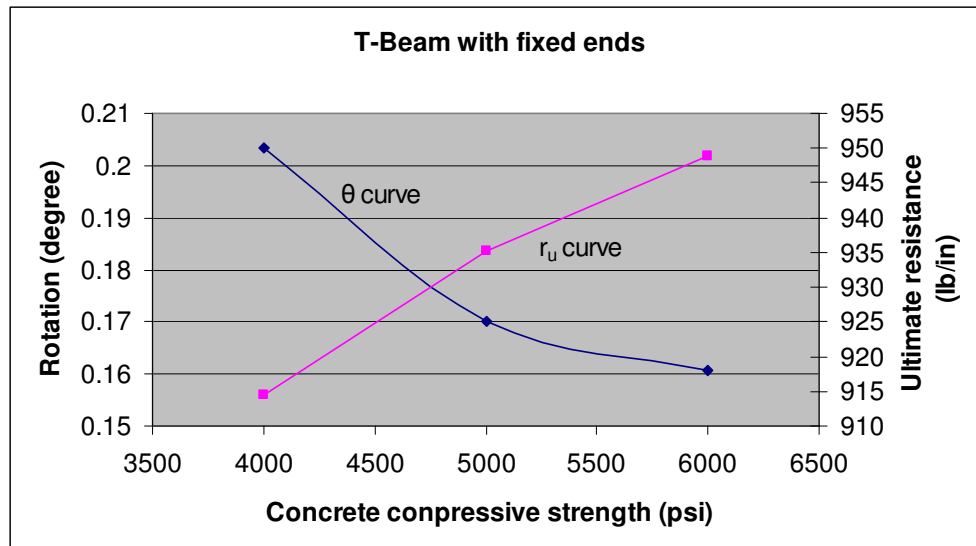
Figures 6.2.5a and 6.2.5b show the relation between the concrete compressive strengths, the ultimate resistance and support rotation for the different boundary conditions. As it is seen, the support rotation decreases, and the ultimate resistance increase with the increase in the compressive strength of concrete. It can be observed from the figures that the ultimate resistance is much higher for the bridge with fixed ends than for the simply supported condition. The support rotation for the bridge with fixed ends is less than that of the simply support solid slab bridge.

6.2.6 Case Study 6:

A T-Beam deck bridge with a span of 504 in. is analyzed for fixed ends and simply supported boundary conditions for different concrete compressive strengths and the results are shown in **Table 6.2.6a**, and **Table 6.2.6b** respectively.

Table 6.2.6a T-Beam with fixed ends

f'_c	A_s	r_u	K_E	x_E	T_N	x_m	θ
Psi	in ²	lb /in.	lb/in/in	in.	ms	in.	degree
4000	6 No. 9= 5.964	914.592	1023	0.89	86.98	0.89	0.203
5000	6 No. 9= 5.964	935.101	1100	0.85	83.87	0.75	0.170
6000	6 No. 9= 5.964	948.774	1182	0.80	80.92	0.71	0.161

**Figure 6.2.6a Concrete compressive strength Vs Rotation and ultimate resistance****Table 6.2.6b Simply supported T-beam**

f'_c	A_s	r_u	K_E	x_E	T_N	x_m	θ
psi	in ²	lb /in.	lb/in/in	in.	ms	in.	degree
4000	6 No. 9= 5.964	460.761	254.9	1.81	149.0	5.24	1.192
5000	6 No. 9= 5.964	471.016	276.9	1.70	143	4.59	1.044
6000	6 No. 9= 5.964	477.852	293.5	1.63	138.9	4.23	0.963

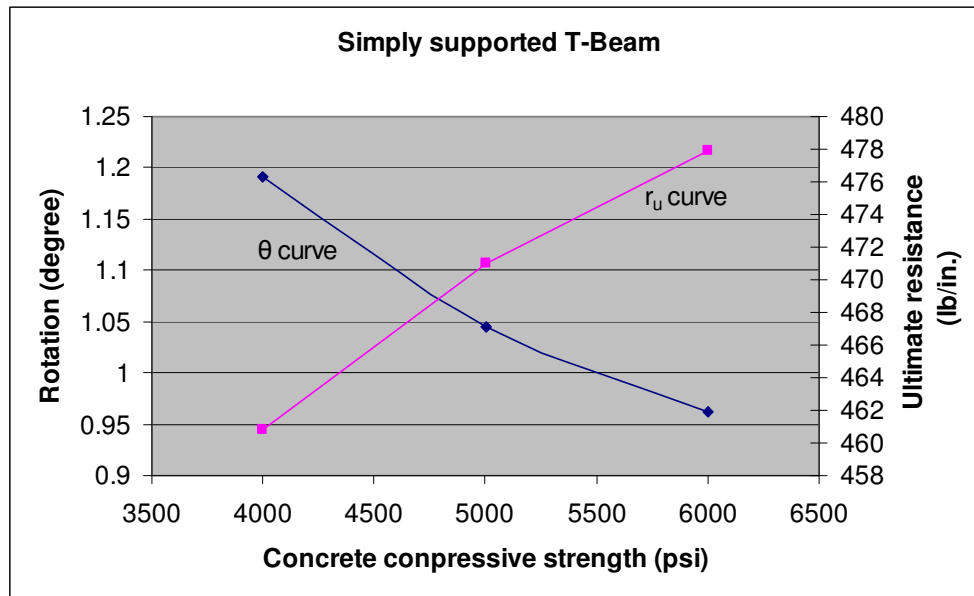


Figure 6.2.6b Concrete compressive strength Vs Rotation and ultimate resistance.

Discussions:

Figures 6.2.6a and 6.2.6b show the relation between the concrete compressive strengths and the ultimate resistance and support rotation for the fixed ends and simply supported boundary conditions of a T-Beam bridge respectively. The comparison of results from these figures shows the effect of the boundary conditions. The support rotation decreases with an increase in the ultimate resistance corresponding to the increase in the concrete compressive strengths. Moreover, although one can see an increase in capacity in both the solid slab and the T-Beam deck bridges with the increase in the concrete compressive strength, the increase is not significant.

6.2.7 Case Study 7:

This case study considers a T-Beam deck bridge of 504 in. span strengthened with Carbon Fiber Reinforced Polymer CFRP for both fixed ends and simply supported boundary condition. The results are shown in **Table 6.2.7.**

Table 6.2.7 Comparison between boundary conditions for T-Beam strengthened with CFRP

Boundary condition	L in.	f'_c psi	A_s in ²	r_u lb /in.	K_E lb/in/in	x_E in.	T_N ms	x_m in.	θ degree
Simply supported	504	4000	5.964	595.9	251.5	2.37	150	4.26	0.969
Fixed ends	504	4000	5.964	1192	1005	1.18	87.73	0.97	0.221

Discussions:

A comparison of the results for the simply supported and fixed end boundary conditions for a T-beam bridge shows an increase of 100% for the ultimate resistance and a decrease of 77% for the support rotation for the fixed end boundary conditions. Moreover, an increase of 300% for the effective stiffness corresponding to a decrease of 42% in natural period of the bridge is observed. As for the elastic and maximum deflection, the elastic deflection in the fixed end case decreases to the half of the one for

the simply supported bridge, while the maximum deflection for the fixed end decreases to one fourth of the one for the simply supported bridge.

6.2.8 Case Study 8:

In this case study, two simply supported T-Beam bridge are analyzed. Only one of them is strengthened with CFRP. The results of the bridge strengthened with CFRP are compared with the conventional reinforced concrete bridge without strengthening. The results are shown in **Table 6.2.8**.

Table 6.2.8 Simply supported T-Beam with and without CFRP

Parameters	L in.	f'_c psi	A_s in ²	r_u lb /in.	K_E lb/in/in	x_E in.	T_N ms	x_m in.	θ degree
With CFRP	504	4000	5.964	595.9	251.5	2.37	150	4.26	0.969
Without CFRP	504	4000	5.964	460.8	254.9	1.81	149	5.42	1.233

Discussions:

It can be seen from **Table 6.2.8** that the ultimate resistance has increased by 29% with a corresponding decrease of 21% in the support rotation due to the effect of the CFRP strengthening. It is observed from the results that there is neither significant change in the stiffness, nor in the natural period of the beam because the thickness of the CFRP laminates is relatively small compared to the depth of the sections. Moreover, the elastic deflection is

increased as an effect of the use of the CFRP and the maximum deflection in the strengthened bridge is less than that without strengthening.

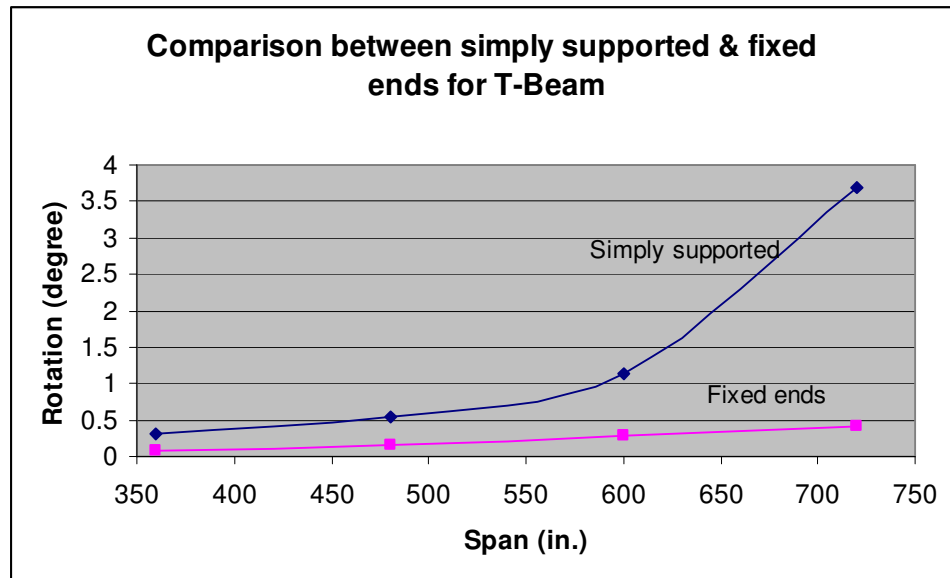


Figure 6.3 Span Vs Rotation (comparison)

6.3 Summary

The structural integrity of the bridges in general depend greatly on the ability of the bridge structure to deform inelastically under extreme loading events by dissipating large amount of energy, prior to failure. The prevention of progressive collapse cannot be guaranteed unless the connection at the supports of the bridge possesses very high rotation capacities required due to excessive loads.

It was found that 20 lb of TNT applied 6 ft over the deck of the bridge at mid-span is able to cause a failure in a simply supported T-beam with a span of 720 in; however, the same T- beam bridge with both ends fixed is able to sustain more than applied blast loads.

Results from the case studies analysis show that the boundary conditions play an important role in increasing the bridge capacity to sustain higher loading rate. **(Figure 6.3)**

For this particular study, the increase in capacity of the T-Beam deck bridge due to the increase in the strength of concrete is not significant. Moreover, the use of the CFRP shows a significant increase in the bridge resistance capacity, however, no increase in the stiffness of the bridge is observed as the thickness of the added CFRP layers is much smaller than the overall depth of the T-beam section.

Chapter 7: Conclusions and Recommendations

7.1 Introduction

The objective of the study is to analyze blast resistant reinforced concrete solid slab and T-beam bridges. A numerical method is developed to calculate ultimate resistance, equivalent elastic stiffness, equivalent elastic deflection, natural period of the beam, the maximum deflection, and the maximum rotation in the support for solid slab and T-Beam bridges.

7.2 Conclusions

Blast resistant bridge design, although very vital to ensure transportation infrastructure safety, this area has not been addressed adequately. The present study evaluates the performance of solid slab and T-beam bridges under blast loads. The performance of the CFRP strengthened bridge is also examined under blast loads.

A reinforced concrete bridge responds in different ways to the blast loads depending on the blast location and magnitude, boundary conditions, structural component, and stand off distance of the explosion from the structure. The following conclusions are made based on the results of the analytical studies:

- i) It was found from the analytical studies that a simply supported T-Beam bridge with a span of 720 in (60 ft) fails at only 20 lb of TNT applied 6 ft over the bridge at mid-span.
- ii) The same 60 ft T-Beam bridge with both ends fixed boundary condition would sustain the 20 lb of TNT successfully.
- iii) The rotation at the support is the indicator of any potential failure; it was found that having fixed ends boundary condition will aid considerably in increasing the sustainability of the bridge.
- iv) The use of high strength concrete was not very effective as the increase in the ultimate resistance was only 4% for an increase of concrete strength from 4000 psi to 6000 psi.
- v) The strengthening of the bridge using CFRP plays an important role in increasing the capacity of the strengthened beam. However, it is recommended that the designer should check the shear capacity.
- vi) It is important to mention that the strength and stiffness of both concrete and steel is increased by increasing the rate of loading. However, the failure mode will be shifted from a ductile flexural to a brittle shear failure.

7.3 Recommendations and Future Research Directions

It is important to mention that before engineers can begin to design bridges to withstand blast loads, they need to develop an understanding of the principles of blast wave propagation and its potential effects on bridge structures.

As for the blast resistant design process for new bridge construction, a preliminary risk assessment should be performed to determine which threats the bridge under construction may face. The preliminary design of critical bridges should consider both security and redundancy. As the stand off distance plays a major role, it can be eliminated by including additional planting protective landscaping. Parking spaces beneath critical bridges, as well as access to critical areas such as piers and abutments should be eliminated.

This research was based on blast loads due to low and intermediate pressures; therefore, further research needs to be done to take into consideration blast loads due to high pressures. Additional research is needed to further develop the proposed blast-resistant design guidelines for critical bridges. Moreover, research is needed to improve the structural response and to mitigate the consequence of an attack.

References

1. Mike P. Byfield "Behavior and Design of Commercial Multistory Buildings Subjected to Blast". Journal of Performance of Constructed Facilities © ASCE/ November 2006.
2. Kirk A. Marchand; Farid Alfawakhiri. "Blast and Progressive Collapse". American Institute of Steel Construction, Inc. © April 2005.
3. American Association of State Highway and Transportation Officials (AASHTO) LRFD Bridge Design Specifications.
4. Bulb-T (BT-72) Single Span, Composite Deck, LRFD Specifications. PCI Bridge Design Manual.
5. M.Y.H. Bangash. "Impact and Explosion Analysis and Design" Published by CRC Press, Inc. 1993
6. Richard M. Barker; Jay A. Puckett. "Design of Highway Bridges, An LRFD Approach; second edition." Published by John Wiley & Sons, Inc © 2007.
7. Multiyear Plan for Bridge and Tunnel Security Research, Development, and Deployment. Published by Federal Highway Administration FHWA-HRT-06-072 March 2006.

8. David G. Winget; Kirk A. Marchand; Eric B. Williamson. "Analysis and Design of Critical Bridges Subjected to Blast Loads, journal of structural engineering © ASCE August 2005.
9. Recommendation for Bridge and Tunnel Security, AASHTO Blue Ribbon Panel on Bridge and Tunnel Security, FHWA September 2003.
10. C. J. Naito; K. P. Wheaton. "Blast Assessment of Load-Bearing Reinforced Concrete Shear Walls", Practice Periodical on Structural Design and Construction © ASCE May 2006.
11. T. Ngo; P. Mendis; A. Gupta; and J. Ramsay. "Blast Loading and Blast Effects on Structures- An Overview", electronic Journal of Science Education EJSE.
12. Masanobu Shinozuka. The Homeland Security and Defense Seminar " Civil Infrastructure Safety and Security".
13. John E. Crawford; L. Javier Malvar; Kenneth B. Morrill; John M. Ferritto; (Karagozian & Case). "Composite Retrofits to Increase the Blast Resistance of Reinforced Concrete Buildings", May 2001.
14. A. K. M. Anwarul Islam. " Performance of AASHTO Girder Bridges Under Blast Loading" PH.D. research FSU, 2005
15. Mario Paz; William Leigh. "Structural Dynamics, Theory and Computation" 5th Edition.
16. Federal Highway Administration FHWA. Abutment and Wingwall Design Example.
17. H. Saadatmanesh; M.R. Ehsani. "Fiber Composites in Infrastructure" 1998.

18. J. R. Allgood; G. R. Swihart. " Design of Flexural Members for Static and Blast Loading", American Concrete Institute Monograph No.5 1970.
19. Cyril M. Harris; Allan G. Piersol. "Harris' Shock and Vibration Handbook", fifth edition 2002.
20. Anatol Longinow and Kim R. Mniszewski. "Protecting Building Against Vehicle Bomb Attacks", Practice Periodical on Structural Design and Construction / February 1996 (Page 51-54).
21. P. Mendis and T. Ngo. "Vulnerability Assessment of Concrete Tall Buildings Subjected to Extreme Loading Conditions". Proceedings of the CIB- CTBUH International Conference on Tall Buildings, Malaysia 8-10 May 2003.
22. L. Javier Malvar and John E. Crawford. "Dynamic Increase Factors for Steel Reinforcing Bars", twenty-eight DDESB Seminar, Orlando, Florida, August 1998.
23. H. C. Fu, M. A. Erki, and M. Sechin. " Review of Effects of Loading Rate on Reinforced Concrete". Journal of Structural Engineering, Vol 117, No. 12, pp. 3660-3679, December 1991.
24. Navy Naval Facilities Engineering Command, "Structures to Resist the Effects of Accidental Explosions, NAVFAC p-397 Design Manual, (also Army TM 5-1300 and air force AFR 88-22), November 1990
25. Naval Facilities Engineering Command "Blast Resistant Structures" Design Manual 2.08, December 1986.

26. N. Uddin, N.S. Farhat, U. Vaidya, and J.C. Serrano-Perez." Vulnerability Reduction for Bridge Piers" University Transportation Center for Alabama, Report 03229, August 2005.
27. Shunsuke Otani, Takashi Kaneko, and Hitoshi Shiohara. "Strain Rate Effect on Performance of Reinforced Concrete Members". Kajima Technical Research Institute, Kajima Corporation, Japan.
28. John E. Crawford. "Protective Design for Blast and Impact Threats" 4th World Conference on Structural Control and Monitoring, 2006.
29. M. J. Chajes, T.A. Thomson, jr and B. Tarantino. "Reinforcement of Concrete Structures Using Externally Bonded Composite Materials", University of Delaware, Newark, USA.
30. Non-Metallic(FRP) Reinforced for Concrete Structures. Edited by L. Taerwe. 1995.
31. J. G. Teng, J.F. Chen, S. T. Smith, L. Lam. "FRP Strengthened RC Structures" Wiley, 2002.
32. P. R. Head " Advanced composites in civil engineering – a critical overview at the high interest, low usage stage of development “, Advanced Composite Materials in Bridges and Structures, Proceeding of the Second International Conference, Quebec, Canada, pp. 3-15, Canadian Society for Civil Engineering, Montreal, Canada, (1996).
33. M. Lopez, A. E. Naaman, and R. D. Till. “ Bending Behavior of Reinforced Concrete Beams Strengthened with CFRP Laminates and Subjected to Freeze – Thaw Cycles” PP. 559 – 576, American Concrete Institute, Farmington Hills, Michigan, USA (1999).

34. O. Buyukozturk, and B. Hearing. "Failure Behavior of Precracked Concrete Beams Retrofitted with FRP", Journal of Composites for Construction, ASCE, Vol. 2, No. 3. PP. 138 – 144. (1998).
35. V. Tamuzs, and R. Tepfers. "Ductility of Non-Metallic Hybrid Fiber Composite Reinforcement for Concrete".
36. Benjamin M. Tang. "FRP Composites Technology Brings Advantages to the American Bridge Building Industry". Proceedings published in the 2nd international workshop on structural composites for infrastructure application, Cairo, Egypt. December 2003.
37. F. K. Kong, R. H. Evans. "Reinforced and Prestressed Concrete" 3rd edition. Incorporating BS 8110 and microcomputer application, UK 1987.
38. Edward G. Nawy. "Reinforced Concrete". A Fundamental Approach, fifth edition 2005.
39. H. B. Pham, R. Al-Mahaidi. "Finite Element Modeling of RC Beams Retrofitted with CFRP Fabrics", pp 499 – 514 (2004).